NASA CONTRACTOR REPORT 159334

NASA-CR-159334
19810004509

CALCULATION OF TWO-DIMENSIONAL VORTEX-SURFACE INTERFERENCE USING PANEL METHODS

B. MASKEW

ANALYTICAL METHODS, INC.

CONTRACT NAS1-15495

DECEMBER 1980

National Aeronautics and Space Administration

Langley Research Center
Hampton, Virginia 23665

1. Report No.	2. Government Accession No.	3. Recipient's Catalog No.
NASA CR-159334		

4. Title and Subtitle	5. Report Date
CALCULATION OF TWO-DIMENSIONAL VORTEX/SURFACE INTERFERENCE USING PANEL METHODS	December 1980
	6. Performing Organization Code
7. Author(s)	8. Performing Organization Report No.
B. Maskew	79-13
	10. Work Unit No.
9. Performing Organization Name and Address	11. Contract or Grant No.
Analytical Methods, Inc. 100 - 116th Avenue S.E. Bellevue, Washington 98004	NAS1-15495
	13. Type of Report and Period Covered
12. Sponsoring Agency Name and Address	Contractor Report
National Aeronautics and Space Administration Washington, D.C. 20546	14. Sponsoring Agency Code

15. Supplementary Notes

Langley Technical Monitor: Mr. Elliot Schoonover, Jr.
Final Report

16. Abstract

The calculation of vortex/surface interference effects using panel methods is studied for two-dimensional flow conditions. The method of approach first considers the simple situation of the vortex standing above an infinite plane and proceeds through to the case of vortex separation from a prescribed point on a smooth surface using a time-step technique. Two basic singularity methods are used, a piecewise constant doublet and a piecewise quadratic doublet model. Initially, the Neumann boundary condition of zero normal velocity is used, but the final cases of separation from a thick section employ the internal Dirichlet boundary condition of zero total potential. The accuracy of the calculation is affected mainly by the ratio of the distance between control stations and the height of the vortex above the surface; this ratio should be kept below 1.0. In relation to the effect of control point spacing, the improvement in accuracy offered by the higher-order singularity distribution is insignificant. However, a technique is developed based on subpanels and an applied doublet distribution which significantly improves the accuracy of the flow predictions in the vortex interference region..

17. Key Words (Suggested by Author(s))	18. Distribution Statement
Vortex Flow Vortex Separation Panel Method	Unclassified -- Unlimited

19. Security Classif. (of this report)	20. Security Classif. (of this page)	21. No. of Pages	22. Price*
Unclassified	Unclassified		

ABSTRACT

The application of panel methods to the calculation of vortex/surface interference characteristics in two-dimensional flow is studied over a range of situations starting with the simple case of a vortex above a plane and proceeding to the case of vortex separation from a prescribed point on a thick section. Low order and high order panel methods are examined, but the main factor influencing the accuracy of the solution is the distance between control stations in relation to the height of the vortex above the surface. Improvements over the basic solutions are demonstrated using a technique based on subpanels and an applied doublet distribution.

SUMMARY

The calculation of vortex/surface interference effects using panel methods is studied for two-dimensional flow conditions. The method of approach first considers the simple situation of the vortex standing above an infinite plane and proceeds through to the case of vortex separation from a prescribed point on a smooth surface using a time-step technique.

Two basic singularity methods are used, a piecewise constant doublet and a piecewise quadratic doublet model. Initially, the Neumann boundary condition of zero normal velocity is used, but the final cases of separation from a thick section employ the internal Dirichlet boundary condition of zero total potential.

The accuracy of the calculation is affected mainly by the ratio of the distance between control stations and the height of the vortex above the surface; this ratio should be kept below 1.0. In relation to the effect of control point spacing, the improvement in accuracy offered by the higher-order singularity distribution is insignificant. However, a technique is developed based on subpanels and an applied doublet distribution which significantly improves the accuracy of the flow predictions in the vortex interference region.

TABLE OF CONTENTS

TABLE OF CONTENTS (CONTINUED)

LIST OF FIGURES

LIST OF FIGURES (Continued)

LIST OF FIGURES (Concluded)

1.0 INTRODUCTION

1.1 Background

Vortex separations from highly swept edges of wing planforms lead to important non-linear lift characteristics at moderate to high anglesof attack. A recent review (1) of the subject describes a number of inviscid fluid models which have been used in the past to predict the vortex characteristics.

The suction analogy put forward by Polhamus (e.g., Reference 2) predicts the wing lift for a broad class of wing planforms, but does not provide flow-field details or surface pressure distribution information. Various methods based on conical flow assumptions (e.g., Reference 3) provide such details for a limited class of slender configurations, but fail towards the trailing-edge region because the trailing-edge Kutta condition is excluded.

More recently surface singularity panel methods have been applied to the problem (e.g., Reference 4). In principle, such methods should offer a wide range of application. These approaches are necessarily based on iterative procedures in order to satisfy all the boundary conditions on the solid surface, the free vortex sheet, feeding sheet and vortex core.

So far, panel methods have given good solutions for thin wings having fairly regular, sharp-edged planforms. The number of iterations for vortex structure shape are minimized by starting the calculations with the conical flow solution. However, in situations where the conical flow assumptions are not valid--as on more general planforms--a large number of iterations are required to obtain a converged solution and solutions for thick sections (with prescribed separation line) have so far failed to converge. motto !

1.2 Present Approach

The objective of the present work is to examine the behavior of surface singularity panel methods applied to the calculation of vortex/surface interference. The method of approach is to examine the calculations in two-dimensional flow and to proceed in steps from the simple vortex/plane problem to the case where a vortex separation occurs from a smooth surface. The following sections describe the results of the investigation starting (in Section 3.0) with the vortex/plane problem in which the basic interference calculation can be observed without the complications of surface

curvature and feeding sheet geometry. The case with surface curvature is considered in Section 4.0 and the case of vortex separation from a sharp-edged plate is considered in Section 5.0 using a time-stepping approach. Extension of this to the case of separation from a thick section is given in Section 6.0, which also includes a preliminary look at the case where the thick section grows with time. The latter was performed with a view of applying the method to the unsteady cross-flow analogy of steady flow about three-dimensional shapes. Such an application could provide an improved initial vortex structure for input to the three-dimensional method with the object of minimizing the number of wake iterations.

2.0 NOMENCLATURE

Except where dimensions are given, the variables listed below are regarded as dimensionless since unit values for the onset flow and characteristic length are set in each problem.

γ	Vorticity strength
Γ	Discrete vortex strength
δt	Time-step increment
θ_{merge}	Angle beyond which vortices on the free sheet are merged with the vortex core in the vortex roll-up calculations, see Figure 22
λ	Ratio of local panel size (or distance between control points) divided by the height of the vortex above the surface
μ	Doublet strength
ϕ	Perturbation potential
ϕ_∞	Uniform onset flow potential
Φ	Total velocity potential
C_p	Pressure coefficient
h	Perpendicular height of the vortex above the local surface on a curved body
$\underline{n}$	Unit vector normal to the surface

NFR	Near-field radius factor; See Section 3.1
NSUB	Subpanel density, i.e., number of subpanels per panel
s	Distance measured along the surface
t	Time in the vortex roll-up calculation
V_N	Velocity component normal to the surface
V_T	Velocity component tangential to the surface

3.0 VORTEX/PLANE PROBLEM

In this section we consider the basic problem of calculating the interference effect between a vortex and an infinite plane using surface singularity methods. This situation, for which an exact solution is known, allows the panel method solution to be examined independently of the effects of surface curvature and feeding sheet. (These factors are considered later.)

3.1 Arrangement of the Flow Model

The arrangement of the vortex/plane problem is shown in Figure 1. For the present calculations, the plane contains the x-coordinate axis and the vortex, strength Γ, is placed at height Z on the z-axis (i.e., at (0,Z). For the x-axis to be a streamline of the flow field, the doublet distribution on the x-axis is (from the image technique):

$$\mu(x) = \frac{\Gamma}{\pi} \tan^{-1}\left(\frac{x}{Z}\right). \quad *$$

The corresponding vorticity distribution is

$$\gamma(x) = \frac{-\Gamma}{\pi}\left\{\frac{Z}{x^2 + Z^2}\right\}. \quad *$$

(This is also the magnitude of the velocity at the surface.)

For the present calculations, only the region $-a \leq x \leq a$ is paneled for the numerical solution. Each panel has a central control point where the boundary condition of zero normal velocity is applied. The normal velocity has three parts:

1. The vortex contribution.
2. The contribution from the two semi-infinite parts of the vortex sheet: $-\infty \leq x \leq -a$, and $a \leq x \leq \infty$.

---

* Note: The convention for positive γ is clockwise and the positive direction for the doublet axis is in the positive z direction; therefore, $\gamma = -\partial\mu/\partial x$.

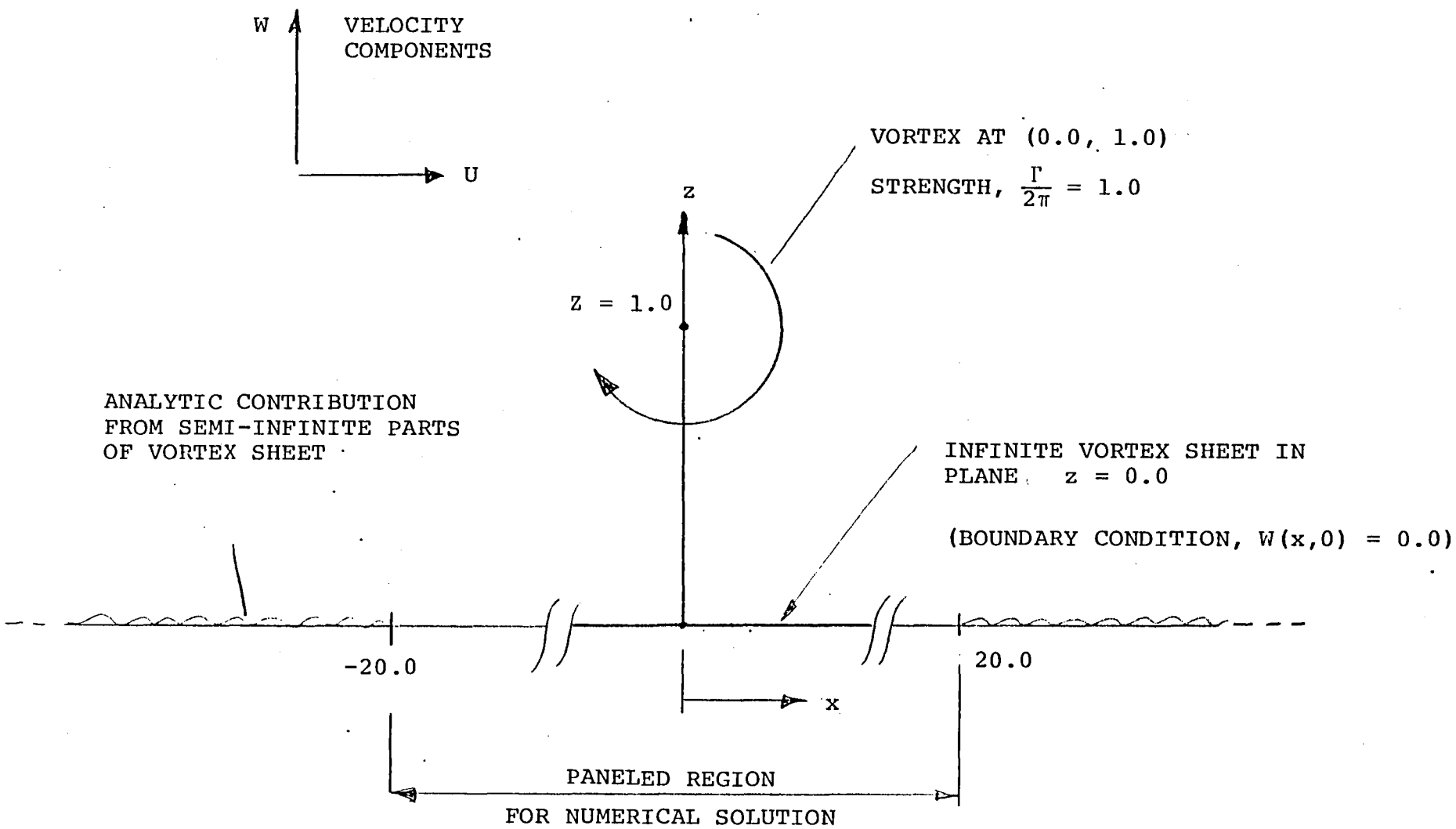

Figure 1. Vortex/Plane Problem.

3. The singularity panel contribution

The sum of parts 1 and 2 can be regarded as the onset flow in this case. Now apply the condition of zero normal velocity at each panel control point:

$$\sum_{k=1}^{N} A_{jk}\,\mu_k - b_j = 0; \qquad j = 1, 2, \ldots, N$$

where A_{jk} is the normal velocity influence coefficient of the doublet value on the k^{th} panel acting on the j^{th} control point, N is the number of panels, and

$$b_j = \frac{\Gamma Z}{2\pi^2 (x_j^2 + Z^2)} \left\{ \log \left| \frac{a + x_j}{a - x_j} \right| + 2 \frac{x_j}{Z} \tan^{-1} \left(\frac{a}{Z} \right) \right\}$$

is the sum of parts 1 and 2 above.

For these calculations, the vortex strength, $\Gamma/2\pi$, is set at 1.0, the vortex height, Z, is set at 1.0, and the extent of the paneled region, a, is set at 20.0.

The region $-a \leq x \leq a$ is divided into N panels: N is considered in the range from 10 to 120. Each panel is divided into an odd number of subpanels, NSUB (Appendix A). NSUB values of 1, 3, 5 and 7 are considered. Each panel's control point is the center point of the middle subpanel on the panel. A panel's set of subpanels provides a more detailed description of the singularity distribution (and also the surface geometry in the general case) when evaluating the panel's contribution to the velocity at a point close to the panel; i.e., at points within the panel's NEAR-FIELD REGION. Use of such detail is unnecessary when the point is far from the panel, in which case the panel, itself, is used. The panel's near-field region is defined by a circle centered on the panel's control point and having radius NFR times panel length. NFR is the near-field radius factor, and values ranging from 2 to 5 are considered here.

Each panel has an unknown doublet value associated with its control point. Doublet values at subpanel center points are obtained using a biquadratic interpolation (cubic)

(Appendix B) through four neighboring panel values; i.e., at the outset each subpanel, except the middle one, has a set of four multipliers applied to a set of four neighboring panel doublet values. Each panel's middle subpanel takes that panel's doublet value.

The vorticity value at each subpanel could be obtained by differentiation of the biquadratic interpolation expression; however, for the time being, and to keep things simple in the three-dimensional case, these quantitles are obtained from simple quadratic fit through three subpanel doublet values (Appendix A).

Two singularity models are considered in the present calculations.

(i) MODEL 1: Piecewise constant doublet distribution on each panel.

(ii) MODEL 2: Piecewise quadratic doublet distribution on each panel.

Model 1 is the two-dimensional equivalent of the vortex-lattice model; i.e., each panel and subpanel doublet value is represented by a pair of opposing discrete vortices positioned at the panel or subpanel corners. The vortex strengths are the same as the doublet values. The calculation involving this first model, therefore, extend the calculations in Reference 5 to the case with subpanels.

Model 2 is equivalent to the widely used piecewise linear-vorticity model except that here we solve for the panel doublet values rather than the vorticity values. This is done with a view to the three-dimensional case where it is an advantage to solve for the (scalar) doublet value. The vorticity values are then evaluated as the doublet gradient.

For the purpose of comparing the results with the exact solution, the vorticity distribution has been selected in order to expose any errors in the doublet gradient evaluation.

3.2 Initial Results

In all the comparisons shown in Figures 2 through 9, the exact vorticity distribution is given by the solid line and boundaries of $\pm 5\%$ error are indicated by dotted lines. Only half the calculated distribution is plotted in the cases where the vortex location is symmetrical with the paneling;

i.e., when the vortex is located above a panel corner. Also, only the portion of the solution extending along the x-axis about two vortex heights is plotted. All computer times are quoted for the CDC 7600 computer.

3.2.1 MODEL 1: Piecewise Constant Doublet

All the piecewise constant doublet calculations here are based on equal panel distributions. Figure 2 shows the calculated vorticity values for various panel densities with no subpanels. Panel sizes range from 4.0 to .33 of the vortex height (i.e., λ values from 4 to .33). Meaningful results are obtained only with panel sizes smaller than the vortex height above the surface ($\lambda < 1.0$).

The effect of using subpanels is shown in Figure 3(a), (b) and (c) for 20, 40 and 80 panels, respectively. The near-field radius value is 3 (i.e., subpanels are not used beyond 3 panel sizes from the calculation point). The use of subpanels gives an immediate increase in the density of information on the calculated vorticity distribution. (Of course, in the present case, similar surface information could be obtained by direct interpolation through the no-subpanel-solutions. But, such interpolation is not always possible in the flow field, and it is here where the subpanel scheme will offer a possible solution.)

The use of subpanels changes the accuracy of the control point solutions only slightly--sometimes improving accuracy; but there are cases of small losses in accuracy. The subpanel solutions can only be as good as the interpolation curve used to represent the doublet distribution--here, a cubic equation is attempting to represent an inverse tangent function. With only 20 panels (Figure 3(a)), the solution is remarkable in that there is only one control station in the plotted region. Using 40 and 80 panels (i.e., panel sizes respectively 1.0 and .5 of the vortex height above the surface) produces very reasonable vorticity distributions that are comparable with the 120-panel (no subpanel) solution from Figure 2. Use of the subpanels gives a significant reduction in computing effort compared with the 120-panel case; e.g., in Figure 3(b) the 40-panel case with 3 subpanels per panel (i.e., a total of 120 subpanels) shows comparable vorticity information to the 120-panel case with no subpanels and yet the computation time is .195 secs. compared with 1.401--i.e., computing time is reduced by a factor of 7. Increasing the number of subpanels to 7 gives even greater density of information for a small increase in computing effort; i.e., .248 secs. c.f. .195 for the 3-subpanel case.

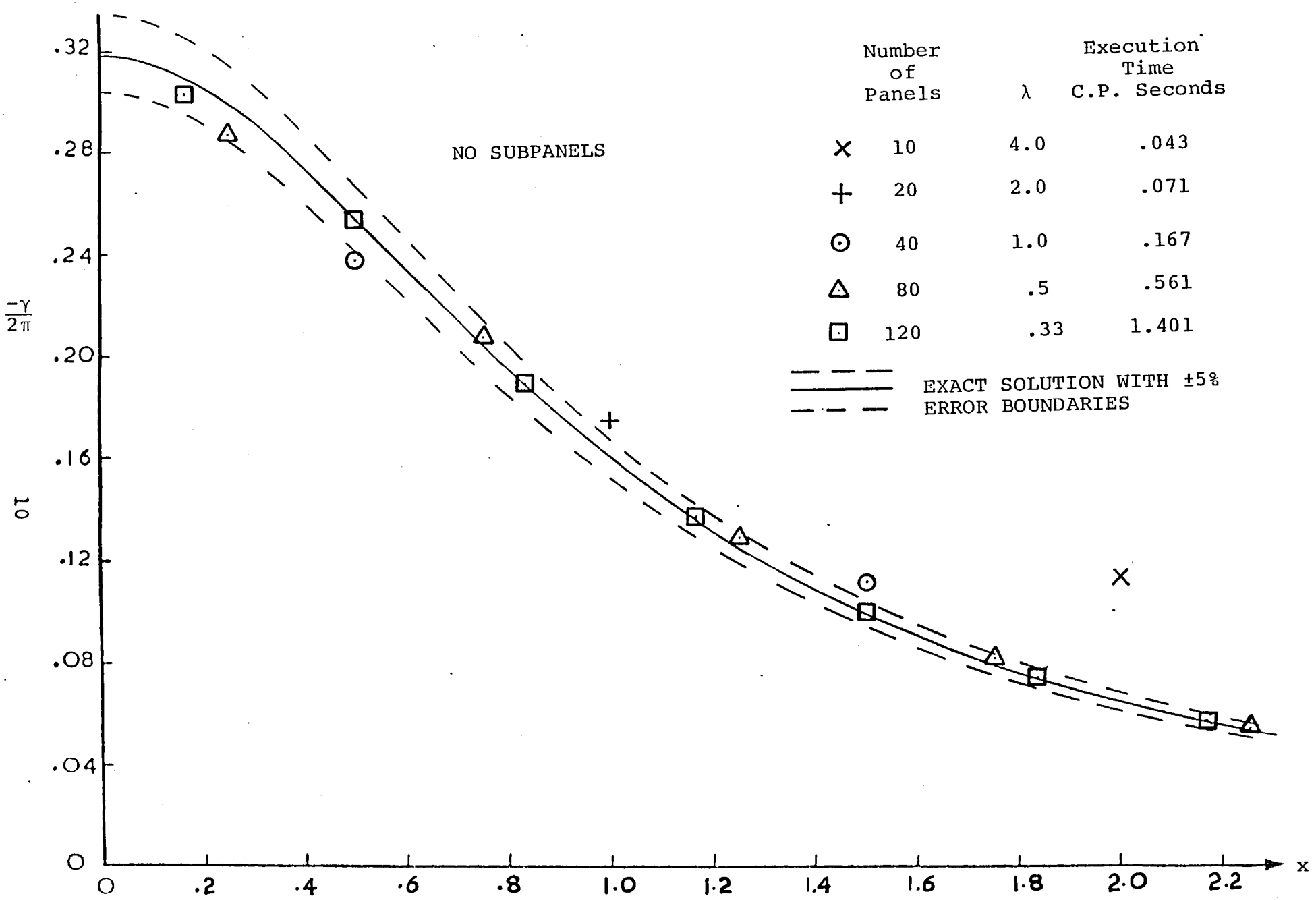

Figure 2. Vortex/Plane Solution. Effect of Panel Density with Model 1.

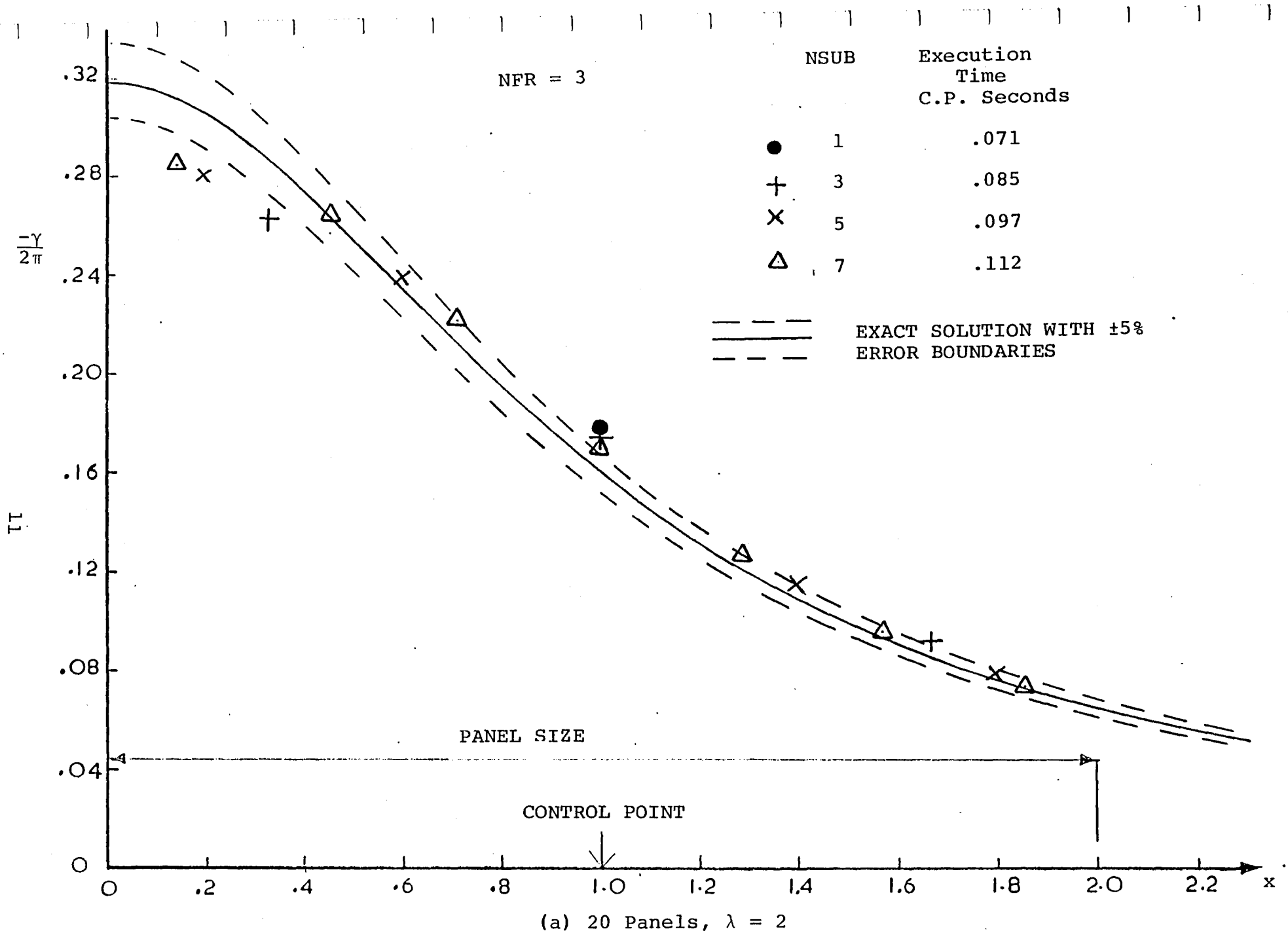

(a) 20 Panels, $\lambda = 2$

Figure 3. Vortex/Plane Solution. Effect of Subpanels with Model 1.

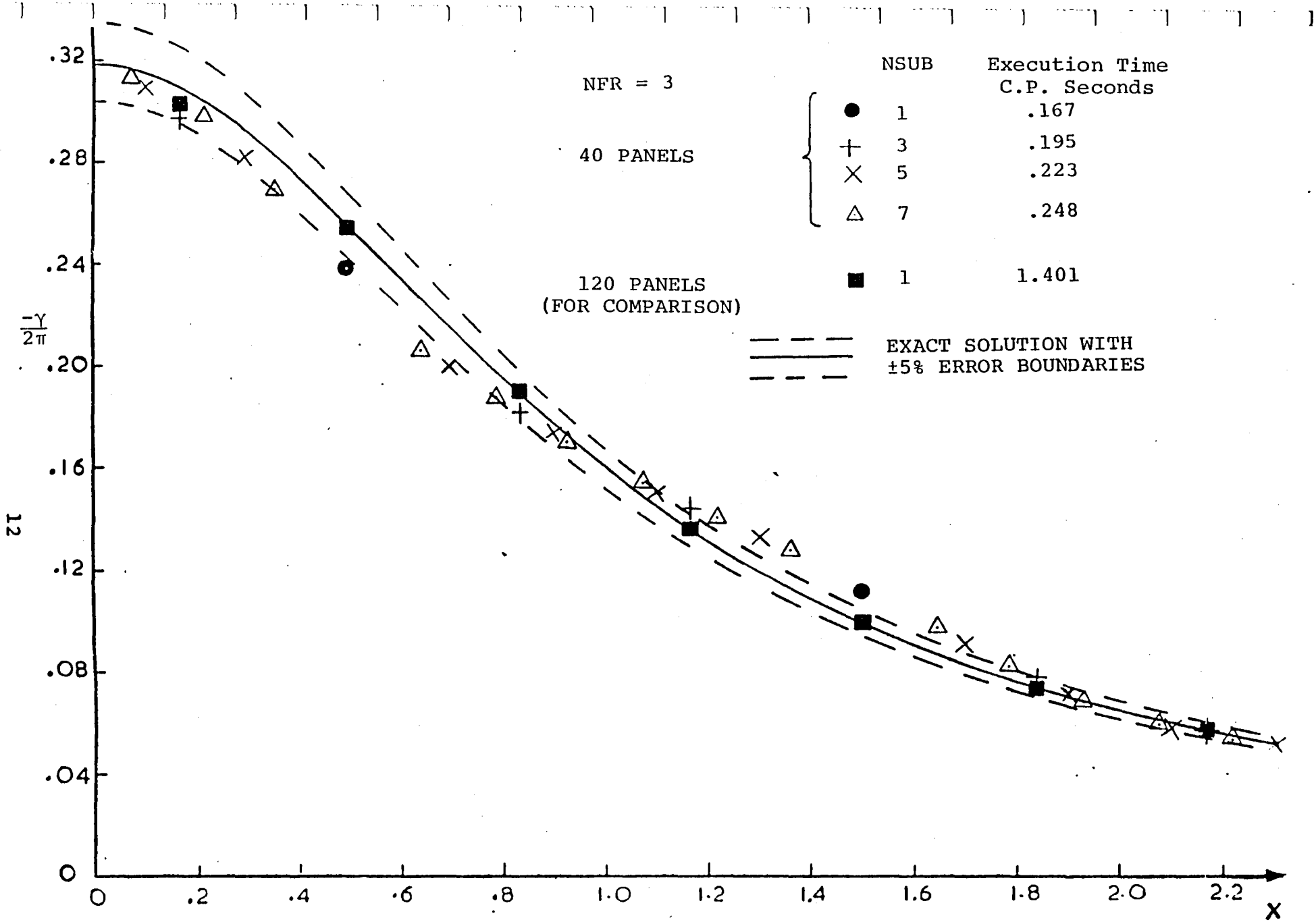

(b) 40 Panels; $\lambda = 1$.

Figure 3. Continued.

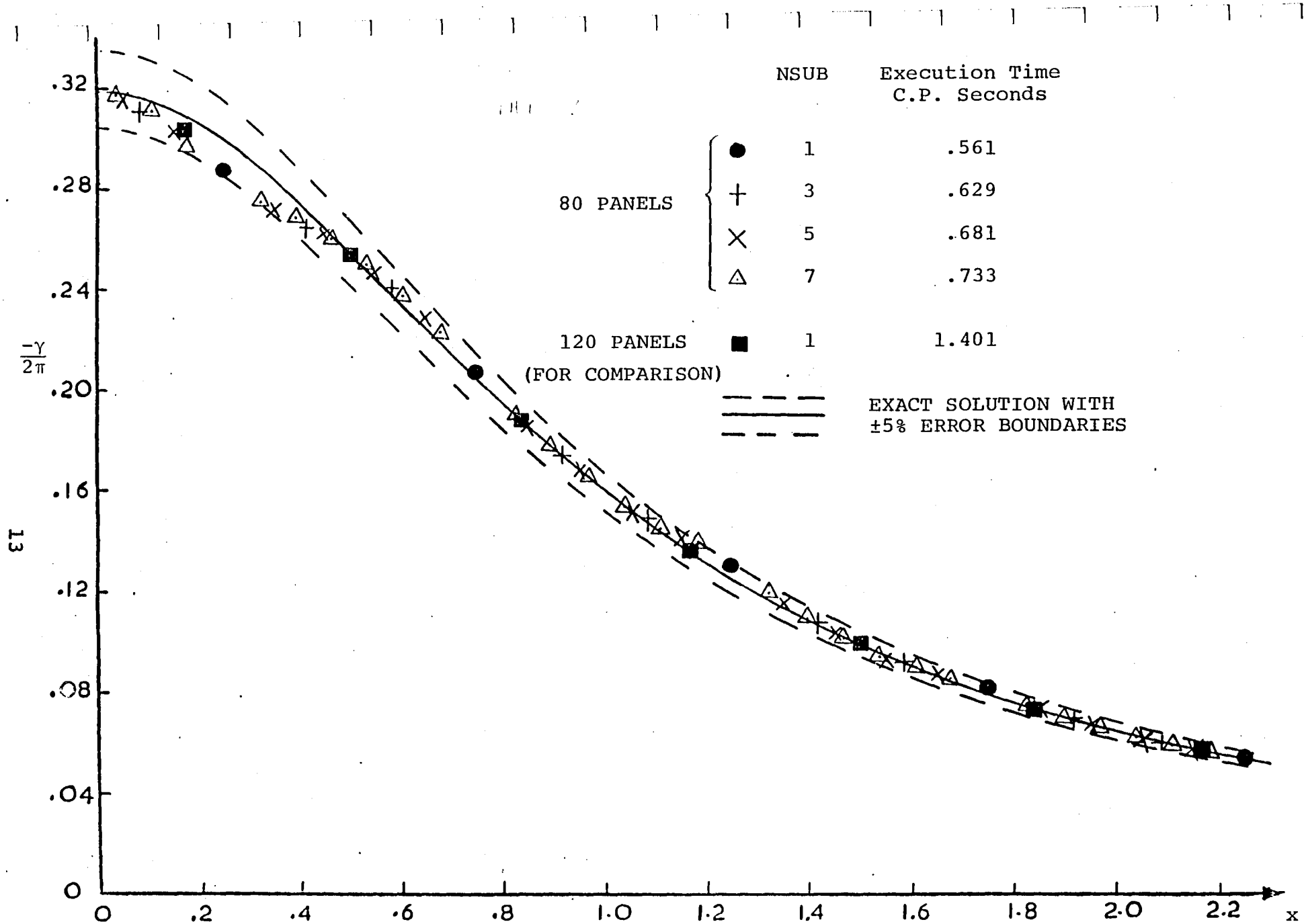

(c) 80 Panels; $\lambda = .5$.

Figure 3. Concluded.

For the 80-panel case (Figure 3(b)), the entire subpanel solution lies within the ± 5% error boundaries, and yet even the 7-subpanel case is achieved with about half the computing effort of the 120-panel case with no subpanels.

Figure 4 shows the effect of near-field radius, NFR, on the calculated vorticity values. NFR values of 2, 3, 4 and 5 are considered with the case of 40 panels ($\lambda = 1.0$) and 5 subpanels per panel. There is only a small effect down to values of 2 for NFR. Use of subpanels beyond 4 panel lengths away has no plottable effect. There is an 8% reduction in computing time going from NFR = 4 to NFR = 2 in this case.

Before leaving the piecewise constant doublet model there is one final feature worth mentioning. In these calculations using equal spacing, the quadratic fit through doublet values to obtain vorticity values is identical to the central difference formula for doublet derivatives. It is remarkable that the vorticity value obtained at panel corners (i.e., vortex locations) from the difference of two neighboring doublet values is considerably more accurate than the value obtained at panel centers (doublet locations) obtained from the difference of the two doublet values on either side of the central point; i.e., the surface interval is twice the value of the first case. For example, in the case of 40 vortices and no subpanels, the vorticity error at the center point is 6.6% compared with .37% at the corner point--an improvement larger than would be accounted for by the halving of the interval.

3.2.2 MODEL 2: Piecewise Quadratic Doublet

Figure 5 shows the effect of panel density (no subpanels) for the piecewise quadratic doublet model. The vorticity errors are reduced only slightly from those of Model 1, c.f., Figure 2 (except in the case of very sparse paneling where the errors are now larger). Clearly, the important factor determining the accuracy of the panel method solution is the panel density--or more significantly the control point density--in relation to the vortex height: the order of the singularity distribution appears to have little influence.

Computing times are only slightly more than for the Model 1 case; for example, the 120-panel case took 1.497 secs. compared with 1.401 secs. for Model 1. (Larger differences in C.P.U. time would be expected in the three-dimensional case).

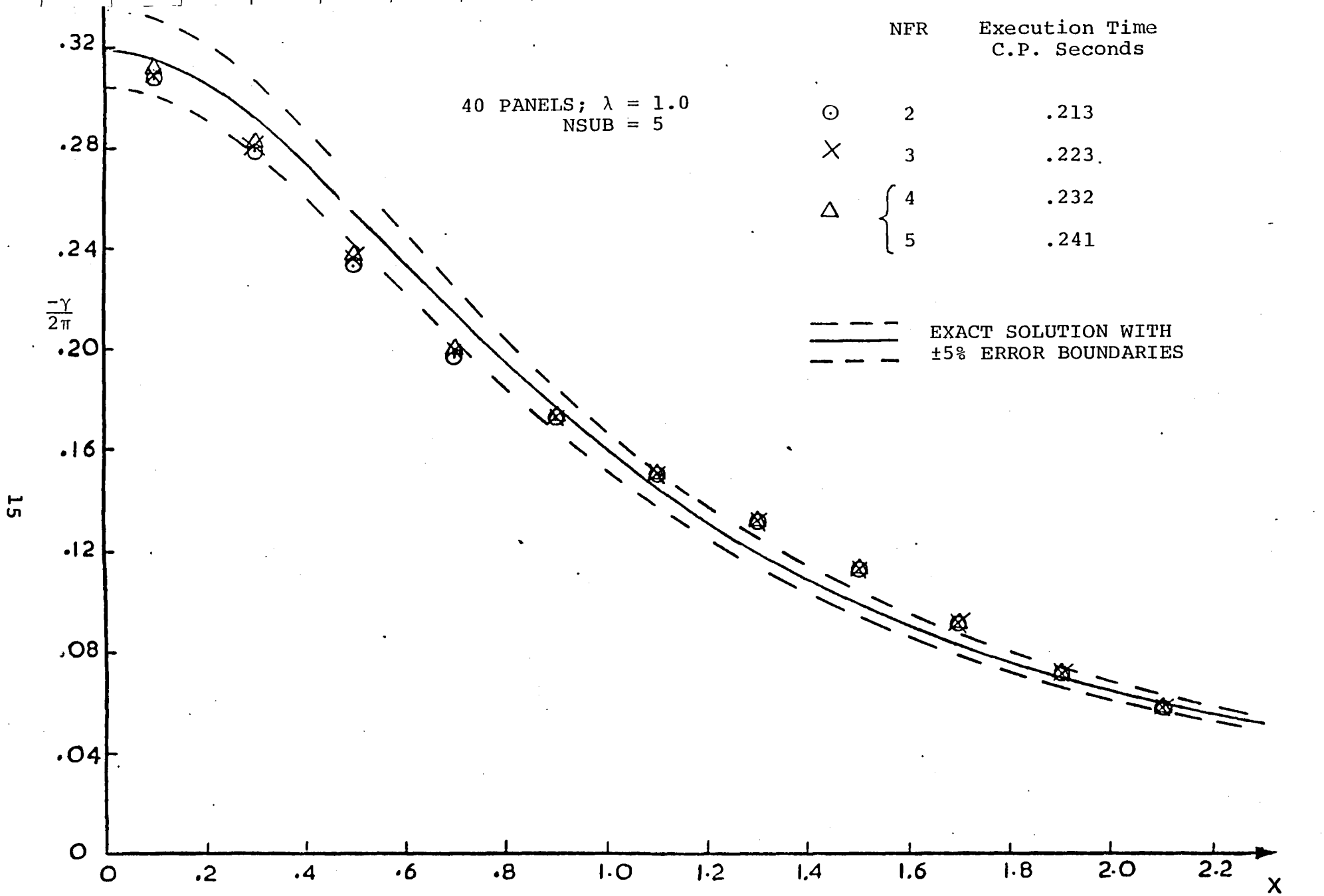

Figure 4. Vortex/Plane Solution. Effect of Near-Field Radius with Model 1.

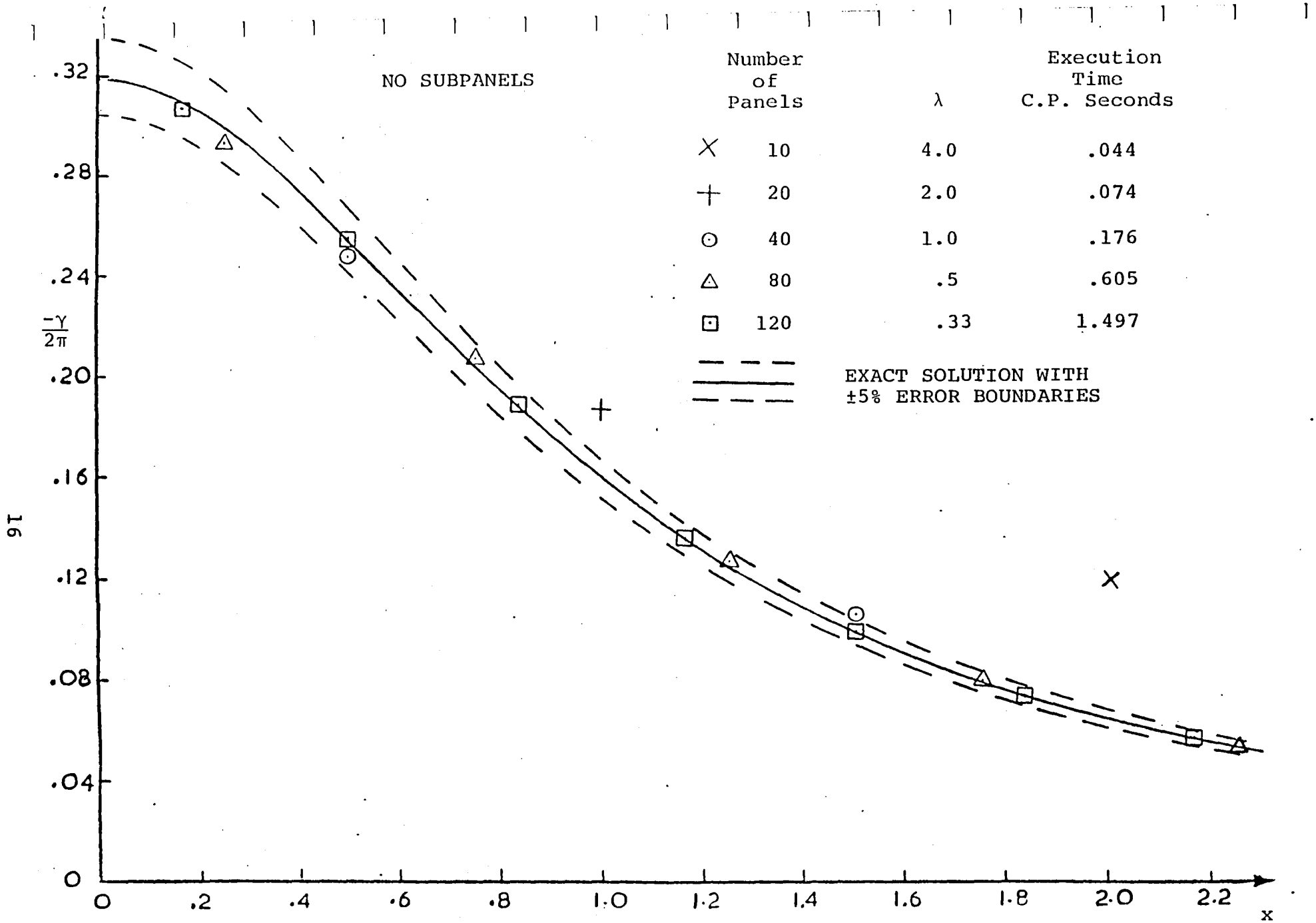

Figure 5. Vortex/Plane Solution. Effect of Panel Density with Model 2.

The effect of using subpanels is shown in Figures 6(a), (b) and (c) for 20, 40 and 80 panels, respectively. These compare with Figures 3(a), (b) and (c), and again show only small improvements in accuracy over Model 1 and a small increase in computing time (~ 6%).

Figure 7 shows the effect of near-field radius, NFR, on the Model 2 calculations using 40 panels and 5 subpanels per panel. In this case there is no plottable difference for NFR values beyond 3.

The effect of using a cosine spacing of panels instead of equal spacing is shown in Figure 8 for the case with 40 panels and 5 subpanels per panel. NFR in this case is 4. The cosine spacing gives increased density of panels in the region of the vortex and also at each end of the panelled region. The increased control point density in the critical region under the vortex clearly improves the vorticity calculation significantly. The closer spacing of control stations helps the cubic interpolation curve to represent the inverse tangent function and produces smaller oscillations in the subpanel solution.

For all the calculations so far, the vortex has been placed directly above a panel corner. In Figure 9, the calculated vorticity distribution is shown for the case where the panel corner point is displaced by .2 of the vortex height along the x-axis. Panel spacing is equal in Figure 9(a). (a = 20.0 still applies, and so there is a small difference in panel size from one side to the other of the x = .2 station.) The calculated results are shown for 40, 80 and 120 panels with no subpanels and for 40 and 80 panels each with 5 subpanels and with NFR = 3. Meaningful results are now obtained only with panel sizes less than .5 of the vortex height above the surface. However, by using cosine spacing, Figure 9(b), with increased panel density in the approximate neighborhood of the vortex, the 40-panel case shows a very reasonable vorticity solution.

All the solutions obtained are evidently limited by the ability of the doublet interpolation curve to represent the exact doublet distribution--in this case a cubic attempting to represent an inverse tangent function. The cubic is convenient to use because of the simple multipliers--one based on an inverse tangent would be more cumbersome to use--particularly in the three-dimensional case.

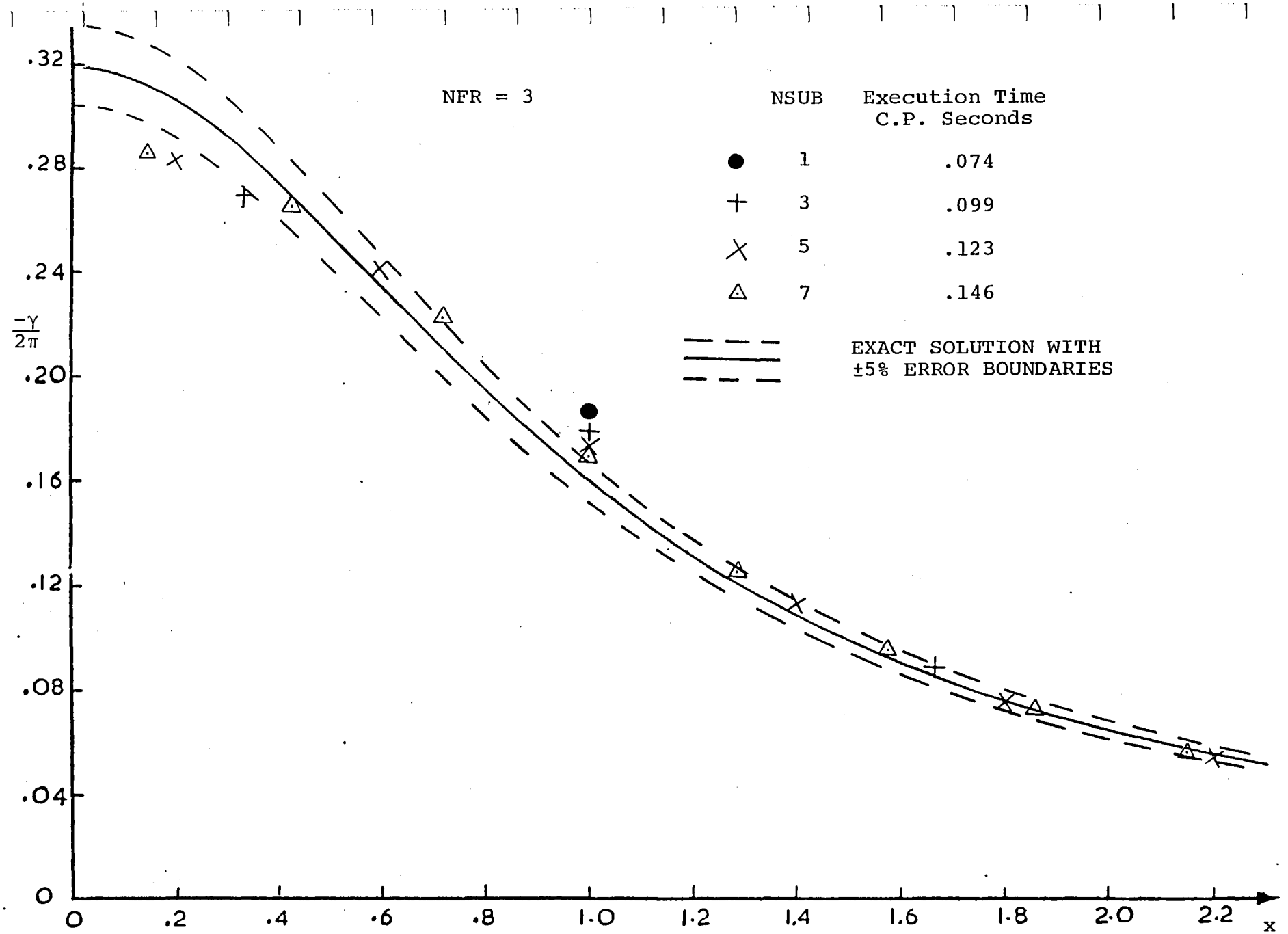

(a) 20 Panels, $\lambda = 2$.

Figure 6. Vortex/Plane Solution. Effect of Subpanels with Model 2.

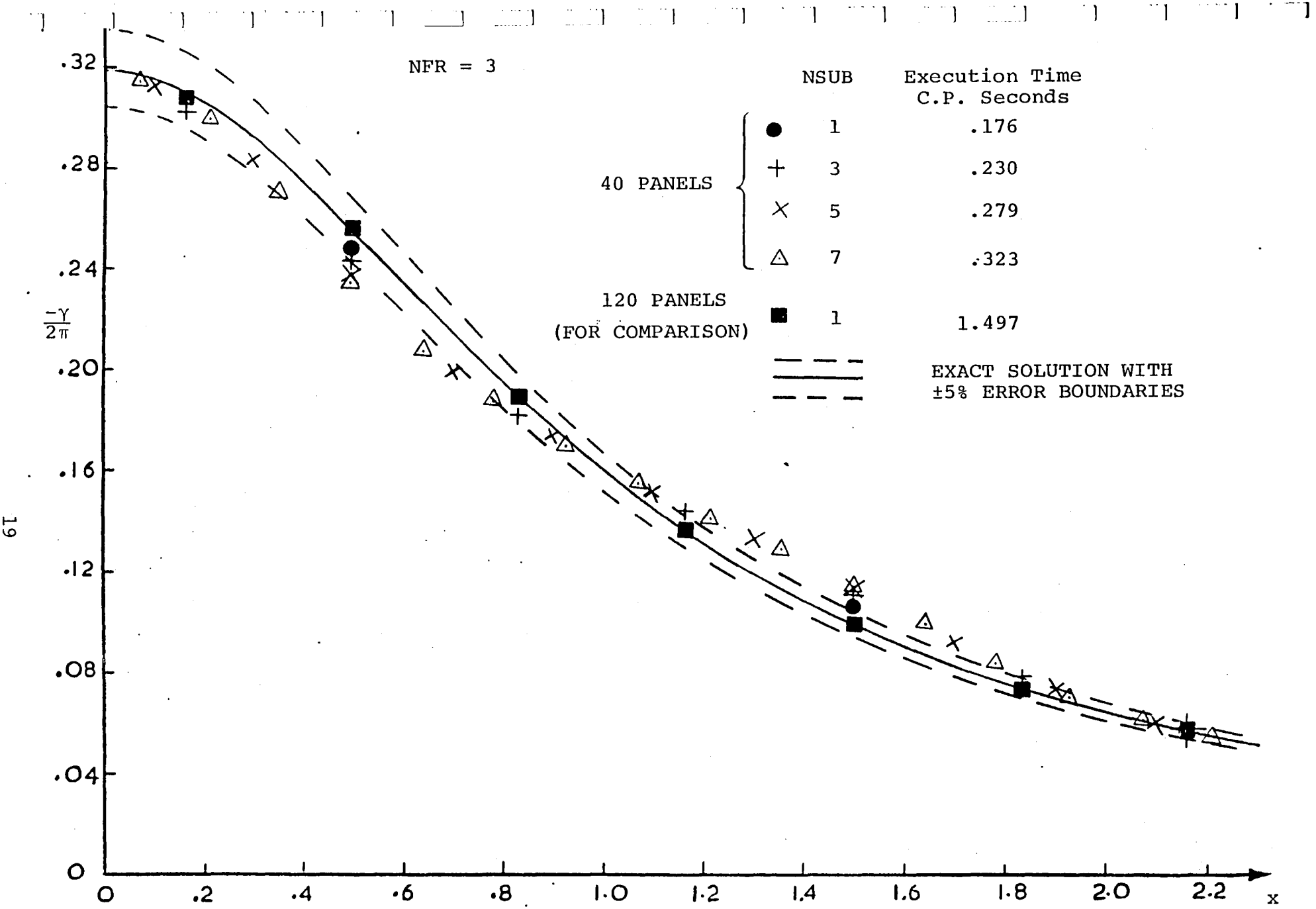

(b) 40 Panels; $\lambda = 1$.

Figure 6. Continued.

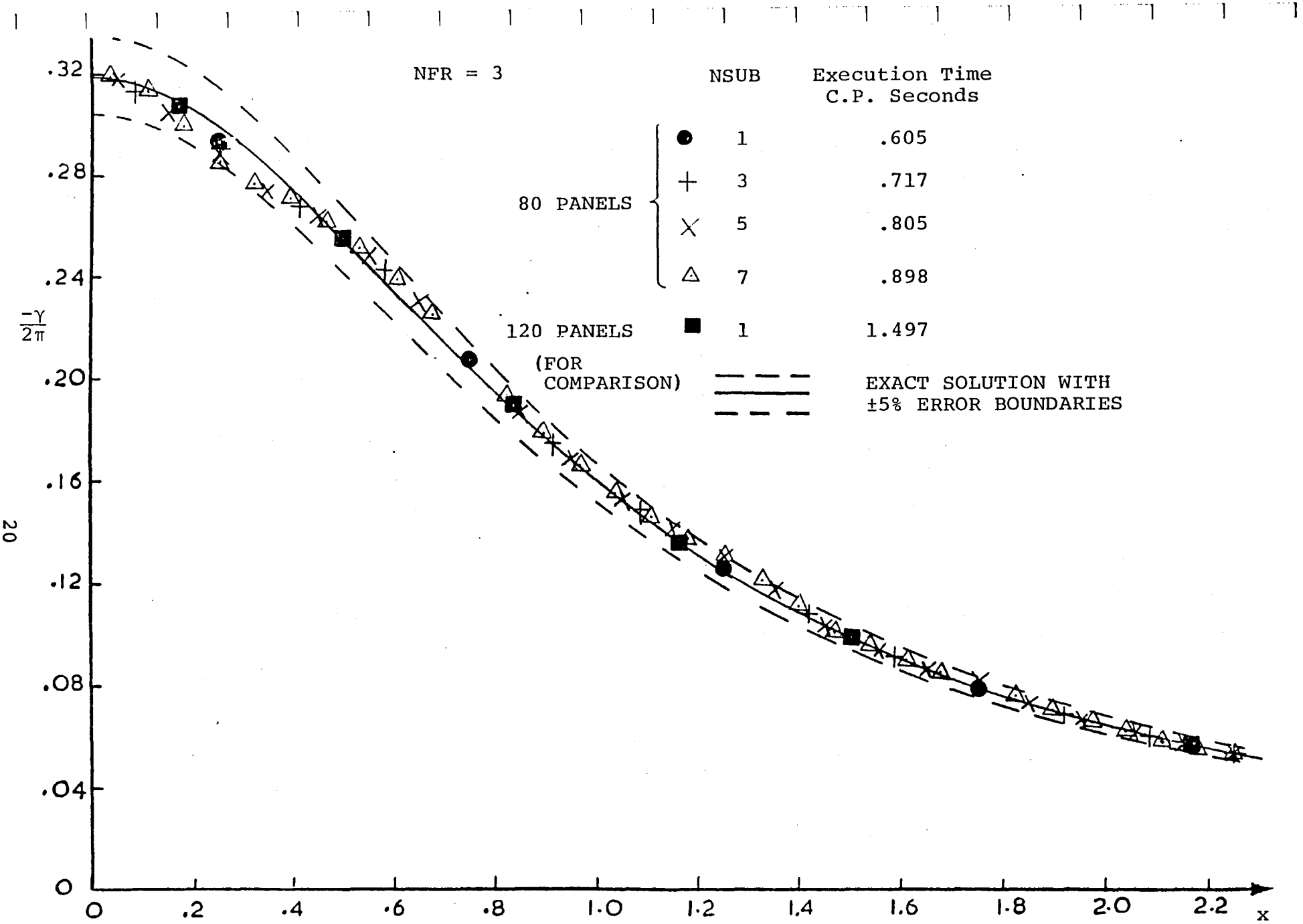

(c) 80 Panels; $\lambda = .5$.

Figure 6. Concluded.

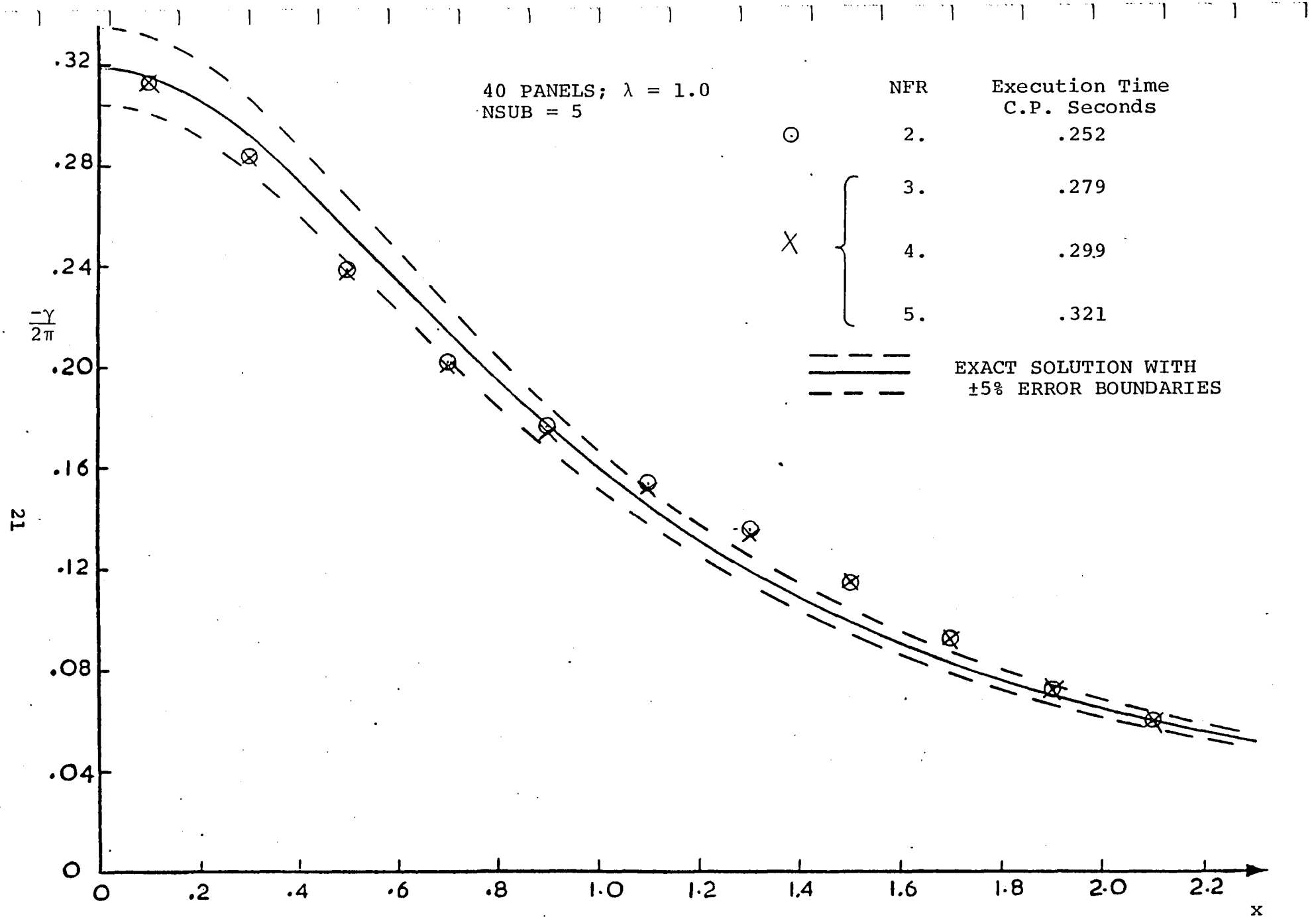

Figure 7. Vortex/Plane Solution. Effect of Near-Field-Radius with Model 2.

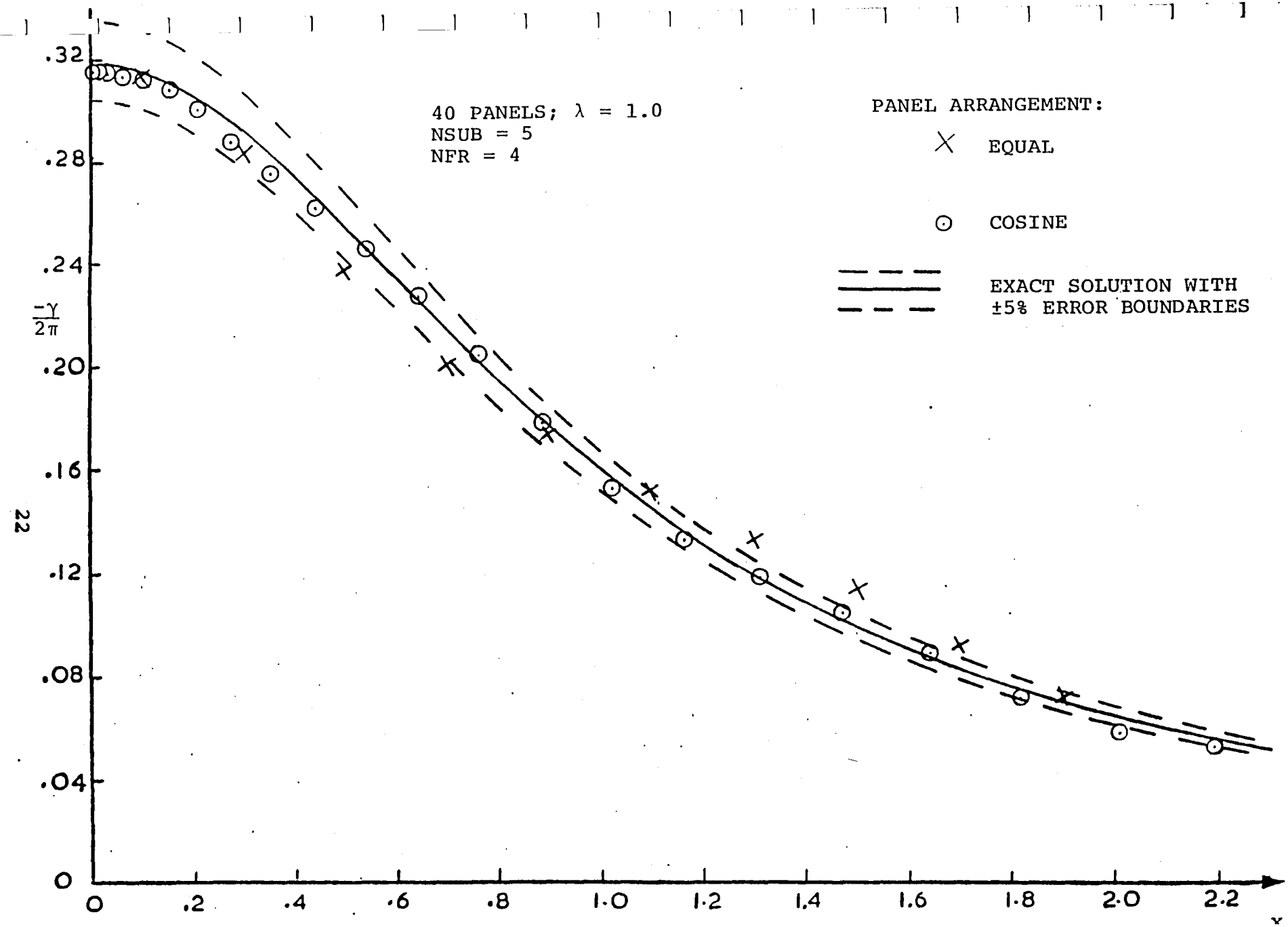

Figure 8. Vortex/Plane Solution. Effect of Panel Arrangement with Model 2.

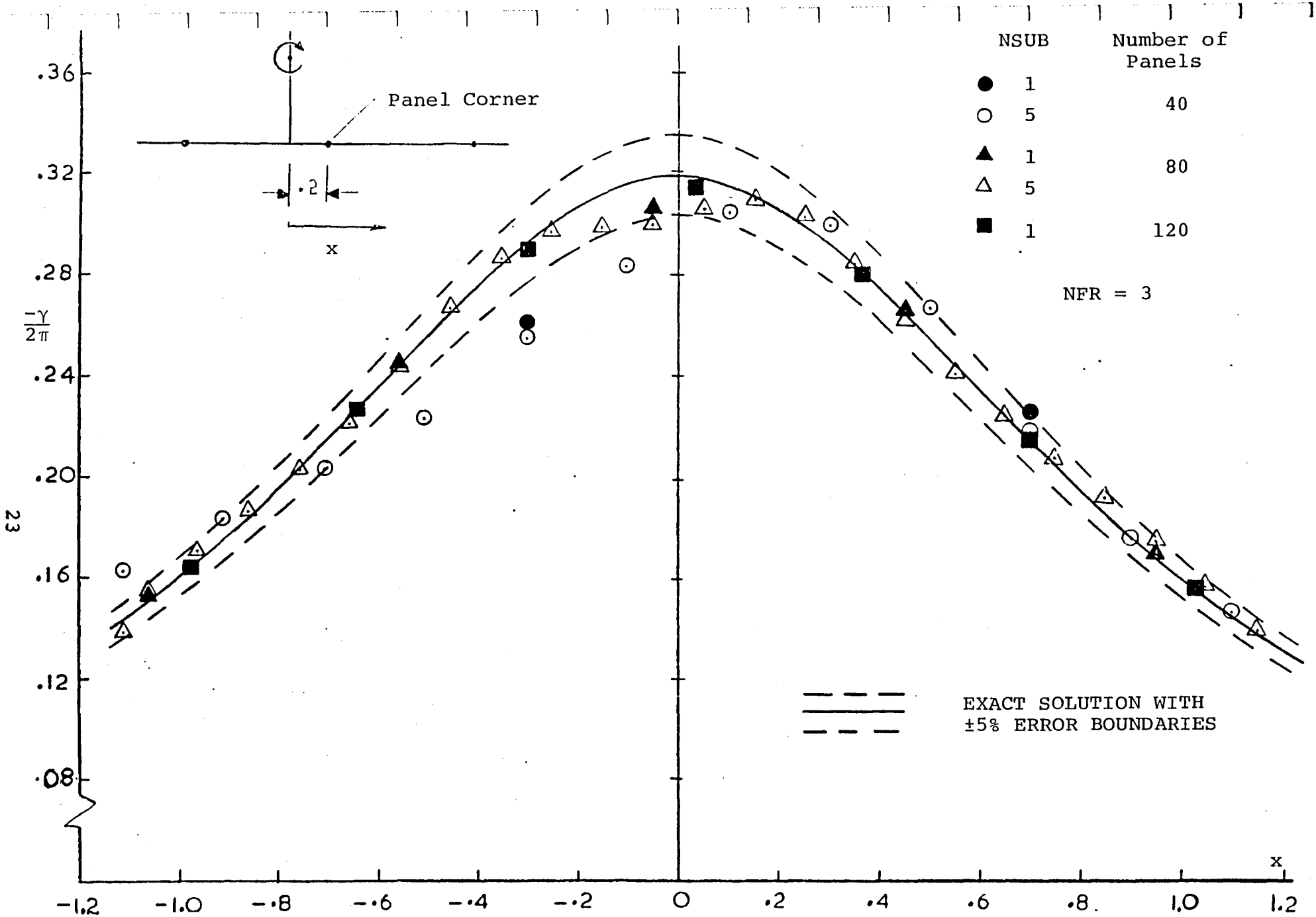

(a) Equal Spacing.

Figure 9. Vortex/Plane Solution. Effect of Vortex Offset by .2 from Panel Edge, Model 2.

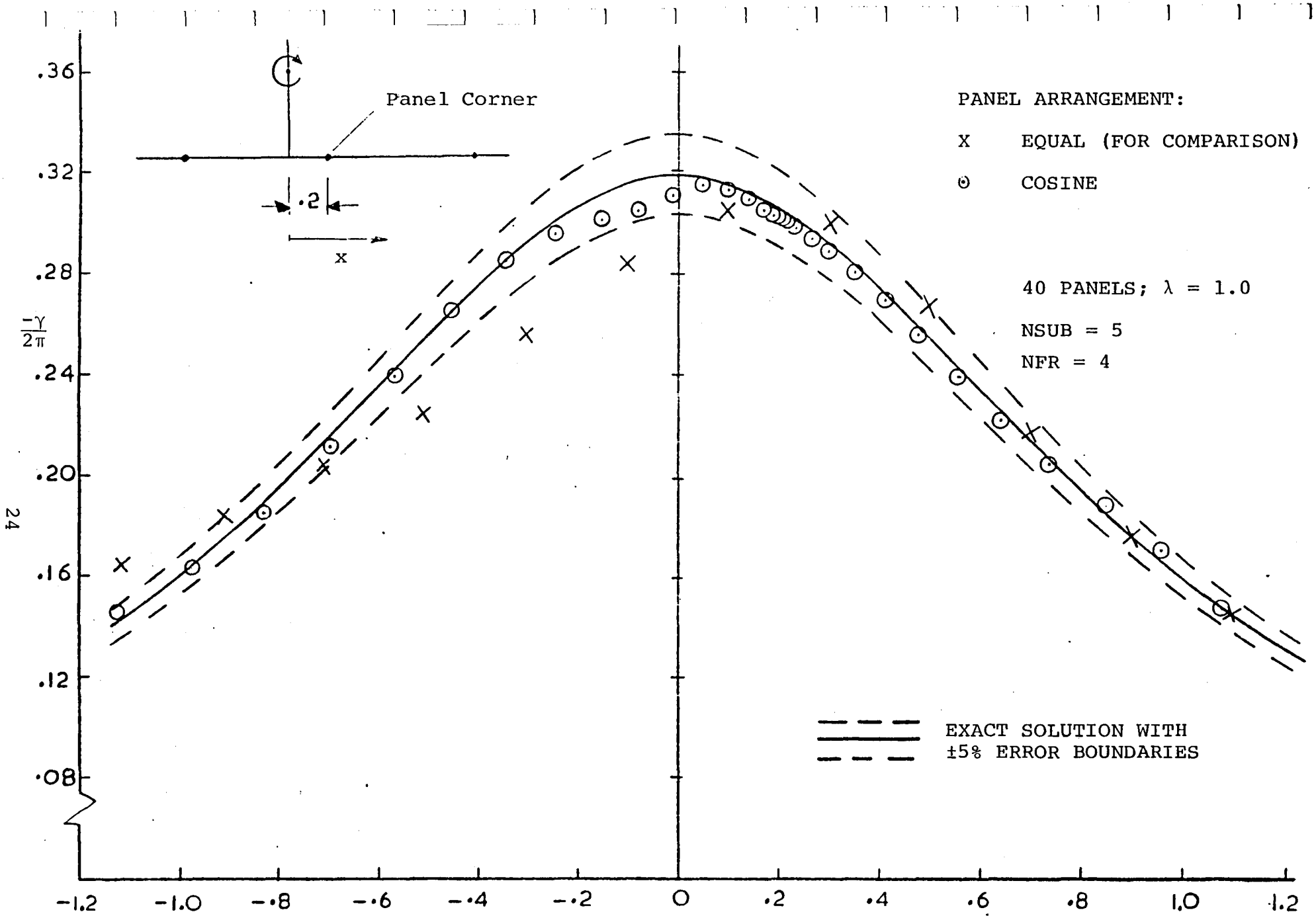

(b) Cosine Spacing.

Figure 9. Concluded.

3.3 Applied Doublet Technique

In order to alleviate the task of the biquadratic to fit the inverse tangent function, the doublet distribution has now been split into two parts. The first part is an applied part being an approximation to the exact solution and appears as a contribution to the right side (i.e., onset flow) of the boundary condition equations; the second part is the unknown part which will be the solution. The solved part should be small if the first part is a good representation.

The applied doublet distribution is evaluated at each subpanel center point. Vorticity values and slopes for the applied distribution are then derived using a quadratic fit through three neighboring subpanel values as before. This is a practical approach which is usable in the three-dimensional case. The solved part of the distribution is treated in the same way as described earlier using the biquadratic multipliers at subpanel locations.

As a preliminary test of the technique an applied distribution of the exact form, i.e., $\mu(x) = \Gamma/\pi \tan^{-1}(x/Z)$, was applied over the entire paneled region (evaluated at each subpanel center point). Of course, in the present problem, the solved doublet distribution should then be zero. The following evaluation might, therefore, appear trivial, but as a result of the practical derivation of vorticity and vorticity gradient (from subpanel center values) and the practical paneling scheme and singularity model (piecewise linear vorticity), the solved distribution reflects the numerical approximations in the procedure. As a result, small residual doublet values appear in the solution. In the general case, the solved part of the doublet distribution would include corrections to the applied part resulting from surface curvature (airfoil shape) circulation and other onset flows.

Figure 10 shows the new calculations using 40 panels (equal spacing) and a range of subpanel densities. For comparison, two solutions from Figure 6 (i.e., with the applied doublet distribution switched off) are also presented. With just the basic panels (i.e., one subpanel per panel) the applied distribution gives no change in the overall distribution of vorticity. (The applied distribution is evaluated only at the panel control points in this case, and therefore offers no improvement in the conditions for calculating vorticity values.)

With subpanels present, there is an immediate improvement in the overall solution with none of the earlier oscillation about the mean line. Unlike the earlier cases,

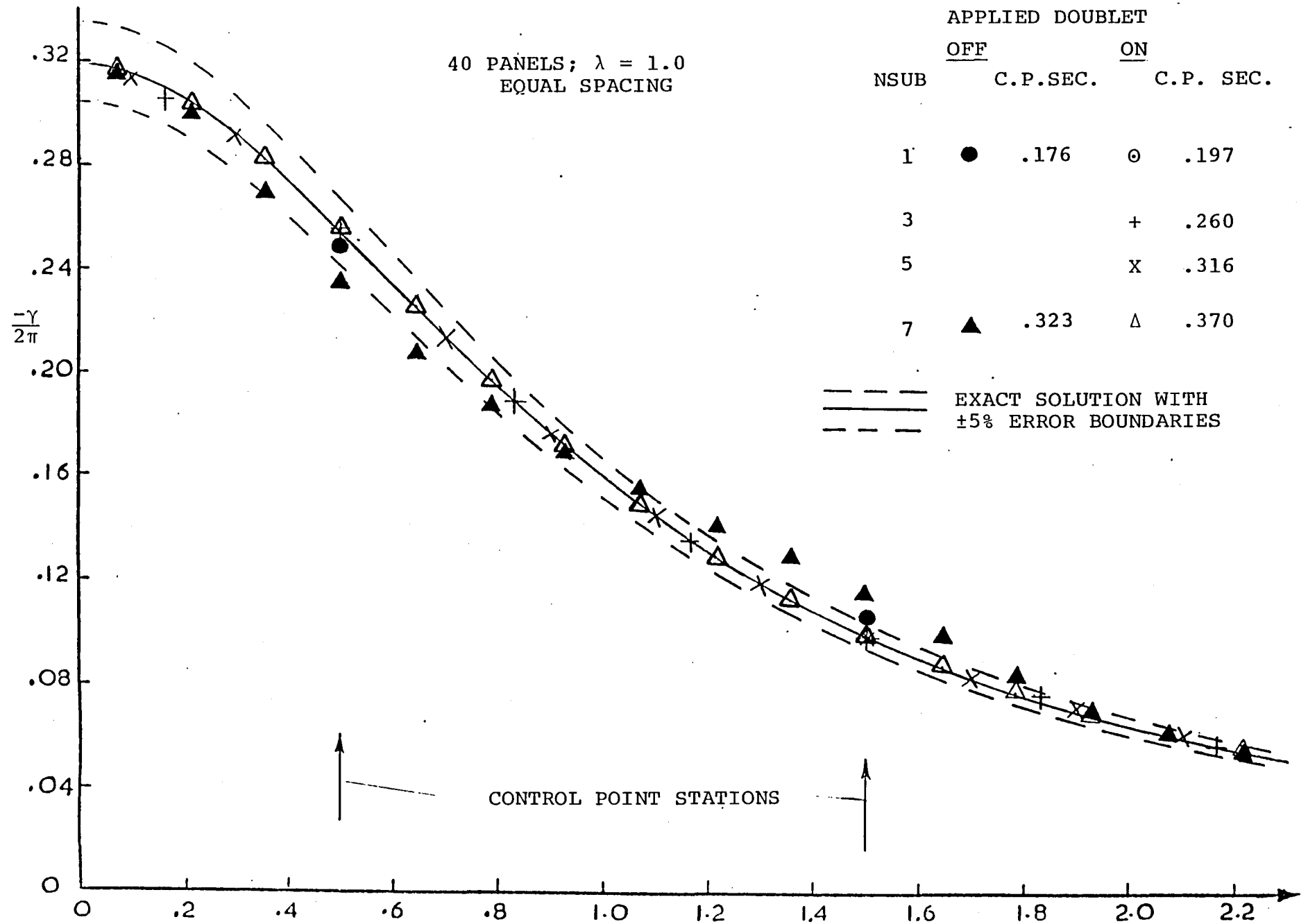

Figure 10. Vortex/Plane Solution. Effect of Applied Doublet Distribution with Model 2.

use of subpanels with the applied doublet distribution switched on always gives an improvement in accuracy at the control stations (some of the basic cases shown earlier indicated a small loss in accuracy at these points when subpanels were used).

Use of the applied doublet routine increases computing time by about 12-15%.

Figure 11 shows results calculated with the vortex offset by .2 from a panel edge. Very good agreement is now obtained using 40 panels equally spaced (panel size equals vortex height above surface) with 5 subpanels per panel, Figure 11(a). Again, the oscillation in the basic results about the exact line has been eliminated. Even the cosine spacing case shows a small improvement over the basic solution, Figure 11(b).

To test the scheme further, a 20-panel case was considered, Figure 11(c). Here the panels are equally spaced with a size twice the vortex height (see inset in Figure 11(c)). This represents a very sparse set of control stations where the boundary conditions are applied and we would expect the numerical approximations in the model to be at their worst. Even so, the detail of the calculated vorticity distribution agrees very closely with the exact curve. In this case, seven subpanels per panel were used (i.e., the applied distribution was evaluated at seven points in each panel).

These results are very encouraging since they indicate a simple procedure whereby the sensitivity of panel density (control point locations) in relation to vortex location can be eliminated. To test the procedure out in the more general case, we now proceed to the case of the vortex/airfoil problem.

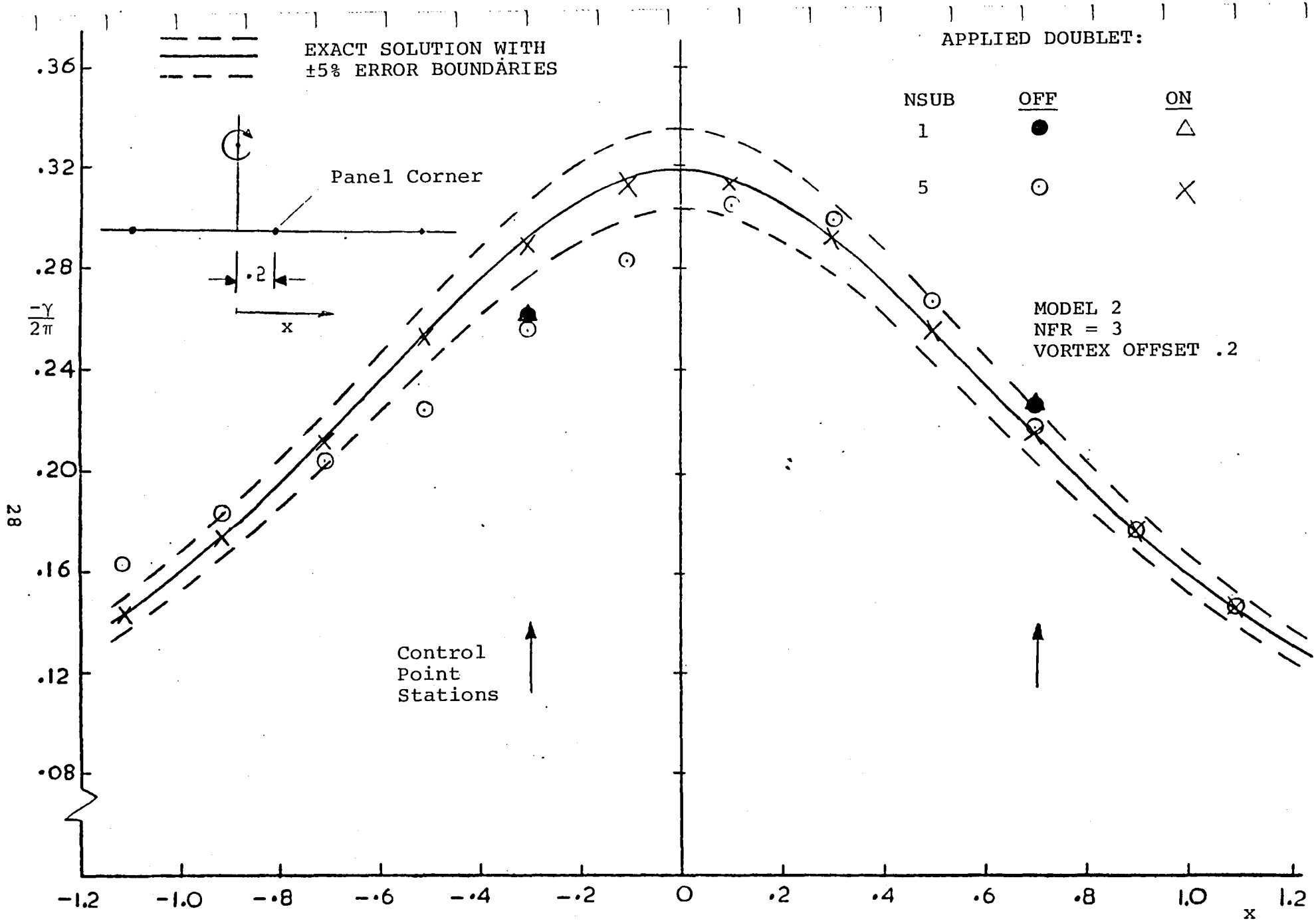

(a) Equal Spacing, 40 Panels.

Figure 11. Vortex/Plane Solution. Effect of Applied Doublet Distribution with Vortex Offset from Panel Edge.

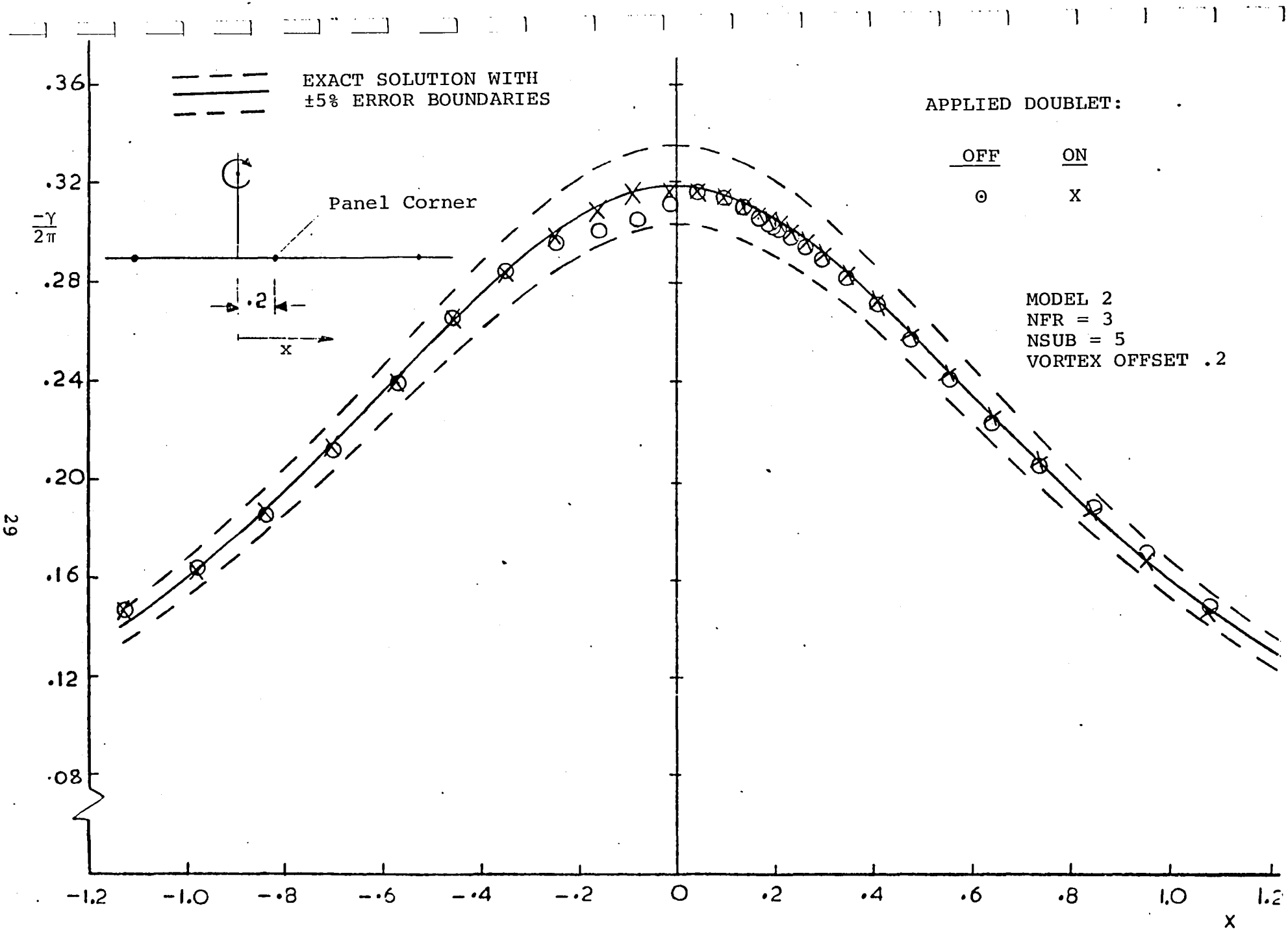

(b) Cosine Spacing; 40 Panels.

Figure 11. Continued.

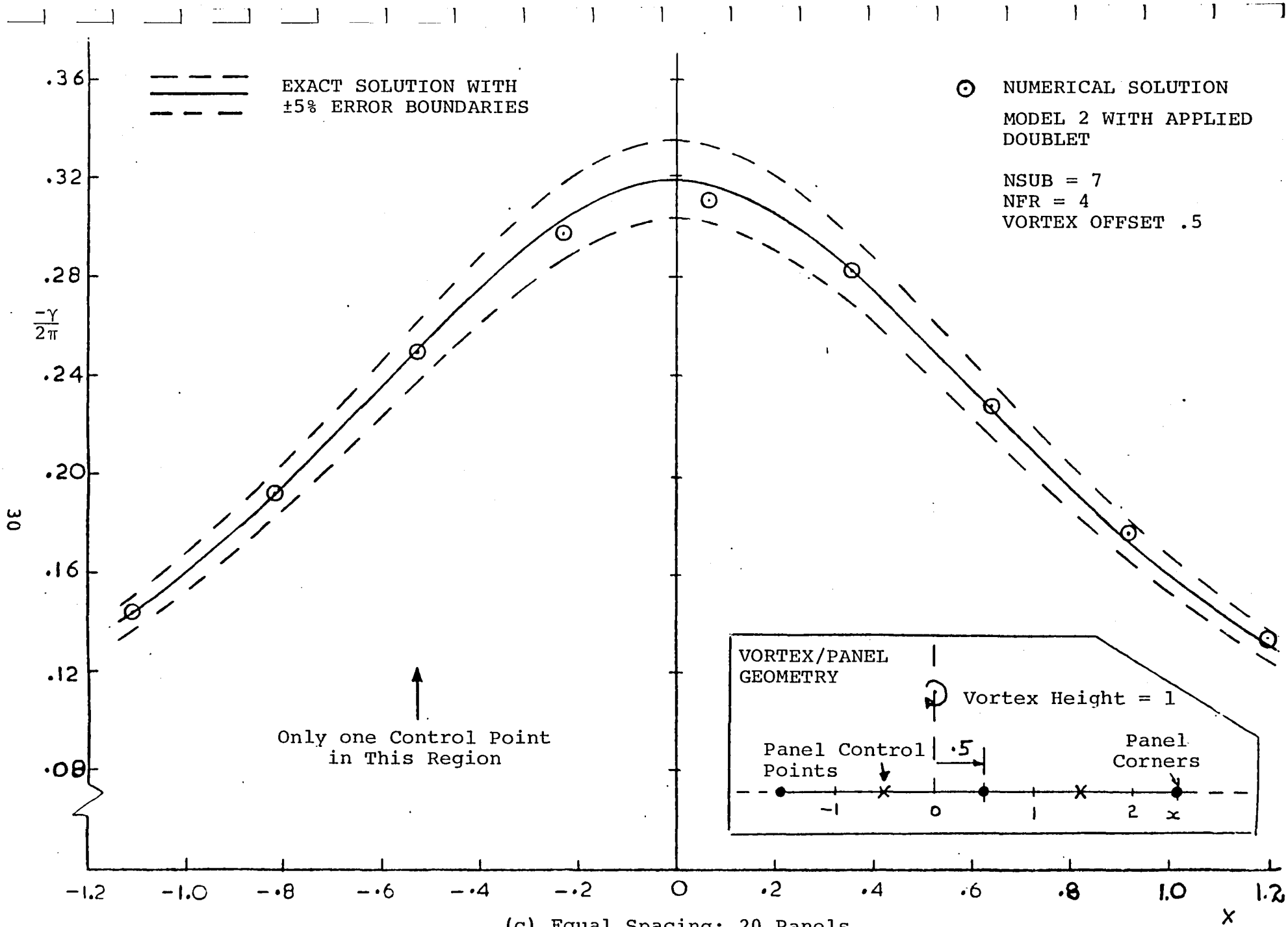

(c) Equal Spacing; 20 Panels.

Figure 11. Concluded.

4.0 VORTEX/AIRFOIL PROBLEM

The results of the previous section are here extended to the case of surface curvature by considering a prescribed vortex standing above an airfoil section. This still excludes the influence of the feeding sheet which is considered later.

4.1 Arrangement of the Flow Model

The applied doublet distribution considered briefly for the vortex/plane problem has to be modified for the general surface. This involves dropping a perpendicular from the vortex onto the airfoil surface to find the projected point and vortex height, h, Figure 12. This also provides the origin for measuring surface distance, s. The applied doublet distribution is then

$$\mu(s) = \frac{\Gamma}{\pi} \tan^{-1}\left(\frac{s}{h}\right)$$

which is evaluated at each subpanel center. This gives the correct behavior on the tangent plane below the vortex and a smooth variation from there to the airfoil trailing edge (upper and lower surfaces). The important feature of the technique is that it removes the vortex-induced steep doublet gradient from the solution part of the distribution.

The basic vortex/airfoil case considered here is based on the CLARK-Y airfoil for which V.J. Rossow of NASA Ames (Ref. 6) provided an exact solution using a transformation technique. The vortex is actually coincident with a sink to stabilize its position. The sink induced velocity is also included in the present calculations.

Detailed surface velocities are calculated here in the neighborhood of the vortex.

4.2 Calculated Results

The general arrangement of the vortex/airfoil case is shown in Figure 13. The vortex location is (-.29364, .17948), and strength, $\frac{\Gamma}{2\pi} = .20009$. The vortex is coincident

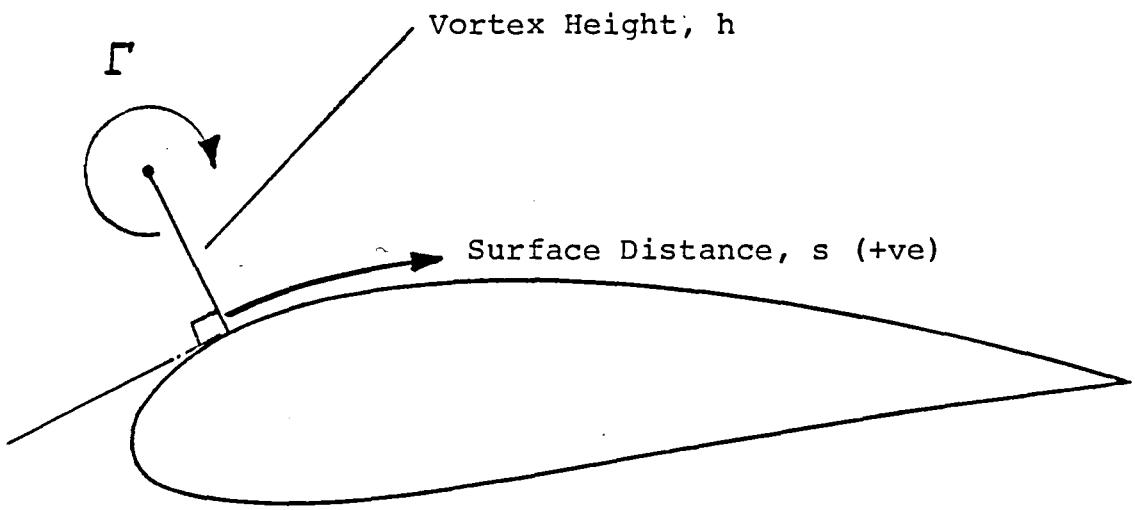

THE APPLIED DOUBLET DISTRIBUTION IS TAKEN AS:

$$\mu(s) = \frac{\Gamma}{\pi} \tan^{-1}\left(\frac{s}{h}\right)$$

Figure 12. Applied Doublet Distribution on the Airfoil. Locating the Vortex.

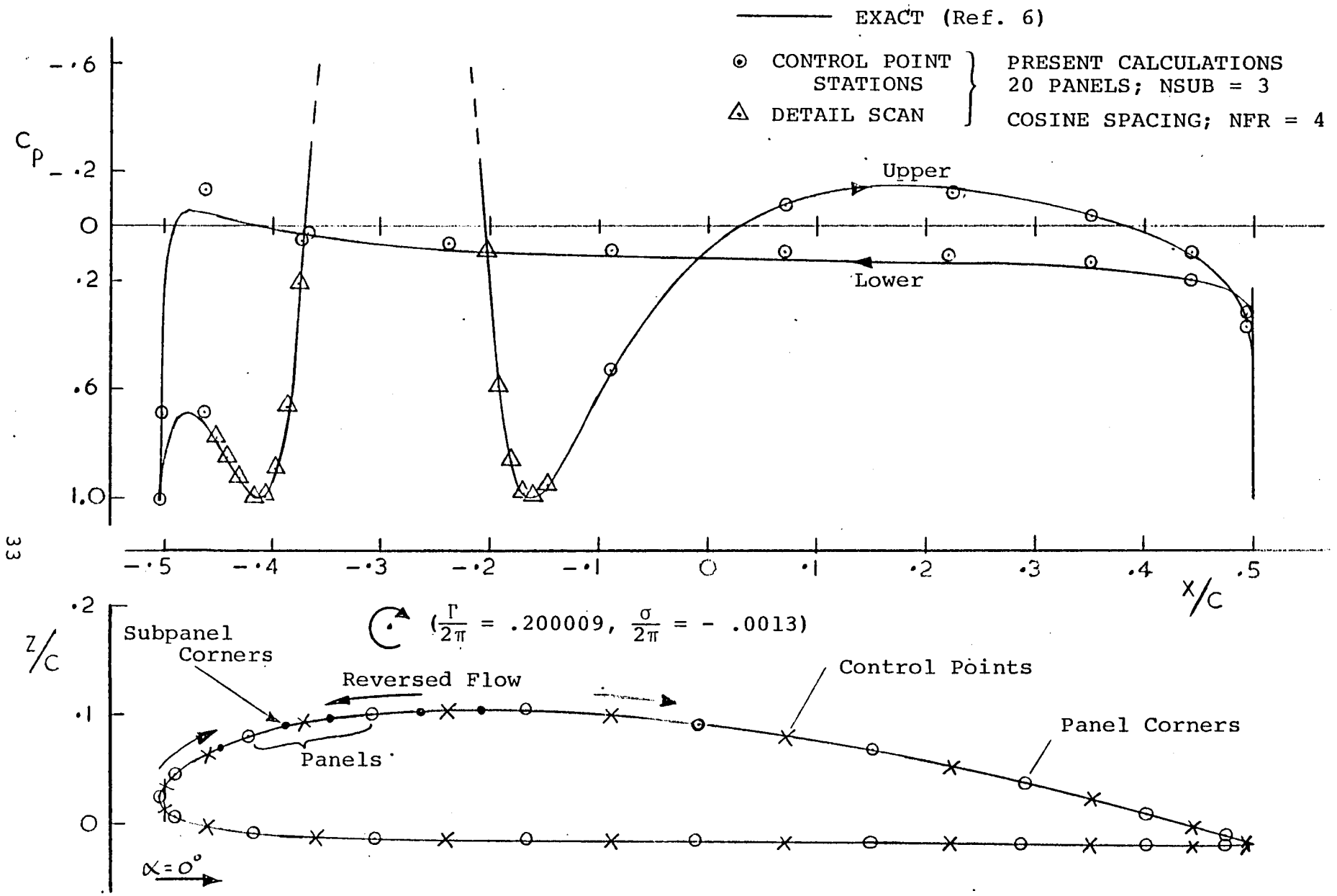

Figure 13. Vortex/Airfoil Case: General Arrangement of Clark-Y Airfoil and Overall Pressure Distribution.

$\frac{\sigma}{2\pi} = -0.00650$

with a source strength, $\frac{\sigma}{2\pi} = -.00130$.

Included in Figure 13 is a comparison of the exact and calculated overall pressure distributions (excluding the peak suction solution which is the feature of the subsequent figures). The present calculations used 20 panels with cosine spacing on the upper and lower surfaces giving increased panel density at the leading and trailing edges, Figure 13. Each panel has 3 subpanels: these are accessed when a velocity calculation point is within 4 panel lengths of the panel center (i.e., NFR = 4). The local panel length/vortex height ratio, λ, is 1.82, which is on the large side (based on the vortex/plane results). Even so, the overall pressure distribution is in good visual agreement with the exact curve, Figure 13. As we shall see below, the subpanel model has a significant effect on the accuracy of this calculation, particularly with so few basic panels. Further, the subpanel model makes it possible to make arbitrary pressure scan lines close to the surface; e.g., a detailed pressure scan initiated in the vicinity of the peak suction provided additional points which give excellent definition of the stagnation regions at the ends of the reversed flow region.

4.2.1 Effect of the Applied Doublet Distribution

The detail of the peak suction region under the vortex is shown in Figure 14 for the 20-panel case. Included are the results with the applied doublet distribution switched off. The applied doublet technique clearly provides a significant improvement in accuracy: without it, the peak suction is not only less accurate, but its location is shifted. (Note: we shall see later (Figure 16) that use of a higher subpanel density with the applied doublet techniques gives even better accuracy).

Figure 15(a) shows the components of the surface doublet distribution. The applied distribution is now in two parts: the symmetrical** part is obtained from a

---

** The symmetrical part of the doublet distribution refers to the component that is the same at corresponding upper and lower points on the surface. This component is associated with the displacement effect of the airfoil, whereas the antisymmetric component is associated with the circulation. The symmetrical component is applied here to remove the "trailing-edge" problem that arises when the Neumann boundary condition is applied to the surface doublet (or vorticity) model--it can be shown that the solution for the symmetrical doublet component suffers ill-conditioning when the upper and lower surfaces came together. Application of the symmetric component is not necessary when the interior Dirichlet boundary condition is used (Section 6.0).

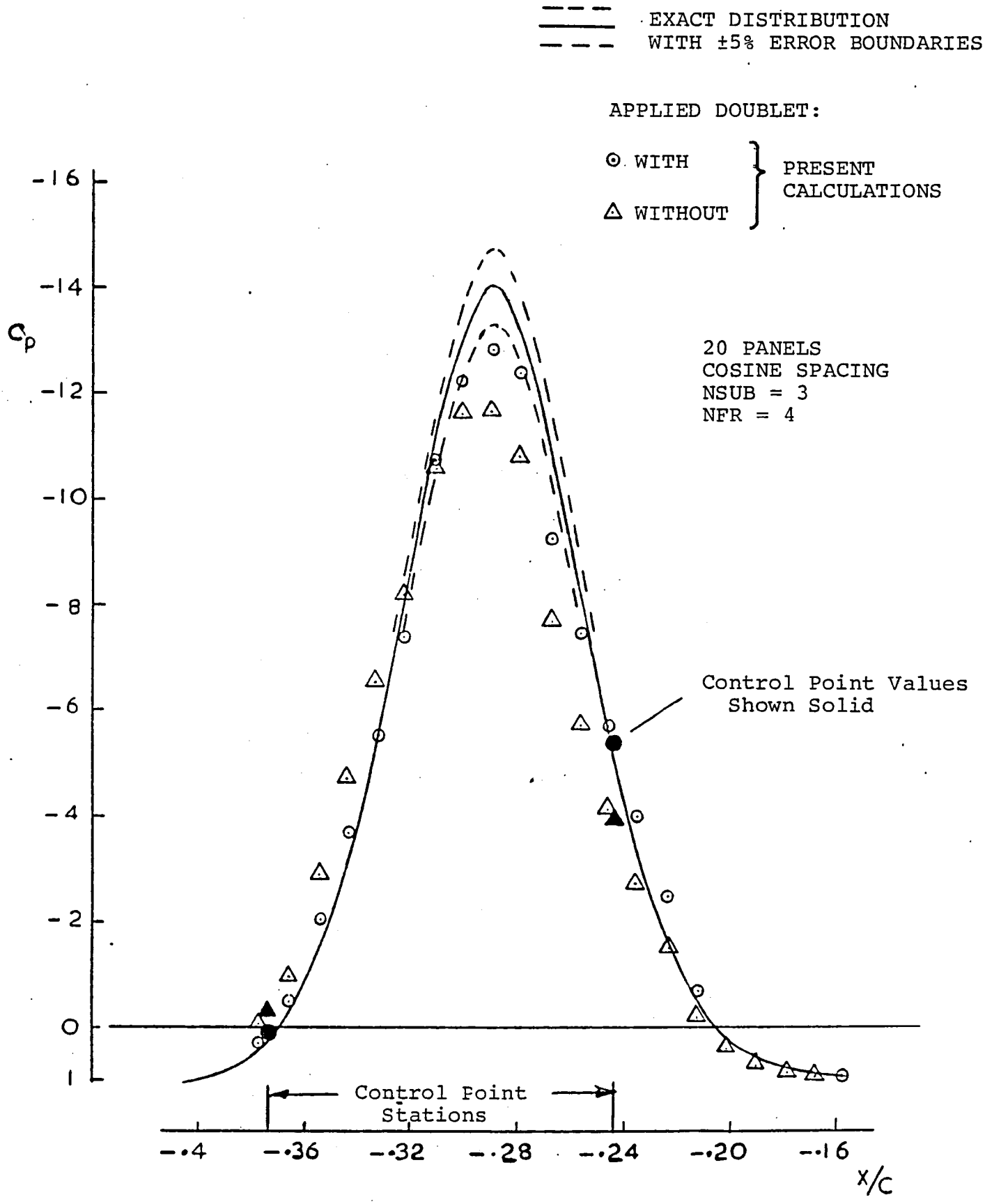

Figure 14. Vortex/Airfoil Case: Effect of Applied Doublet on Peak Suction Region.

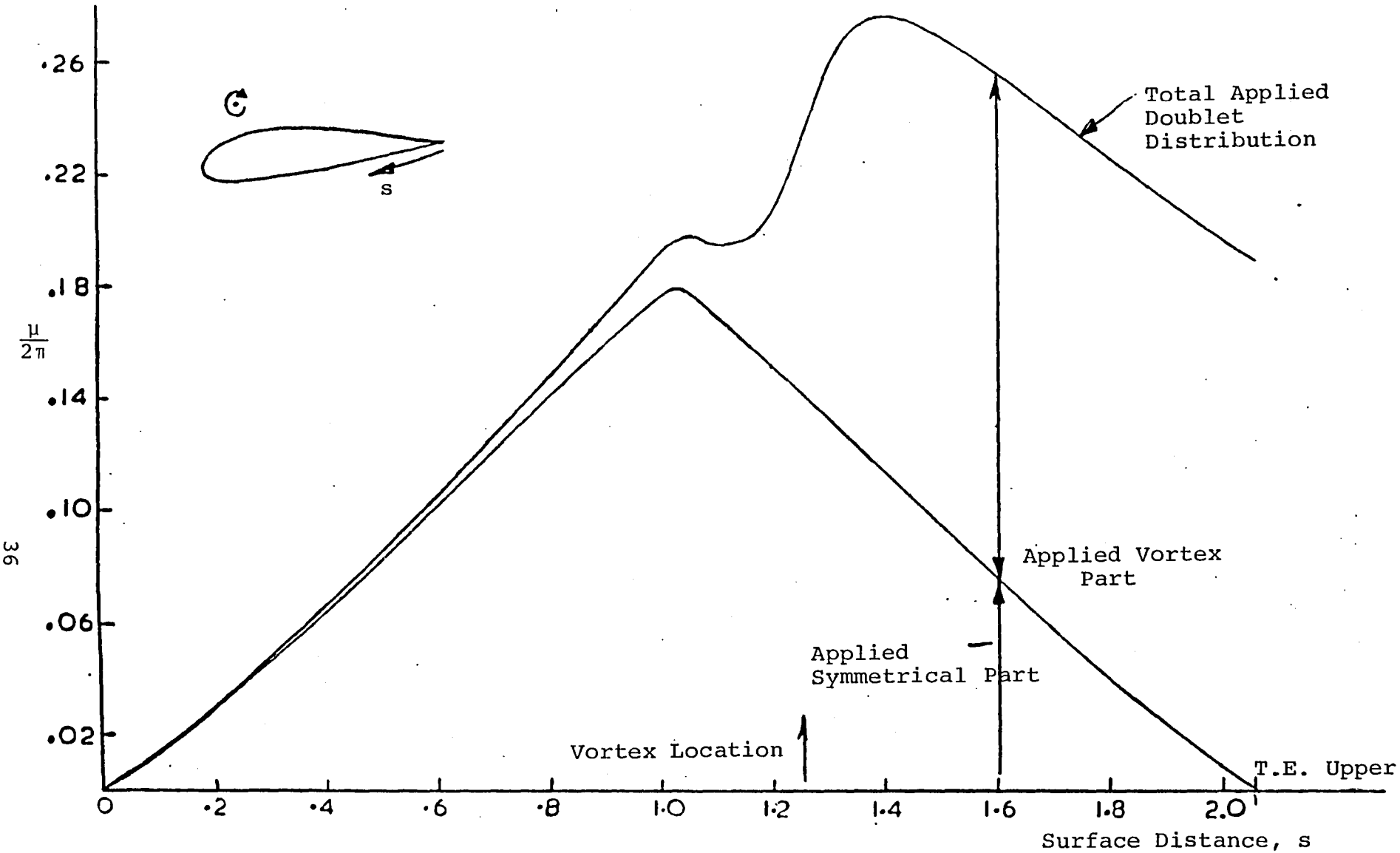

(a) Applied Doublet Distribution.

Figure 15. Vortex/Airfoil Case.

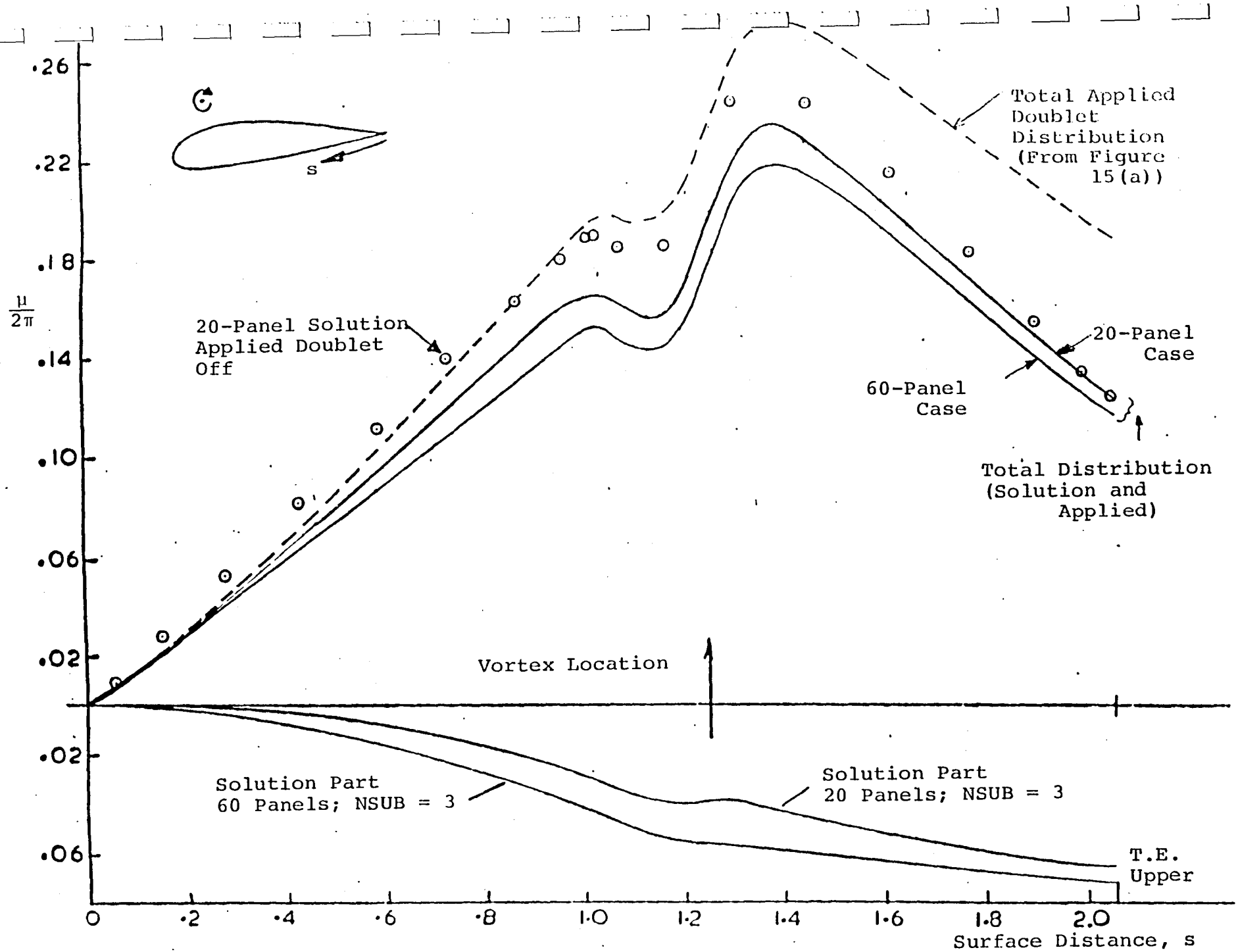

(b) Total Surface Doublet Distribution for Two Panel Densities.

Figure 15. Concluded.

symmetrical Karman-Trefftz section at zero angle of attack and having the same trailing-edge angle and cross section area as the Clark-Y. To this is added the $\tan^{-1}$ distribution due to the vortex, giving the top curve in Figure 15(a). This is evaluated at each subpanel center and the resulting induced velocities are added to the onset flow. The solved part of the distribution (lower part of Figure 15(b)) is then quite small in value, and has a smooth variation which offers little problem to the biquadratic interpolation fit when evaluating local subpanel influences (particularly when using a reasonable panel density--20 is considered too sparse in general). We could reduce the magnitude of this solution part even further by placing the Karman-Trefftz section at the appropriate angle of attack, thereby including the majority of the circulation part (i.e., antisymmetric component) of the doublet distribution with the symmetrical part. In the present case, since the onset flow is non-uniform due to the presence of the vortex, the appropriate angle of attack could be evaluated at the 3/4 chord point on the airfoil (this would be a negative angle in the present case).

The effect of switching off the applied doublet is also shown in Figure 15 (b) for the 20-panel case. In the attempt to represent the "double bump" feature of the distribution, the solution wanders significantly from the earlier solution producing the pressure errors seen in Figure 14.

4.2.2 Effect of Panel Density

Figure 16 shows the peak suction detail for 20, 40 and 60 panels. The local panel length/vortex height ratios, λ, are, respectively, 1.82, .93 and .63. In each case, a density of 3 subpanels per panel was used within a near-field radius of 4 panel lengths. A few pressure values taken from detailed pressure scans augment the control point information at the peak. We observe a significant improvement in accuracy going from 20 to 40 panels; λ decreases from 1.82 to .93, and the peak error decreases from 8.5% to 2.5%. Going to 60 panels (λ = .63) essentially eliminates the peak error, but there are still minor errors away from the peak, possibly resulting from small oscillations from the biquadratic interpolation fit to the solution part of the doublet distribution.

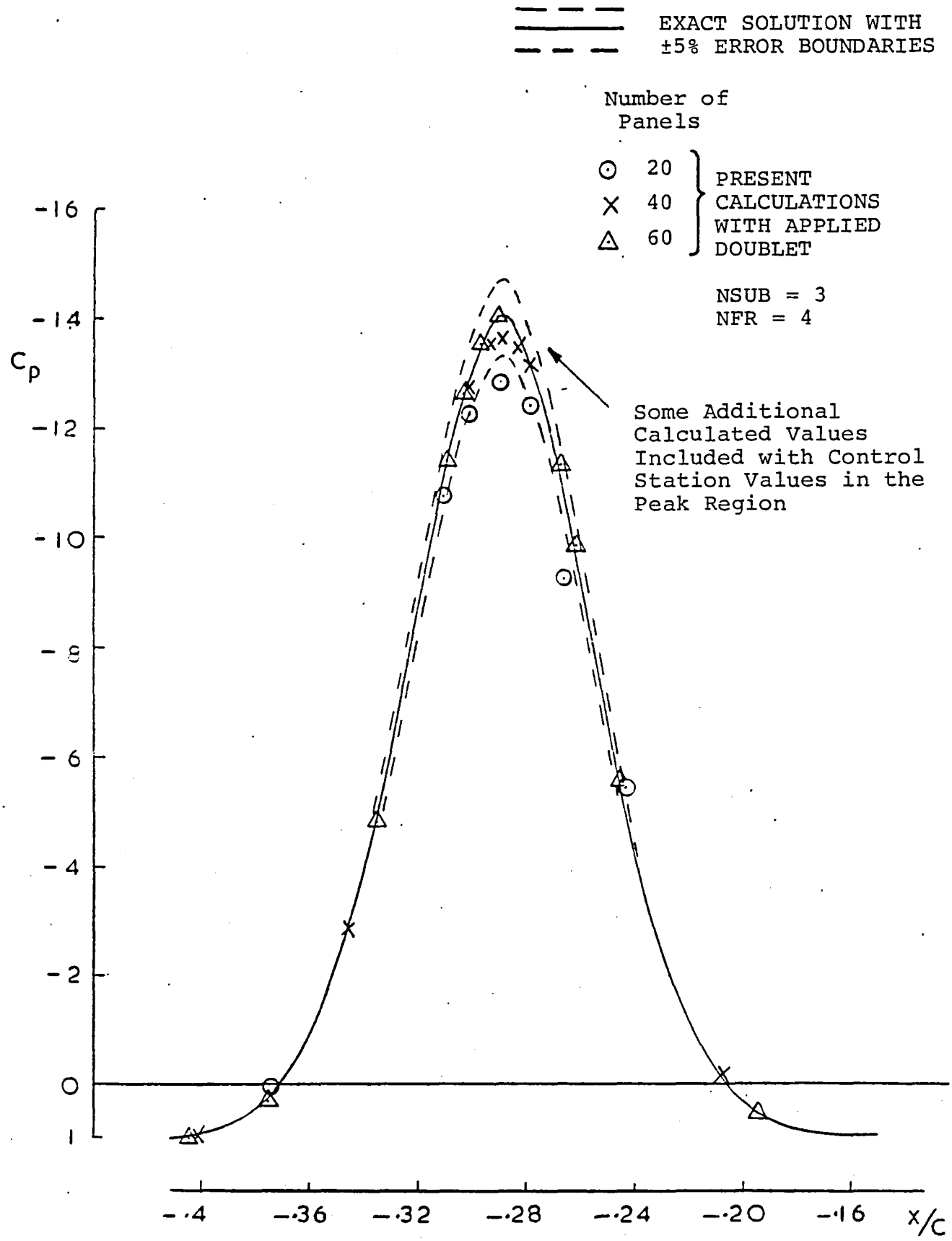

Figure 16. Vortex/Airfoil Case: Effect of Panel Density on Peak Suction Region.

4.2.3 Effect of Subpanel Density

Figure 17 shows the effect of number of subpanels per panel for the 40-panel case. The near-field radius factor is 4.0. The scale of the plot has been expanded further so we are now looking at just the top part of the suction peak. With one subpanel per panel, i.e., the basic paneling only, the peak error is of the order 20%, and the peak location is shifted relative to the exact curve. As noted in the vortex/plane case, the applied doublet distribution does not benefit the solution unless combined with subpanels. The use of 3 subpanels per panel reduces the peak error to 2.5% (as we saw in Figure 16). Increasing the subpanel density further to 5 and 7 reduces the error, but the convergence path with number of subpanels appears to be heading for a small overprediction (~ 1% error).

The near-field velocity calculator is evidently working well, judging from the smoothness of the calculated distribution in Figure 17. There is only one control station in this interval--the rest of the values are from velocity calculations at arbitrary points.

4.2.4 Effect of Near-Field Radius

The calculations so far have accessed the local subpanels for calculations within 4 panel lengths of each panel. Cases were also run for the 40-panel case using near-field radius factors of 3 and 5, but no plottable difference was observed. (In the vortex/plane case, a near-field radius factor of 2 was examined, and this gave only a minor loss in accuracy. However, such a small radius is not recommended in practical cases.)

4.2.5 Effect of Panel Arrangement

The peak suction detail shown in Figure 18 is for a case with 18 panels arranged in 3 regions as shown. The node point ending region 2 was selected close to the vortex location. No attempt was made to match panel densitites from region to region--as a result there is a relatively large panel size ratio (4.2) at the leading edge. The extremely sparse paneling on the lower surface has been offset by specifying 7 subpanels per panel there. The other two regions were given 3 subpanels per panel. The detailed pressure scan shown in Figure 18 shows very close visual agreement with the exact solution--a significant improvement over the basic 20-panel

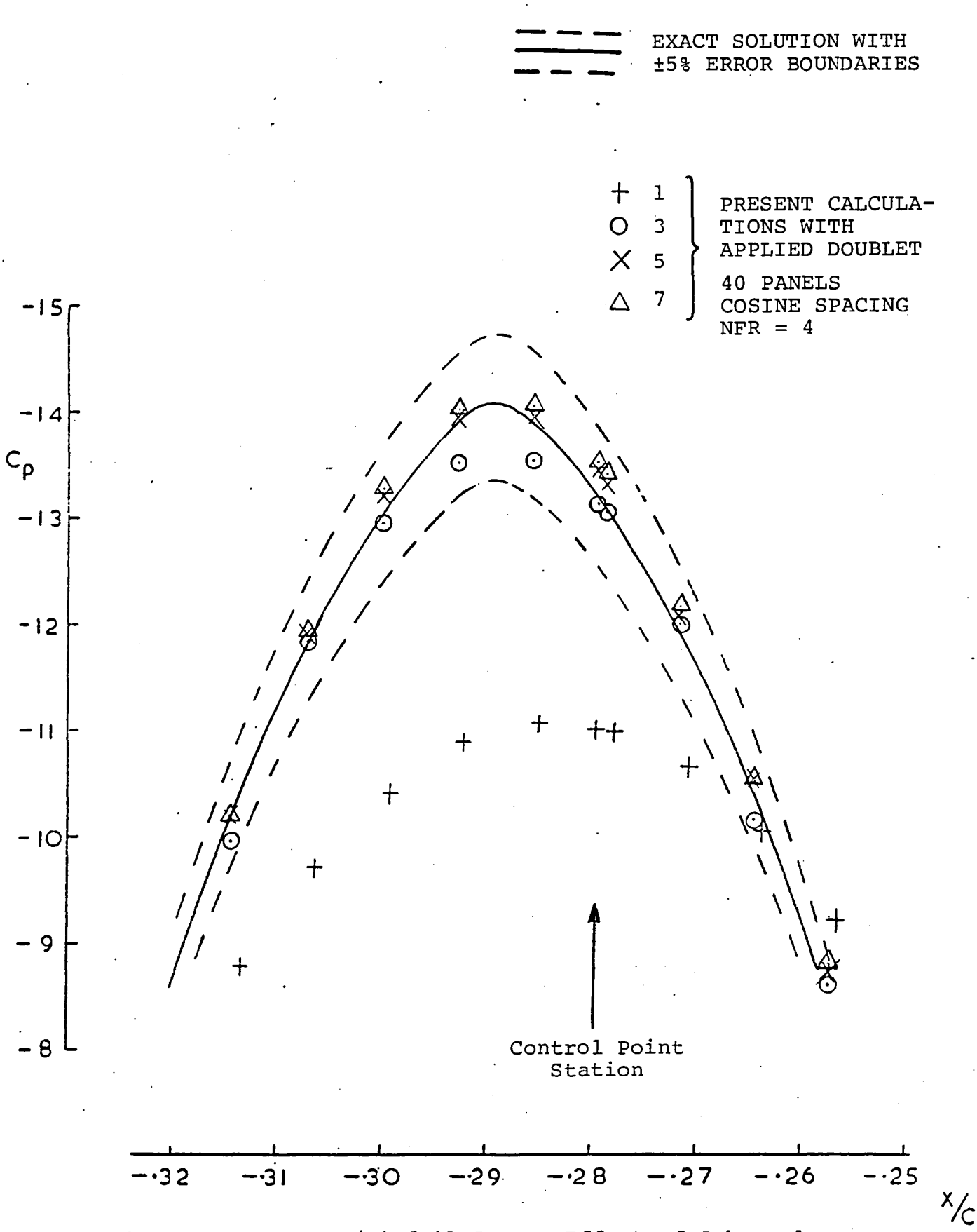

Figure 17. Vortex/Airfoil Case: Effect of Subpanel Density on Peak Suction Region.

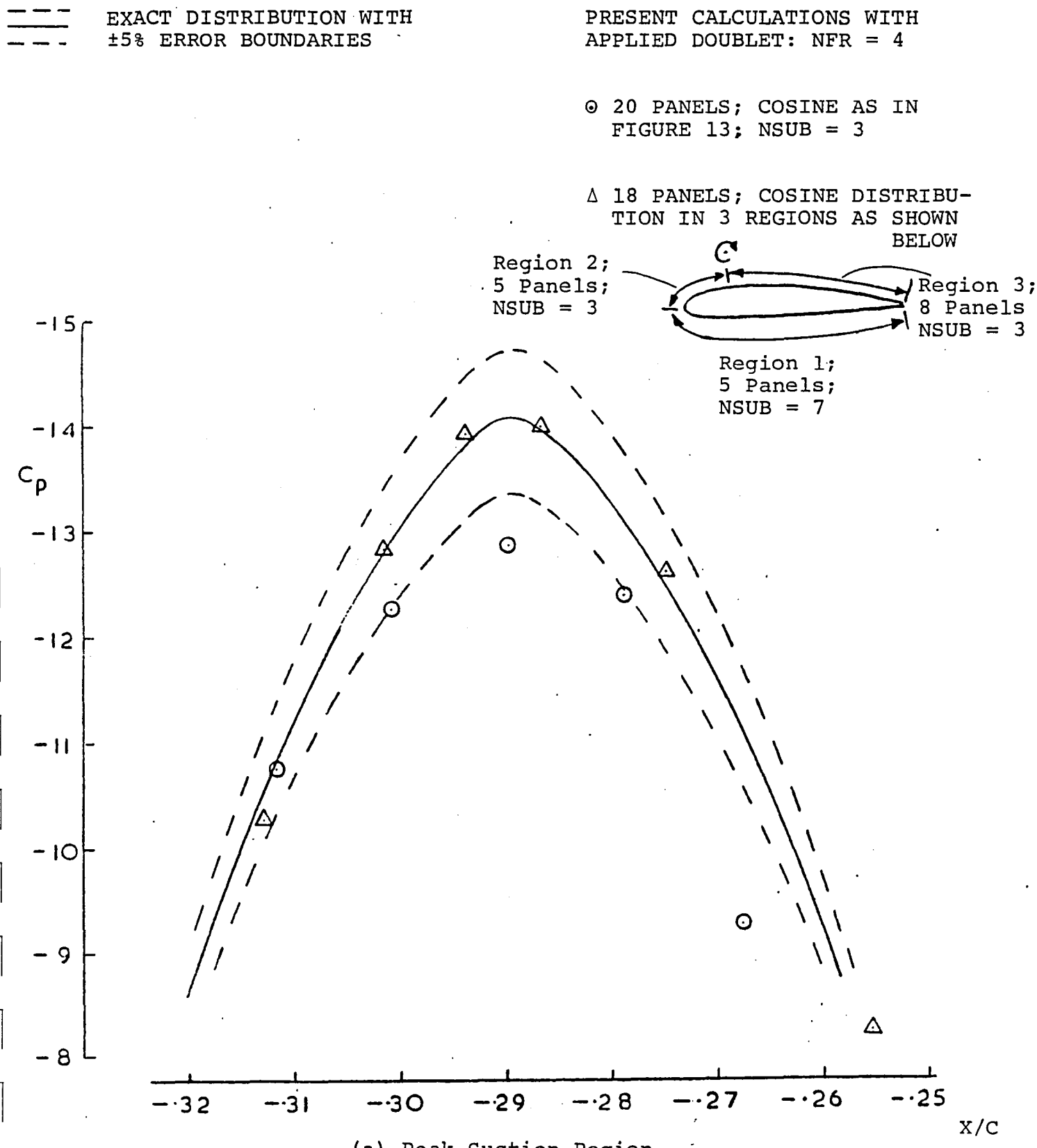

(a) Peak Suction Region.

Figure 18. Vortex/Airfoil Case: Effect of Panel Arrangement.

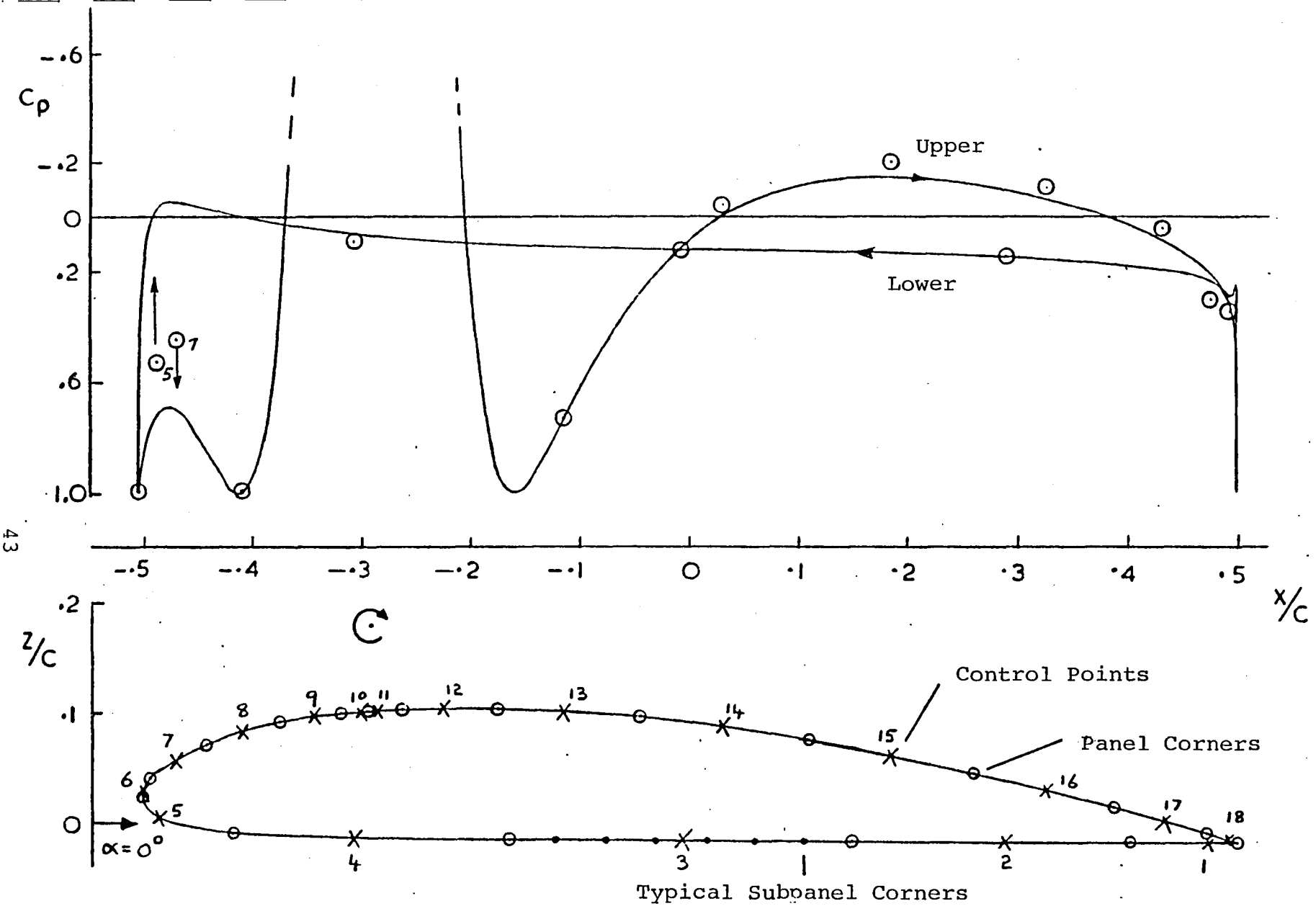

(b) Pressure Distribution Excluding Peak Region.

Figure 18. Concluded.

case and certainly comparable with the 40- (with 5 subpanels) and 60-panel cases. The new case has a local panel length/ vortex height ratio of .4.

The second part of Figure 18 shows the general paneling arrangement and the overall pressure distribution excluding the peak suction. The agreement with the exact pressure distribution is remarkable in view of the very sparse paneling, the obvious mismatching of panels (particularly between upper and lower surfaces near the trailing edge), and the large panel length ratio at the leading edge. The latter has evidently caused the two bad points on panels 5 and 7. The fact that this mismatch has occurred at the high curvature of the leading edge will have contributed to that problem. This situation will not occur in practice when using reasonable panel densitites.

This case demonstrates the flexibility of the procedure in allowing detailed examination of one part of the surface while leaving the rest of the surface sparsely paneled. (of course, one would not be able to make full use of this if, say, the approximate vortex location was not known a priori.)

4.3 Remarks on the Subpanel Technique Usage

From the parametric studies so far, we can assemble the following guidelines for applying the subpanel technique to vortex/surface problems.

Panel Density

The local panel-length/vortex-height ratio should be kept below unity. If the vortex location is known at the beginning, then a local region can be defined with suitable panel density without seriously affecting panel densities on the rest of the airfoil. (Normally, a minimum of 30 panels should be used on an airfoil when dealing with large suction peaks on the high curvature at the leading edge.) If the vortex location is not known a priori, then a suitably dense paneling should be used and the vortex height ratio checked after the solution. Repeat the case using a higher density if necessary.

Subpanel Density

Normally, a subpanel density of 3 per panel appears adequate. However, if low panel density is used, an increased subpanel density should be considered.

For example in the present cases, a 40-panel/5-subpanel case offers slightly better surface definition than a 60-panel/3-subpanel case, and gives essentially the same quality solution for 15% less computing time.

Near-Field Radius

Near-field radius factors should not normally go below 3 unless the panel density is especially uniform and the local surface geometry is flat.

5.0 VORTEX SEPARATION FROM THE EDGE OF A FLAT PLATE

In this section the case of vortex separation from the edge of a flat plate is considered. The plate is moved impulsively from rest in a direction normal to itself and the growth of the vortex structure is followed over a number of small time steps. This extends the Section 3.0 calculations to the case of a feeding sheet with a simple shedding situation (i.e., sharp edge) and leads to the more general problem (Section 6.0) of shedding from a smooth surface.

5.1 Arrangement of the Flow Model

Figure 19 shows the layout of the problem. A flat plate of span 2a is placed on the y-axis with center at the origin and with z-axis vertical. A uniform onset flow, W_∞, is placed normal to the plate. The boundary condition of zero flow across the plate is enforced together with a Kutta condition of zero force carried by the edges.

The panel models considered in Section 3.0 are used here. The models are assembled using the symmetry condition; i.e., only one-half of the plate is paneled, but the image panel and image vortex contributions are included.

Figure 20 shows the layout of the model using N panels on the plate semispan. The boundary condition equation applied to the N control points are solved to give the N doublet values in the presence of the onset flow. At the start of the calculation, the onset flow is the uniform vertical velocity, W_∞. Subsequently, the separated vortex system (and its image) contribute a non-uniform component to the onset flow.

When a doublet solution is obtained, the doublet value, μ_N, on the tip panel causes an edge force because of the finite vortex strength at the edge, Figure 21(a). That doublet value is, therefore, allowed to go free on a new panel, the end of which is obtained by moving a point at the tip distance $\underline{V}\delta t$, $\underline{V}$ being the local calculated velocity and δt a small time step. The vortex at the plate edge is thereby cancelled and reappears on the end of the new panel. Figure 21(b). The panel so formed maintains its doublet value for the rest of the calculations, but the locations of its ends are recalculated at each time step as described below.

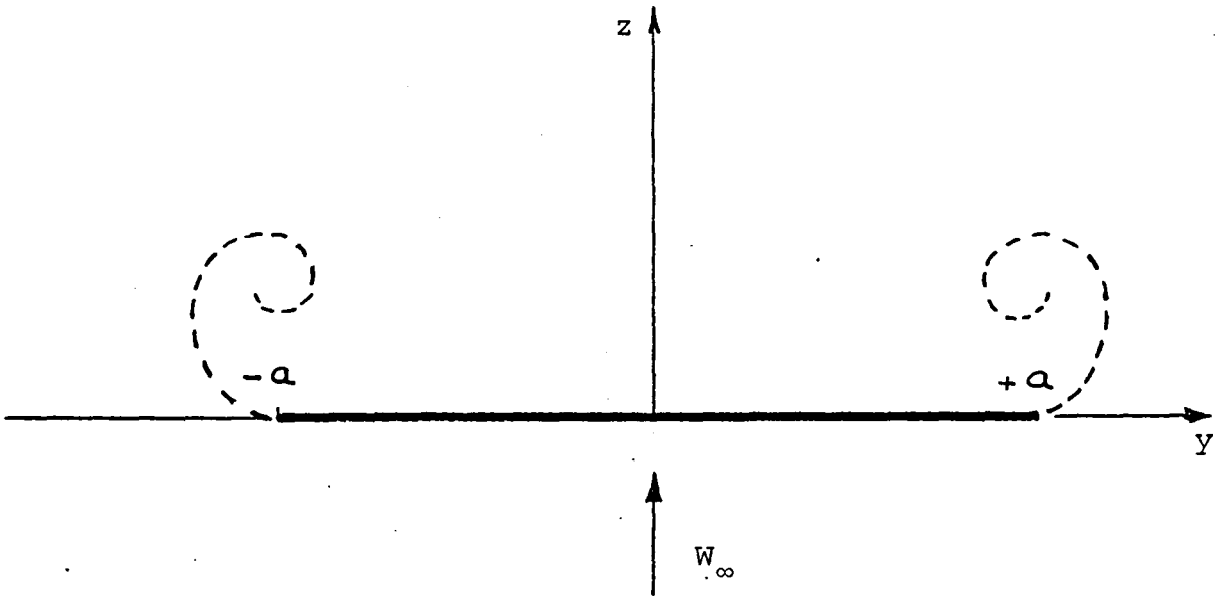

Figure 19. Flat Plate in a Uniform Upwash.

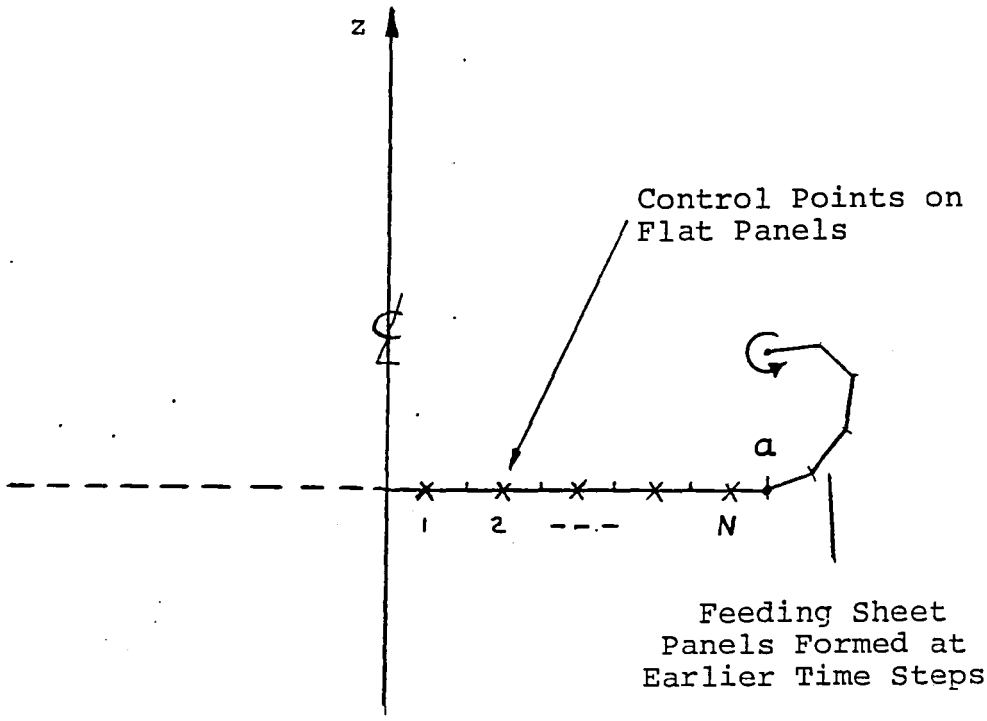

Figure 20. Panel Model for Separation from Flat Plate.

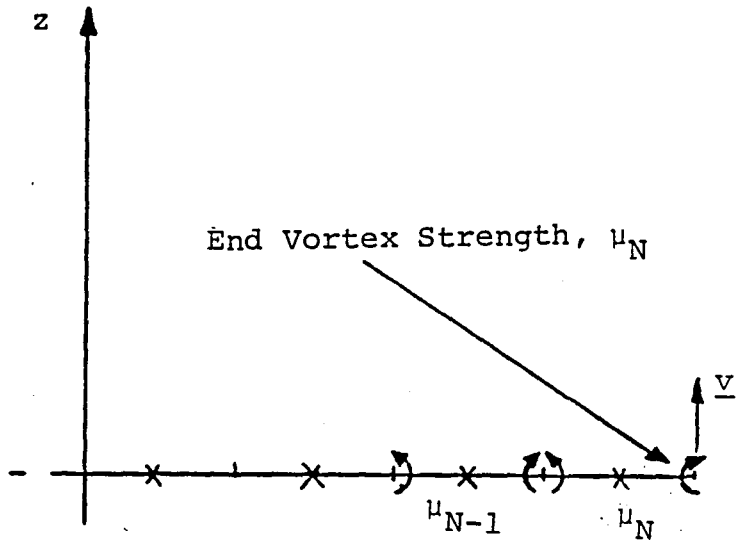

(a) Conditions at Time, t = 0.

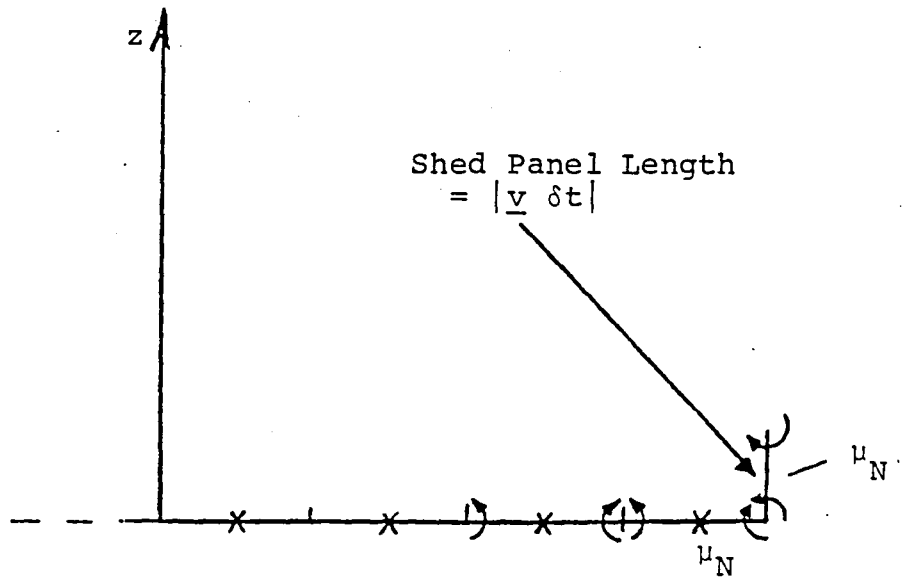

(b) After Time Step, δt.

Figure 21. Shedding Doublet Panels, Separation from Flat Plate.

The location of the feeding sheet is described by a set of panel corner points, $\underline{R}_i$, starting with the flat plate edge. When a doublet solution is obtained at time step, t, the velocity, $\underline{V}_i^t$, is calculated at each point. The points are then moved as follows, assuming constant acceleration:

$$\underline{R}_i^{t+1} = \underline{R}_i^t + (3\underline{V}_i^t - \underline{V}_i^{t-1})\,\delta t/2 + O(\delta t^3)$$

The main requirement of the calculation is for the first turn of the feeding sheet to be represented: thereafter, the detail of the roll-up is probably unimportant as far as surface pressures are concerned. An amalgamation scheme, somewhat similar to that of Moore (7) has been incorporated. This is based on a total angle, θ, through which the roll-up has proceeded (Figure 22). A value of θ_{merge} in the range 2.5π to 3π appears reasonable, but requires further investigation. The effect of θ_{merge} will be considered later in section 6.3. Doublet panels passing beyond θ_{merge} are removed and the last panel edge (i.e., the location of the end vortex) is relocated at the centroid of vortex strength of the amalgamated vortices. In this way, instabilities concerned with calculating the detailed inner roll-up are eliminated.

5.2 Calculated Results

Calculations were performed for MODEL 1 for unit onset flow, W_∞, and unit semispan, a, for the plate. The roll-up of the vortex sheet was followed over a total time, t, of .15. This can be regarded as a dimensionless time, $t^* = W_\infty t/a$, since W_∞ and a are unit values.

Figure 23 shows the shape of the feeding sheet calculated with time step intervals of .01, .005 and .0033. The plate semispan was represented by 10 equal panels and vortex amalgamation was carried out beyond a θ_{merge} value of 3π. A time step of .01 is clearly too large for the basic model: the spacing of the panels is of the same order as the distance between turns of the spiral, and this probably gives rise to distortions. Compared with the other cases, the larger panel size also causes a large difference in the locations of the last panel corner prior to amalgamation, and this will lead to detailed differences in the feeding sheet shape. The time step of .0033 gives such a dense distribution of

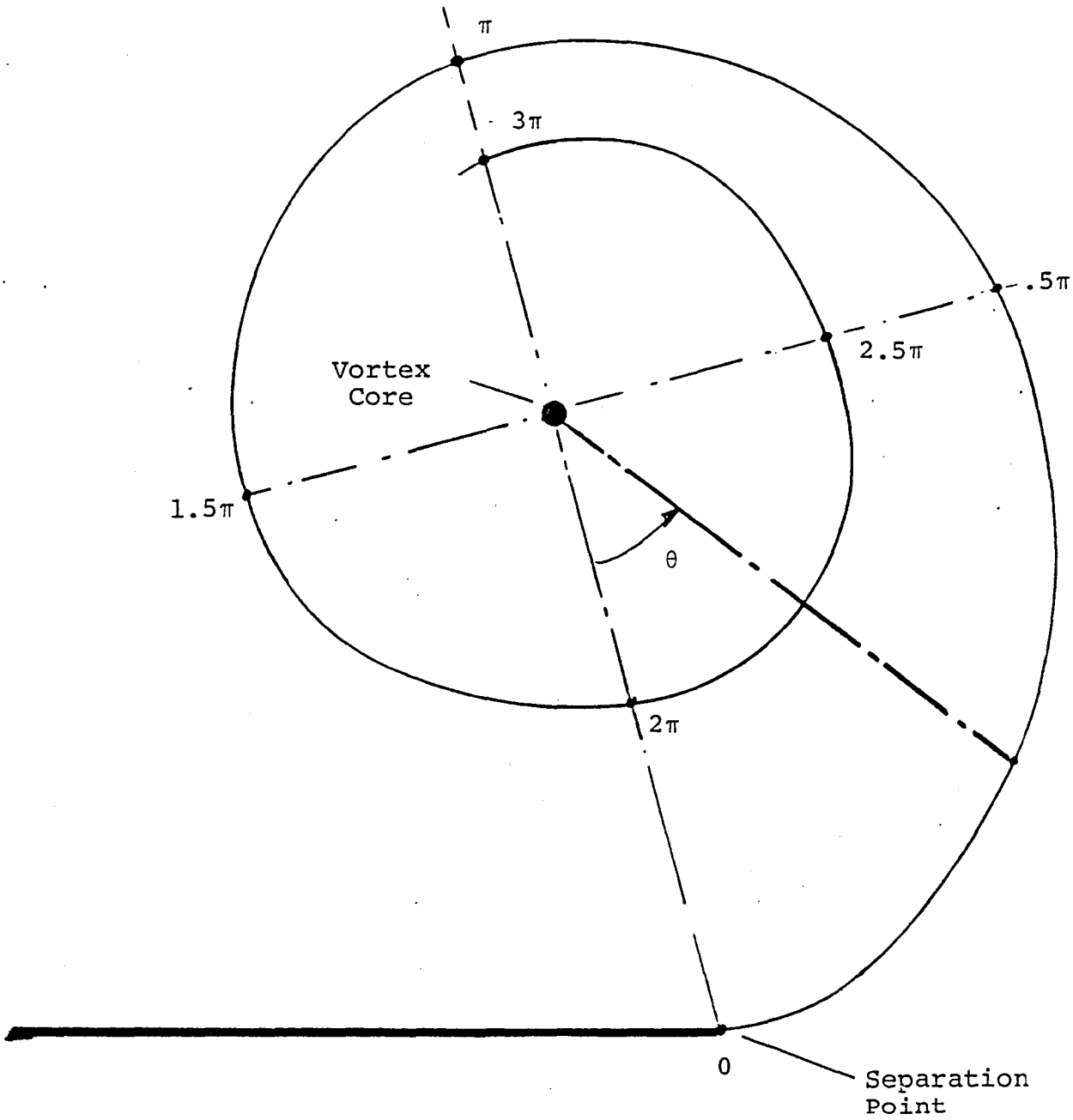

Figure 22. Measurement of Roll-up Angle, θ, for Amalgamation Procedure.

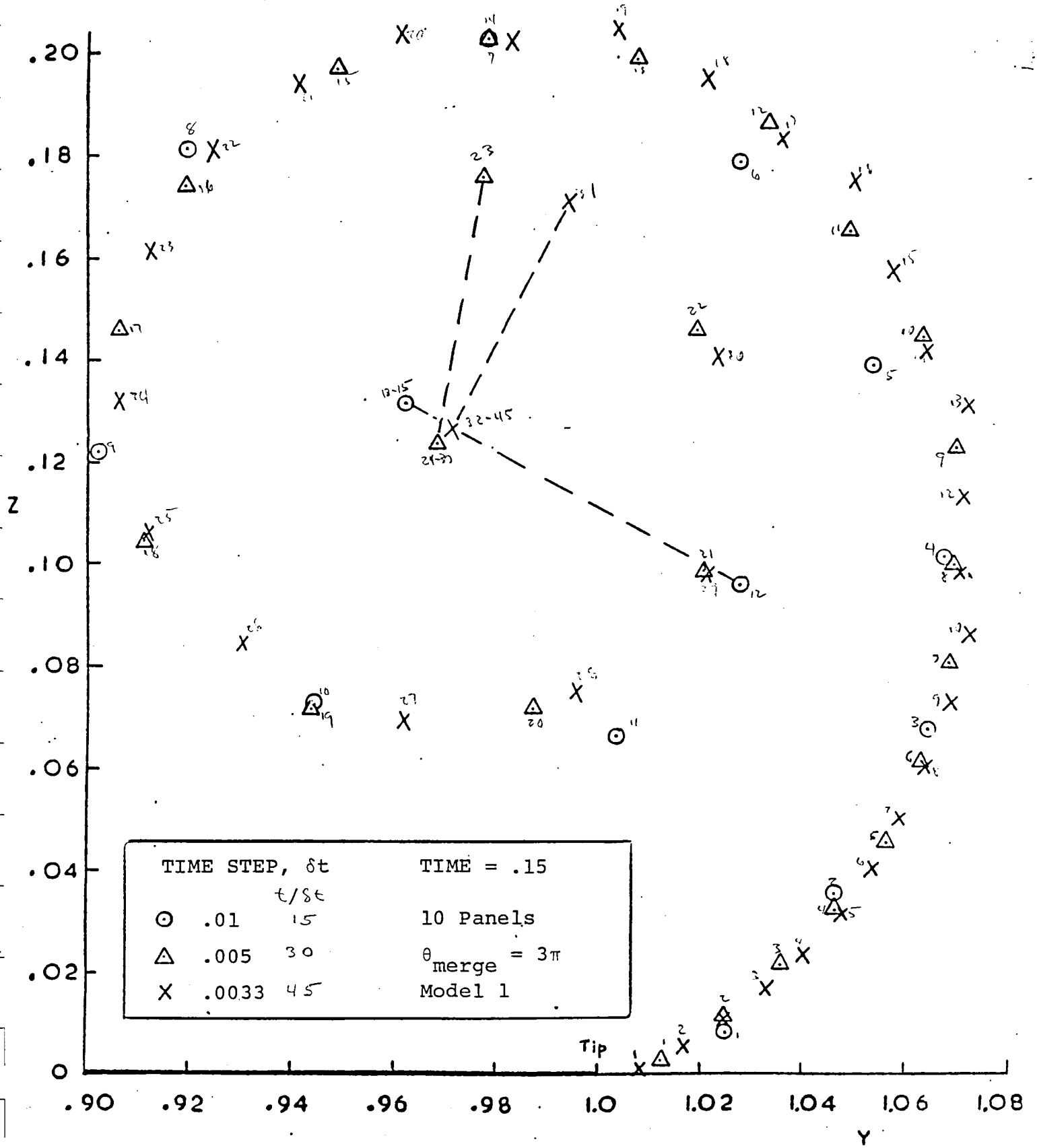

Figure 23. Separation from Flat Plate: Effect of Time-Step Size on Feeding-Sheet Shape.

.0033

panels that numerical instabilities are starting to occur. The .005 time-step case has just the slightest numerical "wobble", but offers a reasonably smooth description of the feeding sheet in relation to the other cases.

The .005 time-step calculation was extended to include the case of 20 and 30 panels on the plate and the resulting feeding sheet shapes are shown in Figure 24. Panel size differences in the inner sheet cause different locations of the last panel corner prior to amalgamation: this probably accounts for small discrepancies in the calculated shape of the feeding sheet. Detail of the inner sheet is affected by panel size on the plate because of early time-step calculations: as the panel density increases, the doublet strength of the leading-edge panel at t = 0 decreases, and, hence, the circulation is more distributed in the early part of the sheet rather than being concentrated in the end vortex. A similar effect occurs with increasing time-step size. As time goes on, these detail differences in the early part of the sheet are collected into the amalgamated vortex core, and the doublet (or circulation) distribution in the feeding sheet becomes less sensitive to changes in the model parameters. For example, the doublet distribution plotted continuously over the plate and feeding sheet is shown in Figure 25(a) for various panel densities and in Figure 25(b) for various time step sizes. Apart from the large time step case, the only differences occur in parts of the feeding sheet shed at early times. The distribution has settled down over essentailly the first 180^0 of roll-up.

The reversal in doublet slope (vorticity) associated with the rolled up vortex acting on the plate is already well established at this time, .15, and can be observed particularly clearly in the vorticity distribution in Figure 26. The vorticity distribution (derived from the doublet distribution in Figure 25(a)) in the feeding sheet has some scatter at this time. This scatter is probably caused by instabilities in the numerical differentiation of the doublet distribution; however, there is a hint of an oscillating vorticity distribution (particularly in the 30-panel case). This would be consistent with an ellipticity in the roll-up spiral due to the presence of the plate. More time should be spent on investigating these characteristics, but unfortunately, the work schedule did not permit this.

Several cases were run for the vortex separation from a flat plate using the linear vorticity subpanel model, MODEL 2. Basic solutions for vorticity, doublet distribution and velocities compared reasonably well with those from MODEL 1. The shapes of the feeding sheet, however, were not in agreement.

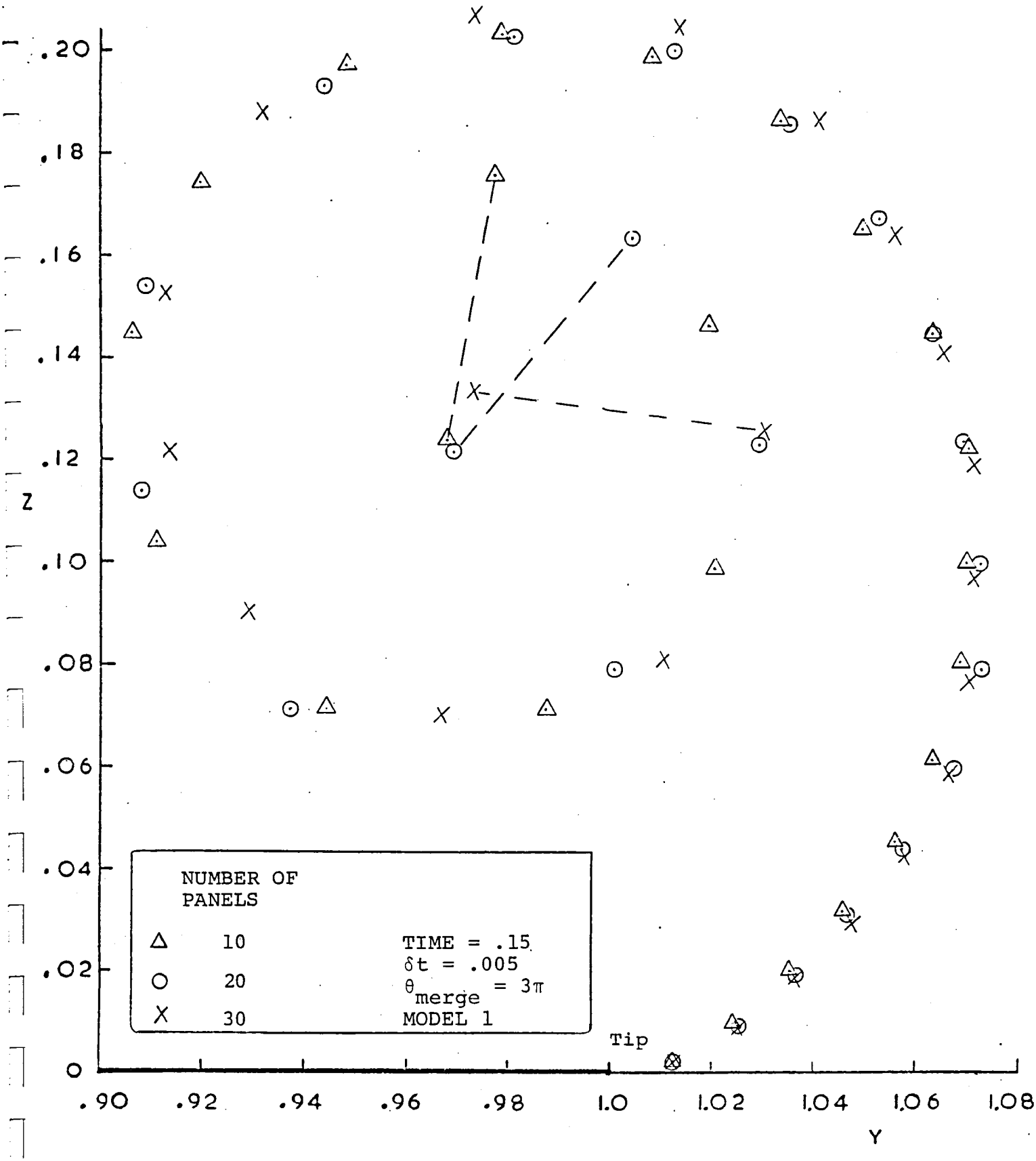

Figure 24. Separation from Flat Plate: Effect of Panel Density on Feeding Sheet Shape.

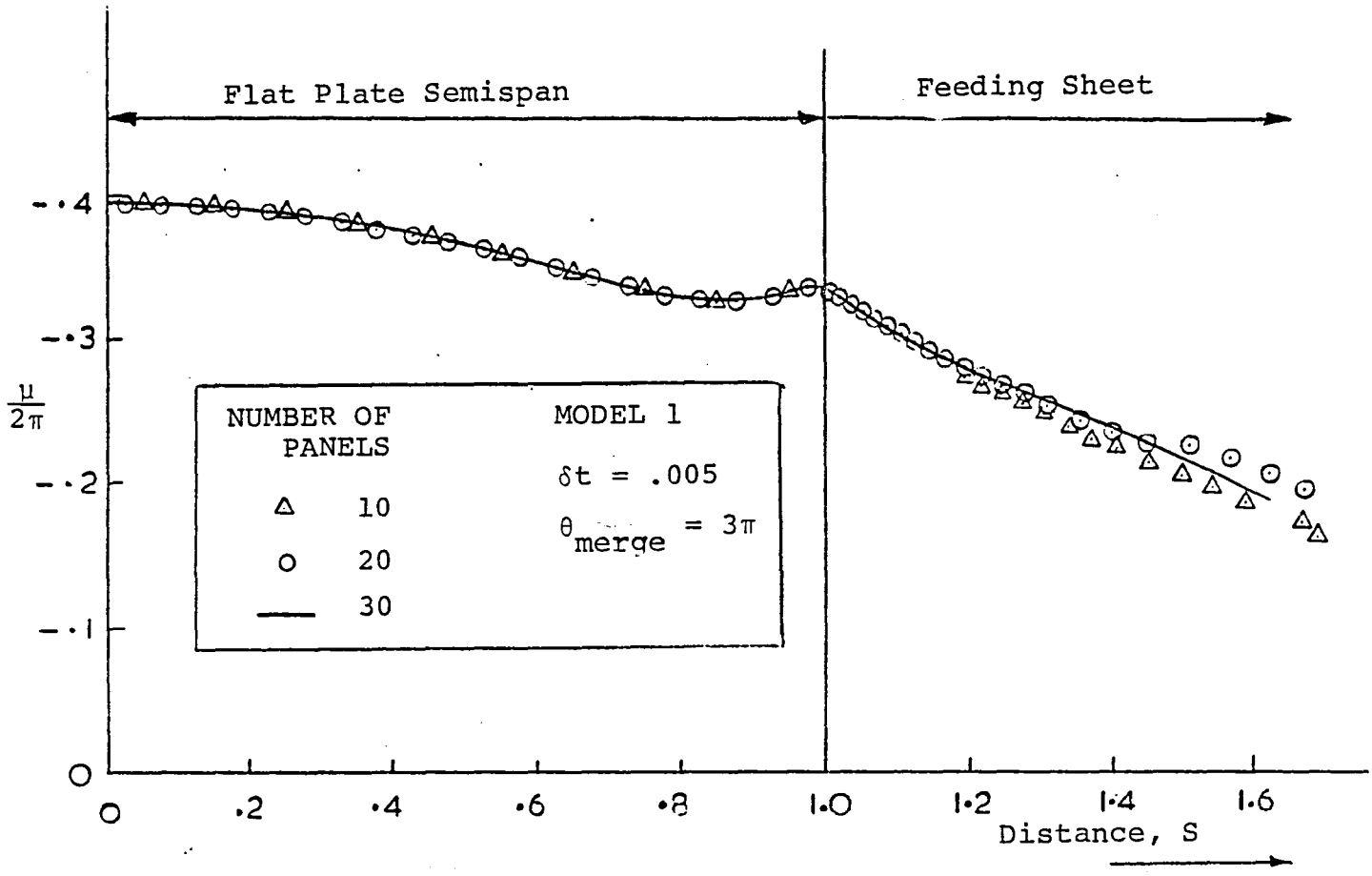

(a) Effect of Panel Density.

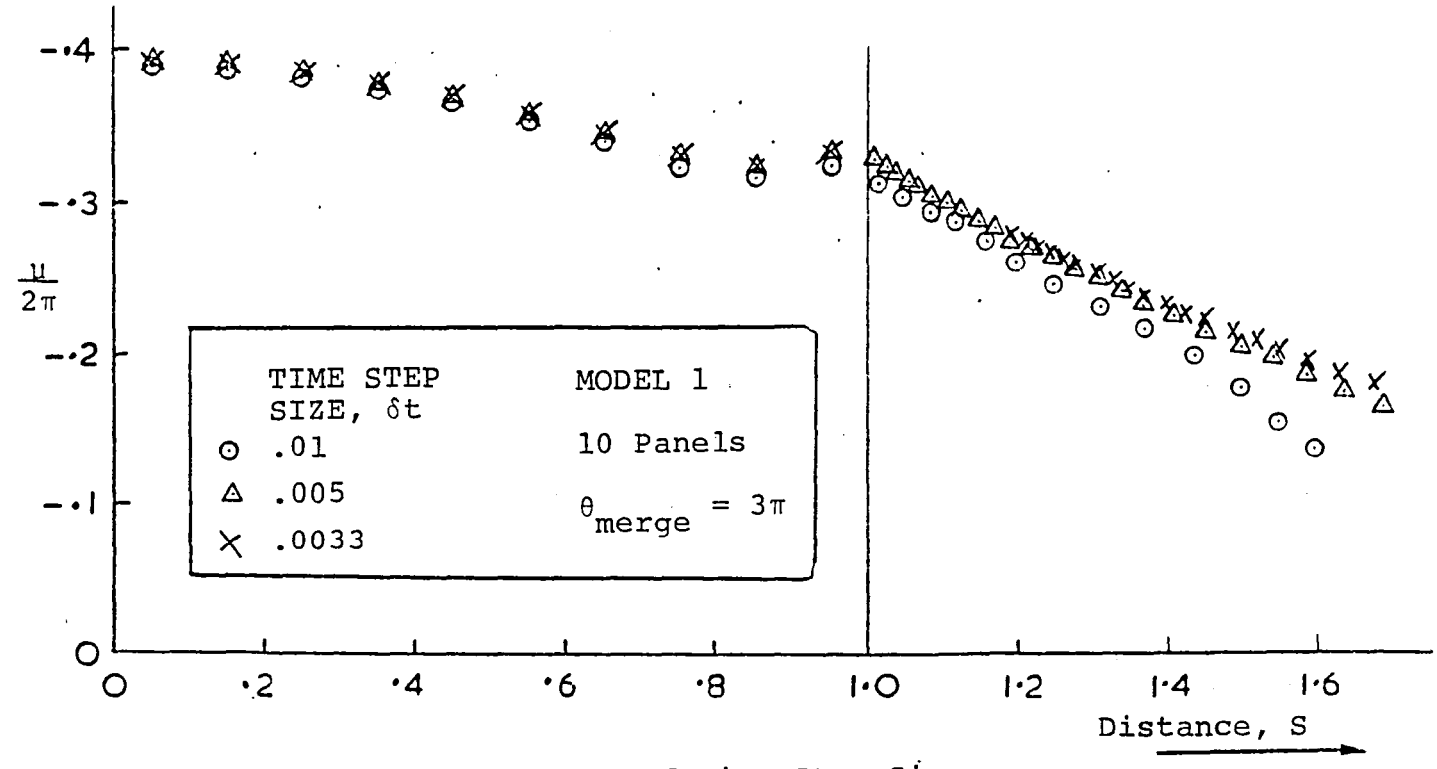

(b) Effect of Time-Step Size.

Figure 25. Separation from Flat Plate: Doublet Distribution at t = .15.

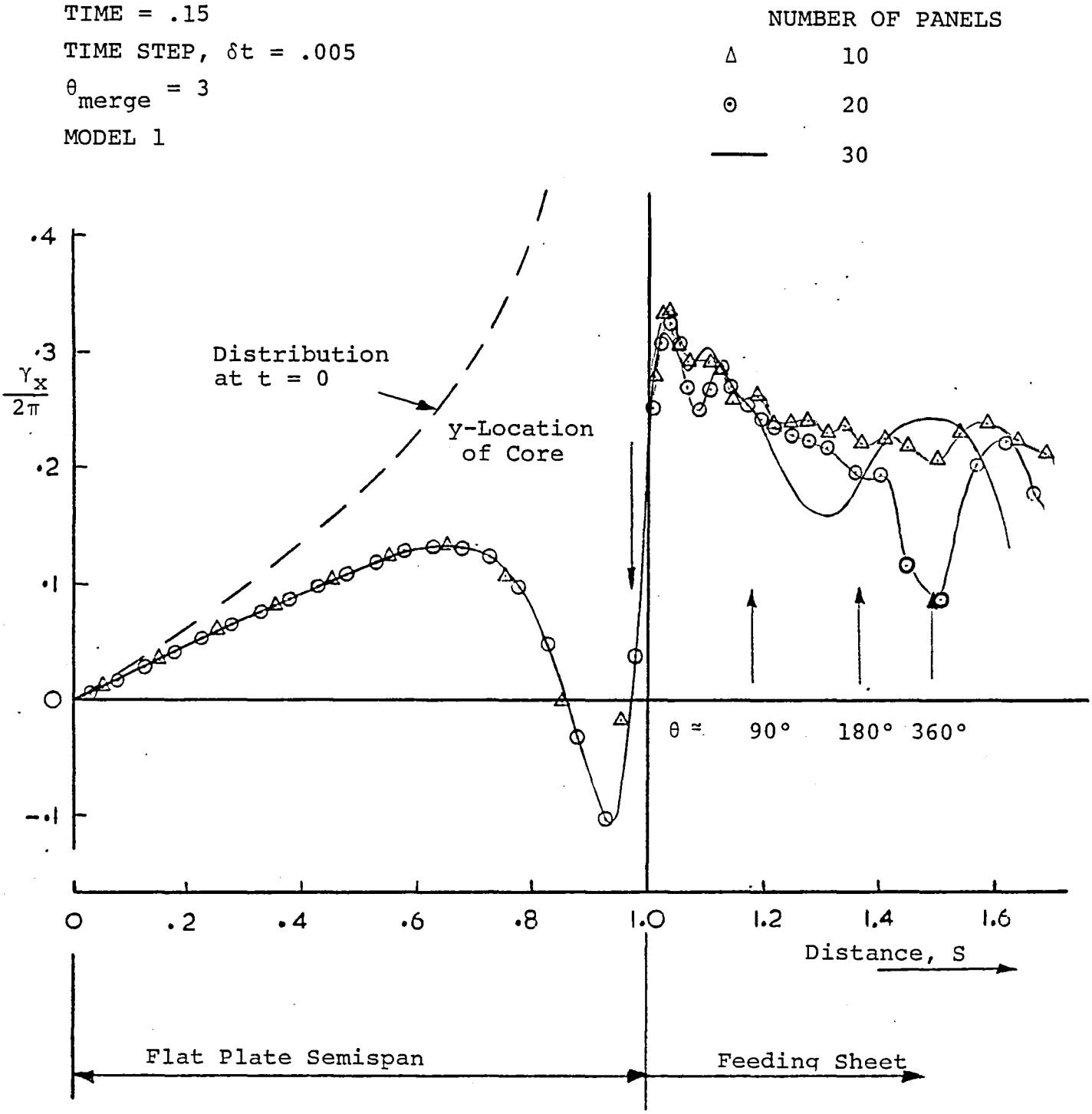

Figure 26. Separation from Flat Plate: Effect of Panel Density on Vorticity Distribution.

Although a number of refinements were applied to the evaluation of vorticity and induced velocities on the feeding sheet, no satisfactory solution to the problem was obtained. As a further test MODEL 2 was assembled in a separate pilot code to check the roll-up calculations in the Westwater case (8); i.e., the roll-up of an initially flat, elliptically loaded vortex sheet. This case has received considerable attention in the past (e.g., Ref. 7) using discrete vortices. In spite of careful evaluation of local velocities, the distributed vorticity model solution did not agree with the earlier solutions, and, in fact, diverged at very early time steps. Small errors in velocity were apparent even at the first time step, and were evidently due to the approximation in circulation distribution given by the piecewise linear vorticity distribution; i.e., even though the basic circulation level has been conserved--because we were following the motion of doublet values--the assumption of piecewise quadratic variation between the points was violating the conservation of circulation by as much as 5% with 40 panels. The conservation of moments of circulation about the centroid was not checked but would clearly be violated, particularly since the distribution errors were more marked in the roll-up region. For these invariants of the vortex sheet motion to be satisfied by a distributed vorticity model would clearly require a higher-order distribution than linear (vorticity). Unfortunately, the work schedule did not permit further investigation of the problem and in view of the satisfactory behavior of MODEL 1 (which does satisfy the vortex motion invariants to quite large times) it was decided to proceed to the thick airfoil case with that model only.

6.0 VORTEX SEPARATIONS FROM THICK SECTIONS

We now come to the difficult problem of vortex separation from the smooth surface of a thick section where location of separation is not known a priori. At this stage we are going to prescribe the separation point with a view to evaluating the inviscid model. We therefore assume that at some future date the inviscid analysis will be coupled with a boundary layer analysis whereby the location of the separation line will be obtained by iteration. This would be a similar procedure to that employed in the "CLMAX" program, Reference 9, and discussed in broad terms in Reference 1. At this point of time it has yet to be demonstrated that existing inviscid methods can converge on the right vortex structure given the separation line on a general smooth body.

Before proceeding with the present calculations, it was found necessary to make some changes in the pilot code developed so far. These changes are described below and concern (i) the shedding model, i.e., Kutta condition applied to the separation point, and (ii) the boundary conditions on the solid surface.

6.1 Shedding Model

The edge-shedding model used in Section 5 in which the edge doublet value is simply convected with the flow was found inadequate for the case of shedding from a smooth surface. Here, an extension of the separation model used in the "CLMAX" code (Ref. 9) was considered. We assume, therefore, that the vorticity value, γ_s, just upstream of separation breaks away from the surface and remains constant over a small time increment, δt. The amount of circulation shed in that time interval is therefore

$$\Delta\Gamma = \gamma_s \, U_s \, \delta t$$

where U_s is the mean velocity at the separation point. $(= |\frac{\gamma_s}{2}|$ since the outer velocity $= \gamma_s$, see Section 6.2). The doublet value on the first wake panel on the feeding sheet takes this increment in circulation while sending the old value further along the feeding sheet. Thus at time, t, the new wake doublet value just downstream of separation becomes

$$\mu_w{}^t = \mu_w{}^{t-1} + \gamma_s{}^t U_s{}^t \delta t.$$

(Note: this satisfies the unsteady Kutta condition in the finite difference sense; i.e., $\frac{\partial \mu}{\partial t} + \frac{U \partial \mu}{\partial s} = 0$, noting that $\gamma = - \frac{\partial \mu}{\partial s}$.)

This "smooth-surface" shedding model reduces to the sharp, trailing-edge type when applied to the upper and lower surfaces separately; i.e., the resultant circulation shed onto the wake depends on the resultant vorticity level between upper and lower surfaces. In the steady case, the upper and lower vorticity values cancel, leaving the standard Kutta condition that the wake doublet value is constant and equal to the difference between upper and lower doublet values at the trailing edge. A brief examination of the above shedding model applied to the sharp-edge case (Section 5.0) showed only a minor difference in the solutions.

As time proceeds, all the old wake doublet panel corners are convected along the local calculated velocity vectors, Figure 27. Subpanels are reformed at each step for the purpose of off-wake velocity calculations.

6.2 Surface Boundary Condition

The boundary condition of no flow across the solid boundary was specified by the external Neumann boundary condition of $\underline{V} \cdot \underline{n} = 0$ in the basic coding. This still applies for thin sections (i.e., single surface). For thick sections, however, we can use an alternative internal Dirichlet boundary condition of specifying the velocity potential on the inside surface. This has been under investigation at AMI in connection with other work, but, as we shall see below, it has certain advantages for the "growing-body" problem with arbitrary separation. There are many possibilities for the internal Dirichlet condition. The so called Green's Third Identity approach of setting zero perturbation potential inside the body is just one possibility and requires both source and vorticity singularities which complicate wake shedding at an arbitrary point. The model investigated at AMI sets the total potential to zero inside the section; this gives the simplest formulation.

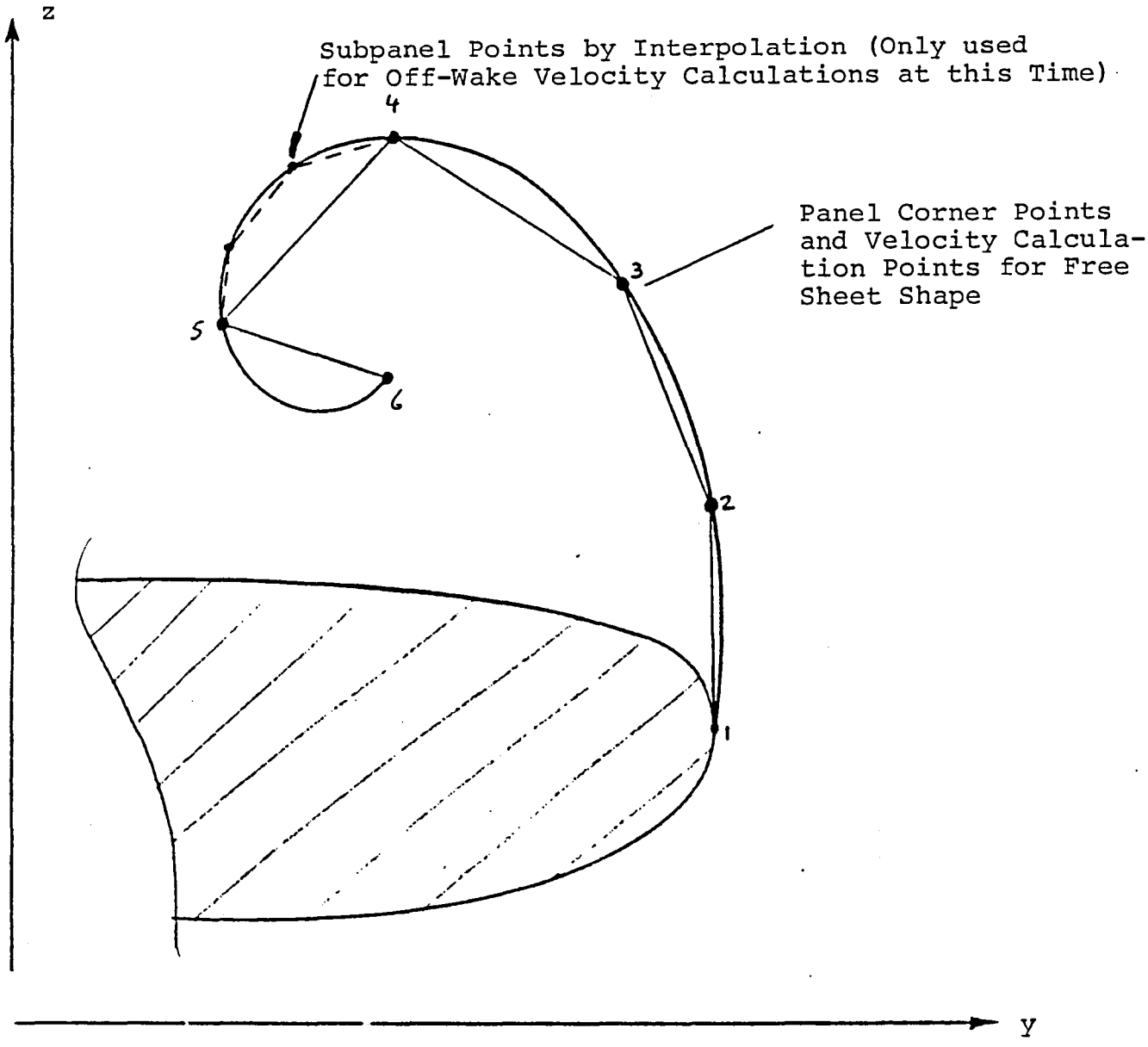

Figure 27. Wake (Free Sheet) Panels.

The formulation from Green's Third Identity for a point, P, on the section interior surface is then

$$\phi_{\infty_p} + \frac{1}{4\pi} \iint_{S-P} \left\{ \mu \underline{n} \cdot \nabla \left(\frac{1}{r}\right) + \frac{1}{r} V_N \right\} dS - \frac{\mu_p}{2} = 0$$

where S-P indicates the integral over the surface excluding point P, r is the distance from an element of the surface to the point P, ϕ_{∞_p} is the onset flow potential at point P, and V_N is the normal velocity at the body surface. (This formulation, which is given for the three-dimensional case, has been used a number of times in the past, usually with V_N set to zero, i.e., the steady case, and usually based on the alternative vorticity model.)

The velocity potential on the outside (i.e., wetted side) of point P is

$$\phi_{\infty_p} + \frac{1}{4\pi} \iint_{S-P} \left\{ \mu \underline{n} \cdot \nabla \left(\frac{1}{r}\right) + \frac{1}{r} V_N \right\} dS + \frac{\mu_p}{2} = \Phi_p$$

Subtracting the first equation from the second yields

$$\Phi_p = \mu_p$$

i.e., the <u>total</u> potential on the wetted surface is identical to the local doublet value with this formulation. Further, the surface gradients of Φ and μ are the same--this is particularly useful from the point of view of shedding a wake from a general point on the contour and is very convenient for evaluating velocities. This relationship between Φ and μ is <u>unaffected</u> by the presence of the source term, $(1/r)V_N$, in the above equations. In fact, with this formulation, the source distribution is given by the <u>total</u> normal velocity at the surface and the vorticity distribution (or doublet

gradient) is the total tangential velocity. Of course, in the steady potential flow case, V_N is zero (in the fixed coordinate system) and so we get the standard doublet only (or vorticity only) formulation with the internal boundary condition. However, in the case of the growing body problem, V_N becomes the local growth rate of the body which is therefore represented by a source distribution. (The pressure equation requires an additional contribution from the integral at infinity due to this growth rate.)

Problems at the trailing edge associated with doublet-only or vorticity-only models with external Neumann boundary condition do not arise with the internal Dirichlet condition, even for a cusped trailing edge.

A further refinement is possible with this model by considering the two parts of μ:

$$\mu = \Phi = \phi_\infty + \phi$$

where ϕ is the perturbation potential.

When calculating the tangential velocity, V_T (i.e., the surface gradient of μ), we can evaluate the onset flow part directly, hence:

$$V_T = \underline{V}_\infty \cdot \underline{t} - \frac{\partial \phi}{\partial s}$$

which should be numerically more accurate than taking the surface gradient of the total potential.

We can take this a step further and solve for the perturbation component of μ (i.e., ϕ) directly:

$$\frac{1}{4\pi} \iint_{S-P} \phi \frac{\underline{n} \cdot \underline{r}}{r^3} \, dS - \frac{\phi_p}{2} + b_p = 0$$

where

$$b_p = \frac{\phi_\infty}{2} p + \frac{1}{4\pi} \iint_{S-P} \left\{ \phi_\infty \frac{\underline{n} \cdot \underline{r}}{r^3} + \frac{1}{r} V_N \right\} dS$$

can be evaluated at each subpanel directly to improve the "onset" flow representation. (Note: these refinements have not been implemented in the pilot code at this time.)

At this time the singularity model is still based on piecewise constant doublet and source distribution on flat panels and subpanels (i.e., MODEL 1).

6.3 Calculated Results

In order to check the thick section separation calculation, the pilot code was applied to a 5:1 ellipse moving impulsively from rest to a uniform unit velocity normal to its major axis, Figure 28. Separation was prescribed at the ends of the major axis and conditions of symmetry about the minor axis were assumed.

The semi-ellipse was represented by 16 panels each with 3 subpanels. The location of the control points is indicated in Figure 28. This panel density is rather sparse for a vortex-surface interaction calculation, but should be adequate to test the procedure.

A time-step size of .01 was used and two amalgamation angles were used; i.e., θ_{merge} = 225° and 370°.

Figure 29 shows the growth of the vortex and its feeding sheet with time up to t = .2. As would be expected, the roll-up structure appears to be somewhat flattened by the presence of the solid surface. Some small irregularities have appeared in the feeding sheet for θ_{merge} = 370°, and will cause problems at later times. The irregularities are essentially eliminated by using an earlier amalgamation; viz., θ_{merge} = 225°, but this can affect the pressure distribution calculated beneath the vortex, Figure 30. If the pressure distribution is of interest (rather than just the vortex location) then at least the first passage of the free sheet over the surface should be maintained--implying θ_{merge}

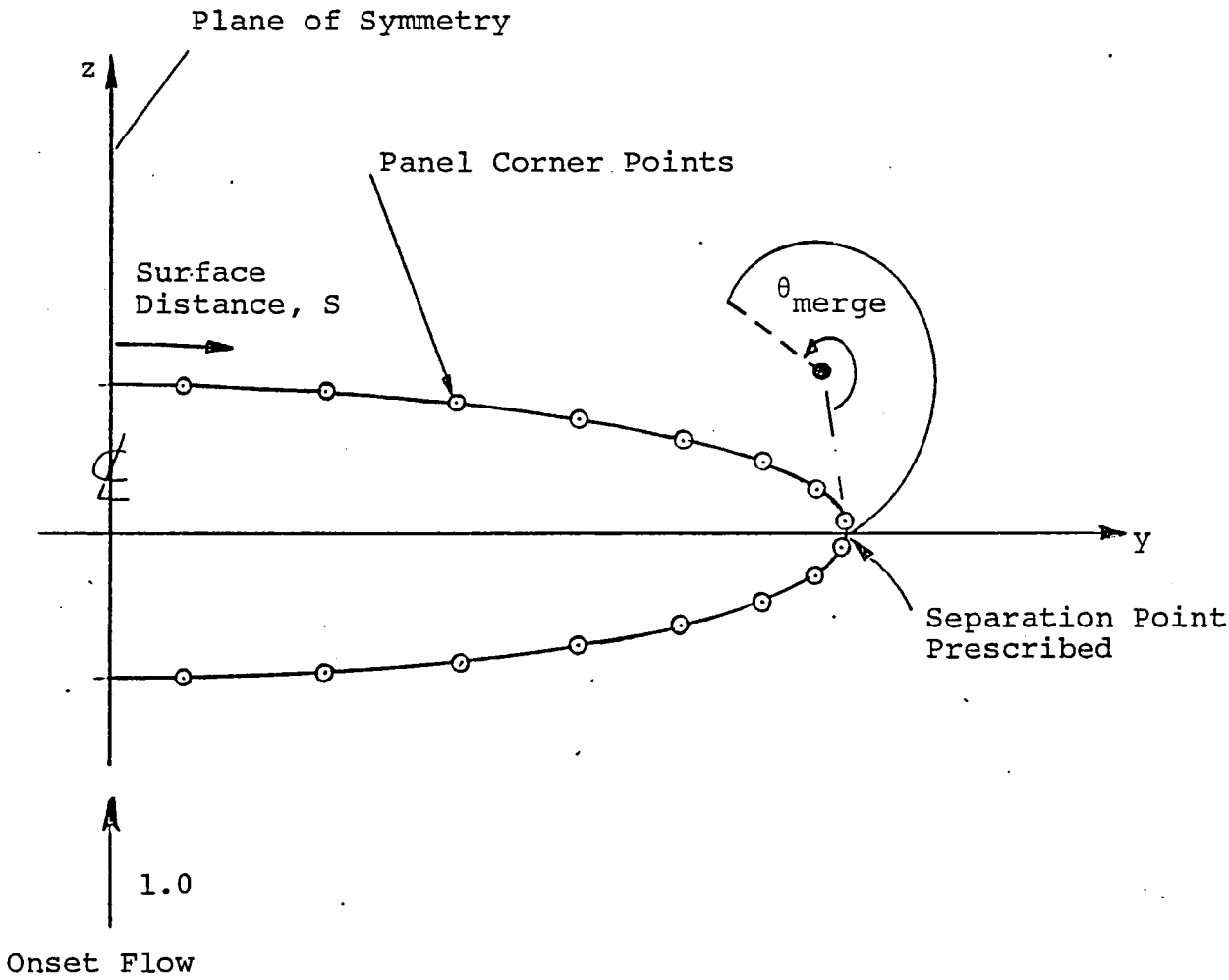

Figure 28. 5:1 Ellipse Moving Impulsively from Rest Normal to Its Major Axis.

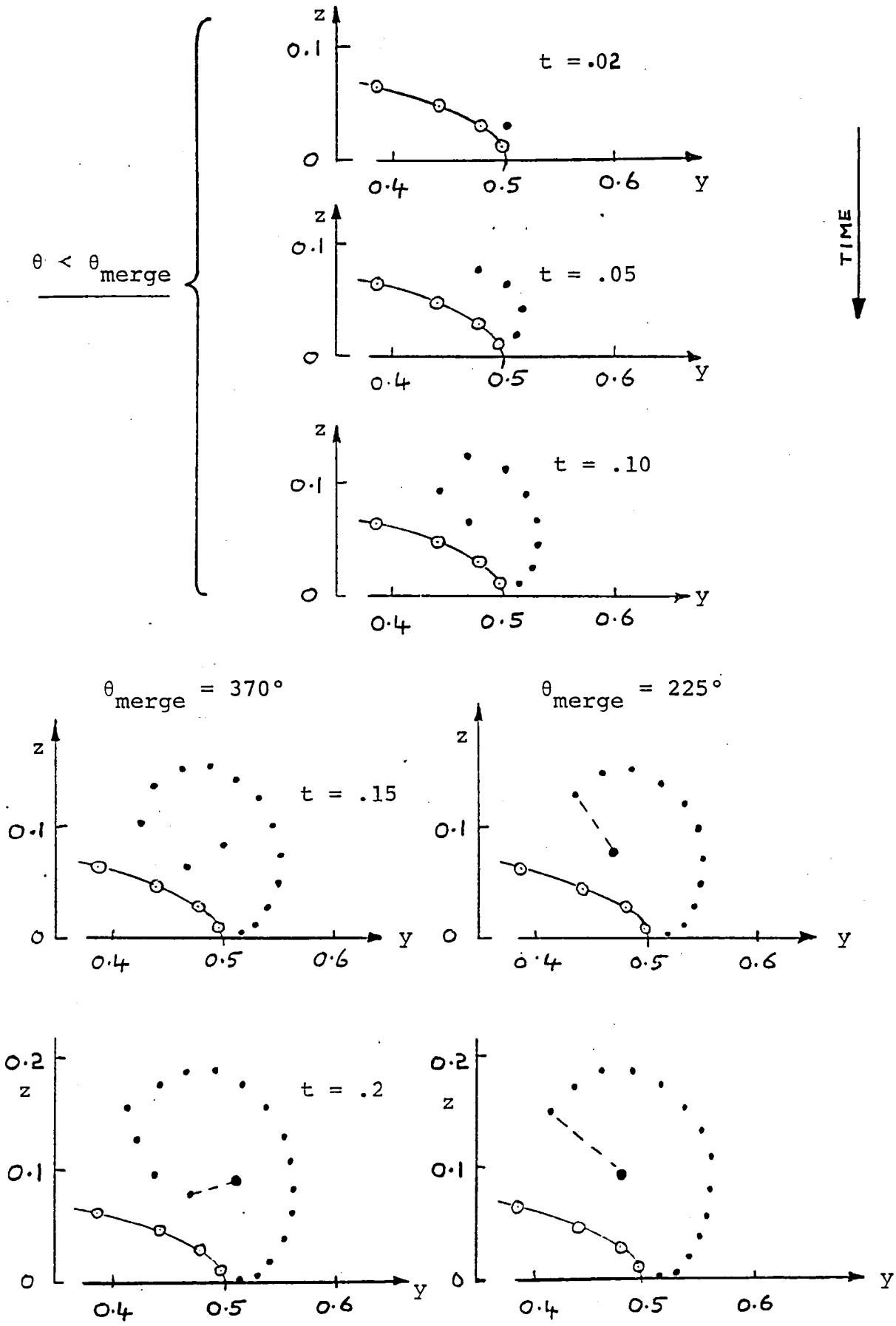

Figure 29. Growth of the Vortex Structure on the 5:1 Ellipse Moving Impulsively from Rest Normal to Its Major Axis; Time Step Size = .01.

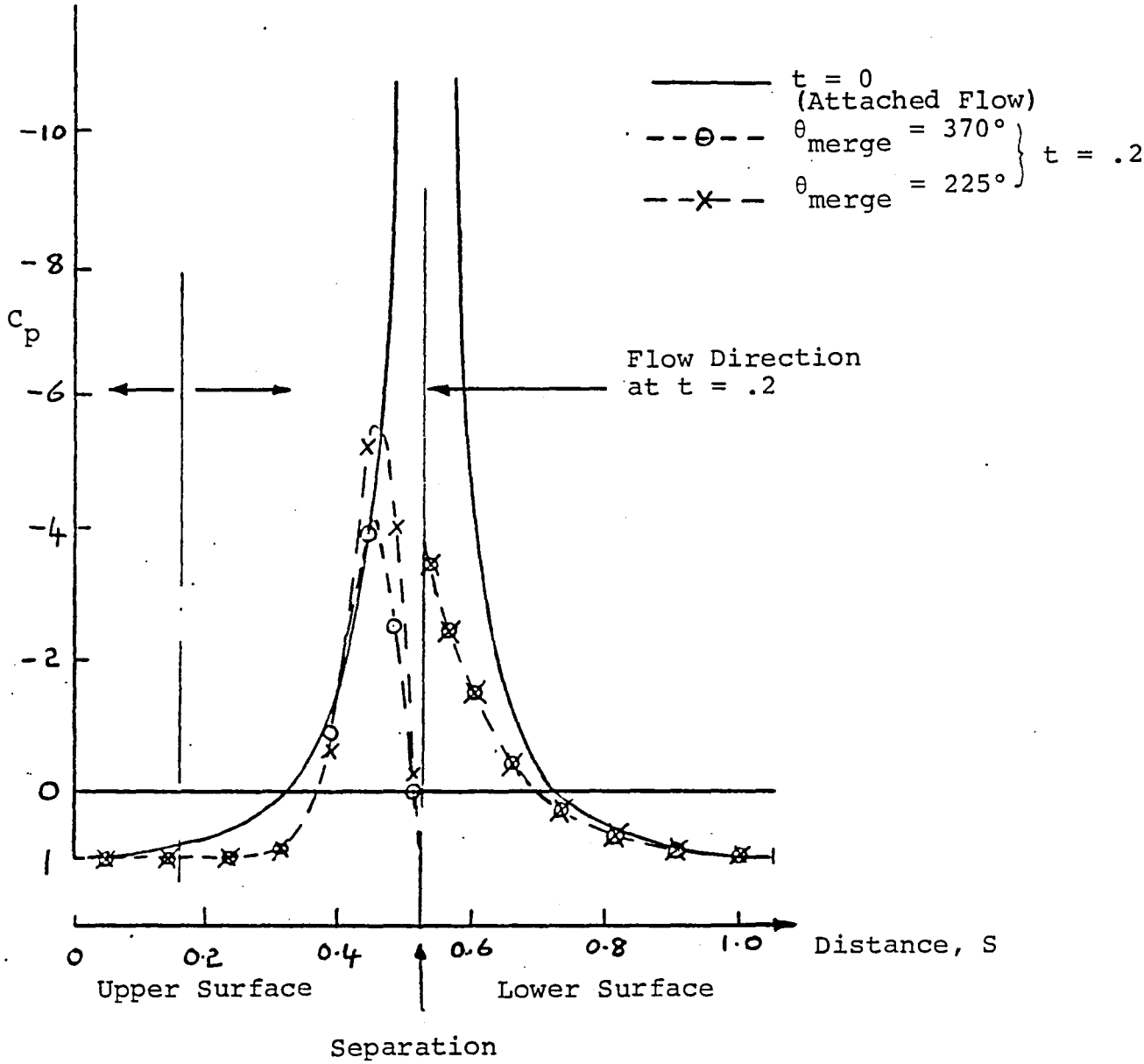

Figure 30. Effect of Vortex Amalgamation on Surface Pressures; 5:1 Ellipse Moving Impulsively from Rest Normal to its Major Axis. Time Step Size = .01.

values exceeding 360°. $\left(\text{Note: here } C_p \doteq 1 - \left(\frac{V_T}{W_\infty}\right)^2 - \frac{2}{W_\infty{}^2}\frac{\partial\phi}{\partial t}\right)$. These θ_{merge} values represent a much later amalgamation than is currently being used in vortex sheet calculations; e.g., Ref. 4 uses only 180°.

The irregularities that occur in the free sheet for large θ_{merge} values may be caused by small perturbations in the shed panels at earlier times. Certainly there is a small discrepancy in relative panel size in the initial part of the wake. In addition, the orientation of the free sheet as it leaves the surface appears too steep at later times. (It could be argued, however, that in view of the large vorticity level still being shed at t = .2 (see Figure 31) some self-induced curvature of the sheet would be expected and would disappear later as the shed vorticity level decreases.) Some detail examination of the shedding model characteristics needs to be carried out to see whether a refinement in the model is called for.

If irregularities in the free sheet persist, then we might consider refining the vortex sheet roll-up routine to improve the stability.

Figure 31 shows the surface tangential velocity distributions (positive convention clockwise) at a number of time steps. The first solution with fully attached flow forms a peak velocity in excess of -25. As time proceeds, the velocity peak in the attached flow region decreases steadily. Downstream of the separation point, the velocity peak decreases rapidly and at t = .05 a small reversed flow region has appeared (i.e., positive velocity) beneath the vortex. This reversed flow region grows with time and forms a second peak larger than the upstream value. The peak value does appear to be converging.

6.4 Vortex Separation on a "Growing" Body

Under the assumptions of the "unsteady cross-flow analogy", the calculations in Subsection 6.3 are equivalent to the separated flow from a three-dimensional body of constant elliptical section moving forward at constant angle of attack. Because of the general capability of the panel method, the section shape can, in principle, be changed with each time step to represent a more general body shape in the three-dimensional case.

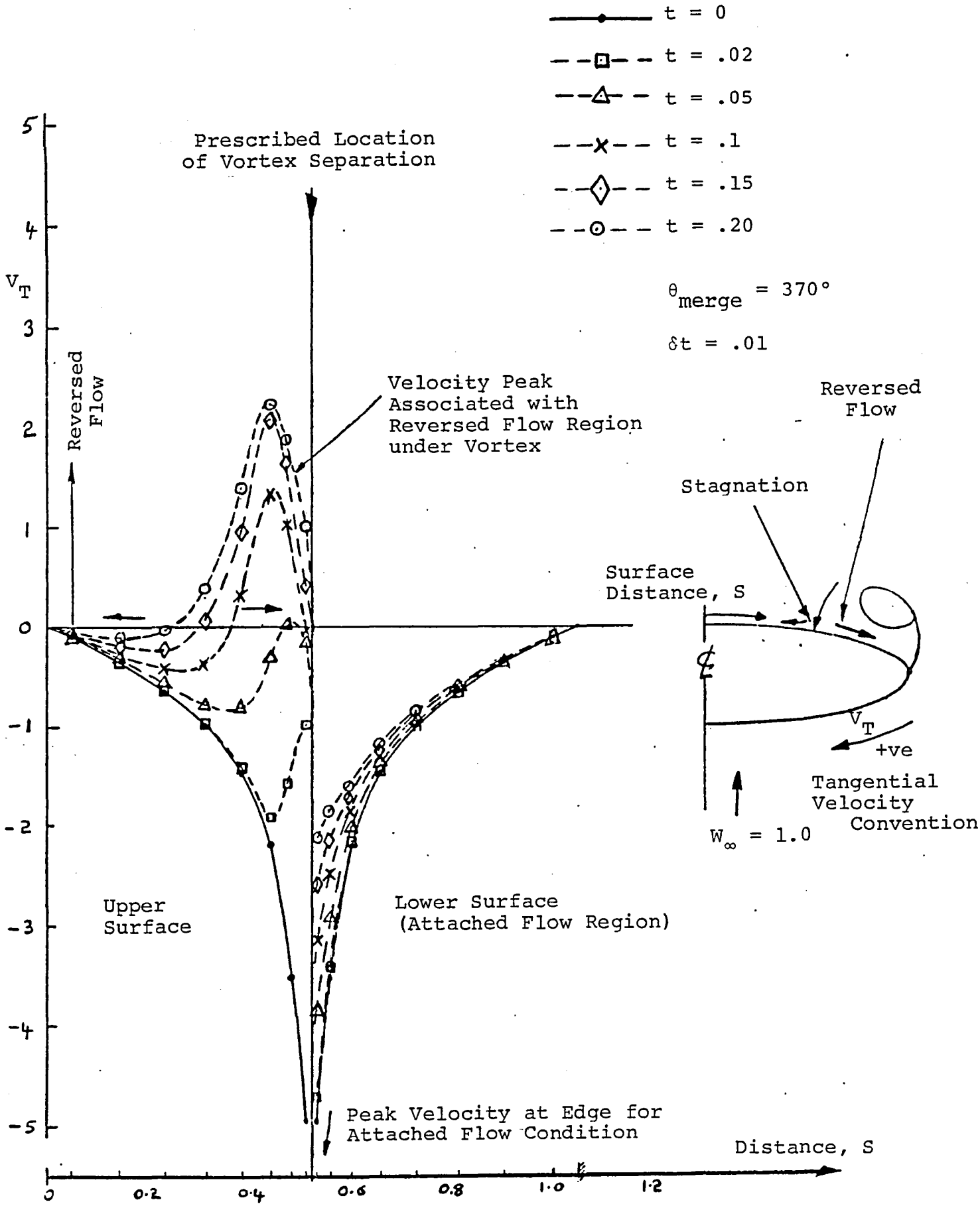

Figure 31. History of Surface Velocity Distribution on 5:1 Ellipse.

For a preliminary check of such an application, the 5:1 ellipse considered above was given a uniform growth rate of 1.025, i.e., a point, $\underline{r}^t$, on the ellipse at time t becomes simply $\underline{r}^{t+\delta t} = 1.025 \times \underline{r}^t$ at time $t + \delta t$. The value for δt used here was .01. The normal motion of the surface is represented by a source distribution (see Subsection 6.2). The source and doublet singularities are the only quantities affecting the growth of the vortex structure with time, i.e., the growth factor is applied only to the surface of the ellipse and not to the free sheet.

Figure 32 shows the shape of the free sheet at several time steps. Except for the growth rate, these calculations were the same as the earlier steady-shape calculations, and so Figure 32 can be compared with Figure 29 to show the effect of the growing body. The free sheet is seen to be pushed ahead of the solid surface and then to be "left behind", forming an even more flattened roll-up region than before. It is interesting to observe that if a larger growth rate were used (equivalent to a smaller sweep angle--or a smaller angle of attack--on the three-dimensional wing) then the free sheet would lie closer to the surface and the conditions for separation would disappear.

Some irregularities in the free sheet are seen at the later time steps using $\theta_{merge} = 225°$. These irregularities are essentially eliminated by using $\theta_{merge} = 180°$ (Figure 32); however, as seen earlier (Figure 30), this does affect the height and shape of the velocity peak associated with the reversed flow beneath the vortex (Figure 33).

Finally, in Figure 34 the locus of the centroid of shed vorticity is shown in relation to the locus of the leading edge of the equivalent three-dimensional body. The shed vorticity locus is not affected by the θ_{merge} assumption. The path of the vortex "core" is, however, affected by θ_{merge}, since this determines the proportion of shed circulation held by the core at each section; i.e., with large θ_{merge} values the shed circulation is still largely distributed in the free sheet and so the "core" will tend to rotate around the locus of the centroid of shed vorticity.

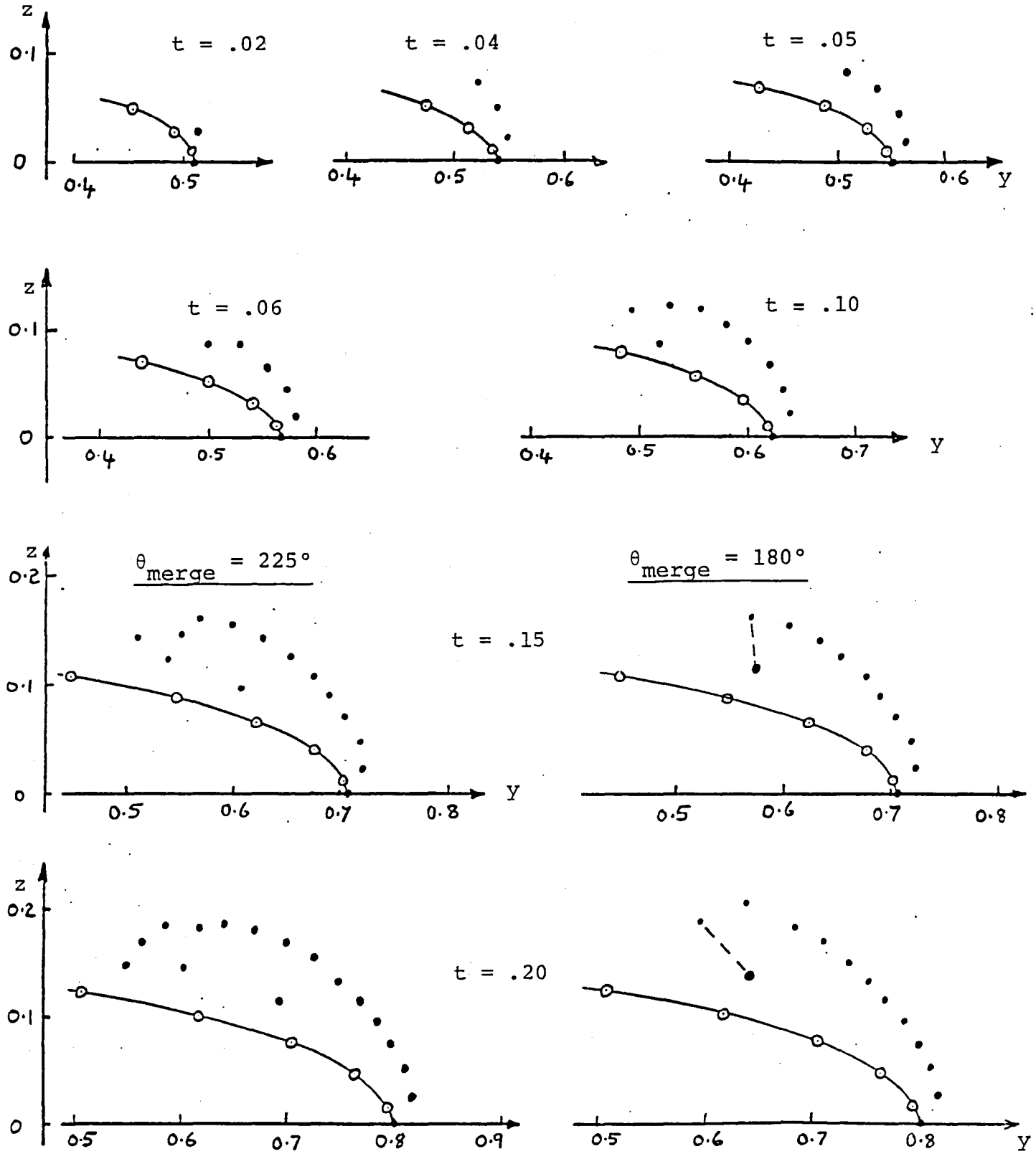

Figure 32. History of the Vortex Structure on the Growing 5:1 Ellipse. Growth Factor = 1.025 at Each Time Step. Time Interval = .01.

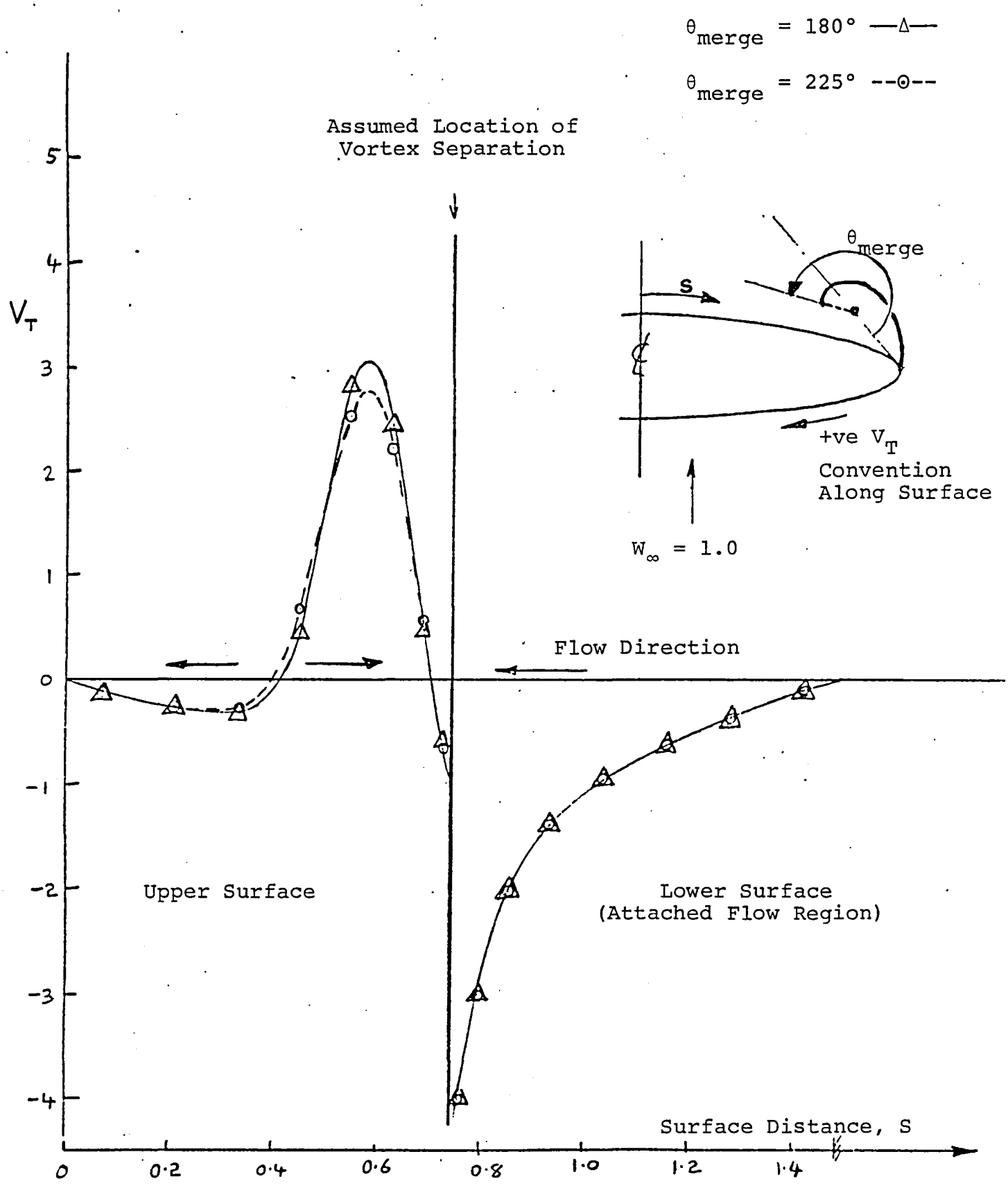

Figure 33. Effect of θ_{merge} on Surface Velocities on the Growing Ellipse. t = .15; Growth Factor 1.025.

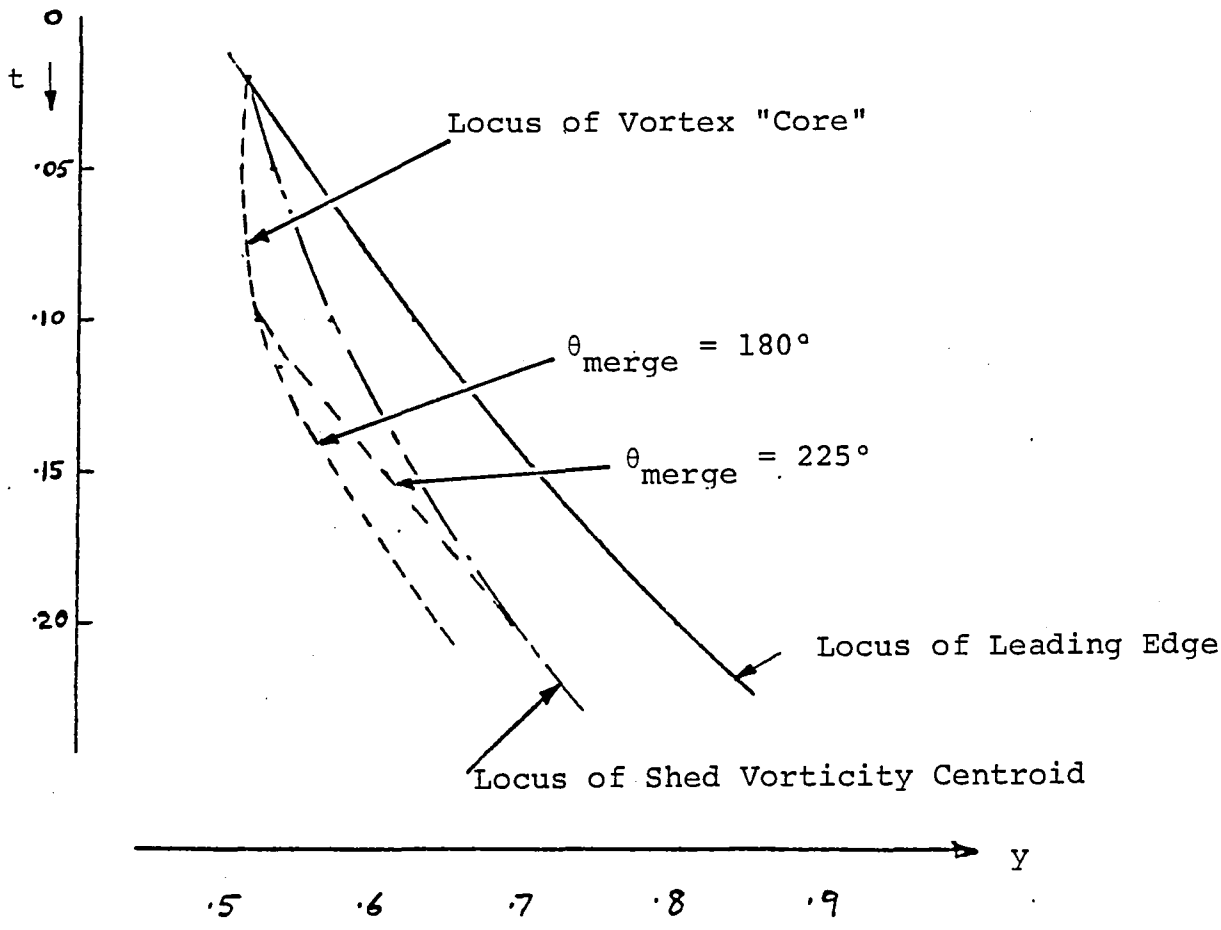

Figure 34. Locus of Shed Vorticity Centroid on Growing 5:1 Ellipse; δt = .01, Growth Factor = 1.025.

7.0 CONCLUSIONS

The application of surface singularity methods to the calculation of vortex/surface interference has been examined in the two-dimensional case in a series of situations of increasing complexity. Two main conclusions may be drawn from the initial set of calculations:

1. The main factor affecting accurate prediction of the vortex/surface interference flow is the distance between control point stations (where the boundary condition is applied) relative to the height of the vortex above the surface. The ratio of these distances, λ, should be kept below 1.

2. In relation to the effect of control point density, the improvement in accuracy offered by a higher-order panel method is insignificant.

A technique was developed based on subpanels and an applied doublet distribution which gave significant improvements in accuracy and detail of the interference flows. The technique, which is applicable to any panel method, has the following features:

(i) The effect of a more detailed representation is obtained without increasing the number of unknowns.

(ii) The technique is a pseudo higher-order method, yet can still be based on a simple influence coefficient expression, thus the technique need not affect the basic versatility of a low-order panel method.

(iii) Subpanels are used only locally in a close-approach situation and so do not increase computing effort significantly for a given density of control point stations.

(iv) The applied doublet part of the technique locates the major term in the interference flow without special relocation of panels and control points.

In time-step calculations involving a feeding sheet from a separation point on the surface, only MODEL 1 (piecewise constant doublet model) has given consistent solutions for the shape of the feeding sheet. The higher-order model diverged at early times and was not considered further.

Preliminary solutions were obtained for the case of vortex separations from a smooth surface (ellipse) including the case when the surface grows with time.

8.0 RECOMMENDATIONS FOR FURTHER WORK

Further refinement is required in the feeding-sheet shape calculation in order to ensure stability at large times and particularly to guarantee the representation of the first turn of the sheet, i.e., the first passage back over the surface. As part of the refinement, particular attention should be given to the behavior of the separation model and the shape of the initial part of the feeding sheet.

The demonstration in Subsection 6.4 of vortex separation from a "growing" body in the unsteady cross-flow analogy of steady three-dimensional flows was for the simple case of uniform growth; i.e., the shape of the body is always the same. The panel method used, however, is not restricted in shape and so the principle can be extended to the case where the body cross section at each time step is arbitrary. This would require the development of a routine for determining the growth rate of each panel at each time step and from this, the equivalent source distribution. Such an extension would be capable of predicting an initial vortex structure for input to the Boeing three-dimensional code (4) and should reduce the number of iterations required for a converged three-dimensional solution. In such an application, the Suction Analogy (2) loading shape could be used to modify the cross flow conditions in order to approximate the trailing-edge Kutta condition. Further development would make it applicable to asymmetric flow (yaw) and multiple separations (e.g., body vortices, wing strake vortices, leading-edge vortices and tip-edge vortices).

9.0 REFERENCES

1. Smith, J.H.B., "Inviscid Fluid Models, Based on Rolled-Up Vortex Sheets, for Three-Dimensional Separation at High Reynolds Number", Paper No. 9, AGARD Lecture Series No. 94 on Three-Dimensional and Unsteady Separation at High Reynolds Numbers, February 1978.

2. Polhamus, E.C., "Predictions of Vortex-Lift Characteristics by a Leading-Edge Suction Analogy", J. Aircraft, Vol. 8, 1971, p. 193.

3. Smith, J.H.B., "Improved Calculations of Leading-Edge Separation from Slender Delta Wings", R.A.E. Technical Report 66070, March 1966.

4. Johnson, F.T. et al., "An Improved Panel Method for the Solution of Three-Dimensional Leading-Edge Vortex Flows", Vol. I--Theory Document, NASA CR-3278, Vol. II--User's Guide and Programmer's Document, NASA CR-3279, 1980.

5. Maskew, B., "A Subvortex Technique for the Close-Approach to a Discretized Vortex Sheet", NASA TM X-62,487, September 1975.

6. Rossow, V.J., "Lift Enhancement by an Externally Trapped Vortex", J. Aircraft, Vol. 15, No. 9, September 1978, pp. 618, 625.

7. Moore, D.W., "A Numerical Study of the Roll-Up of a Finite Vortex Sheet", J. Fluid Mech., Vol. 63, Part 2, 1974, pp. 224-235.

8. Westwater, F.L., "Rolling up of the Surface of Discontinuity Behind an Airfoil of Finite Span", Aero. Res. Council R & M No. 1962, 1935.

9. Maskew, B. and Dvorak, F.A., "The Prediction of C_{LMAX} Using a Separated Flow Model", J. Am. Hel. Soc., April 1978.

APPENDIX A

Subpanel Model

For near-field calculations, a panel is divided into a number of subpanels, Figure A1(a). The subpanel corners are located on the interpolated surface and the subpanel singularity values are obtained using biquadratic interpolation through a local set of panel singularity values. In this way the subpanels offer a more continuous representation of the surface geometry and singularity distribution than is given by the basic panel--even in the case of piecewise constant doublet model--Figure A1(b).

The doublet value at location α is given by

$$\mu(\alpha) = G1(\alpha, \alpha_{1_n})\ \mu_{n-1} + G2(\alpha, \alpha_{1_n}, \alpha_{2_n})\ \mu_n$$

$$+ G2(1 - \alpha, 1 - \alpha_{2_n}, 1 - \alpha_{1_n})\ \mu_{n+1}$$

$$+ G1(1 - \alpha, 1 - \alpha_{2_n})\ \mu_{n+2}$$

where the biquadratic multipliers, G1 and G2, are given in Appendix B. Doublet values, μ_{n-1}, μ_n, etc., are the values on four local panels and the parameter α is the normalised distance along the surface (Appendix B).

The gradient of the doublet distribution (i.e., vorticity) is evaluated assuming a local quadratic doublet distribution through three neighboring values, μ_A, μ_B, μ_C:

$$\left.\frac{\partial \mu}{\partial s}\right|_B = \left(\mu_C\ S_A/S_C - \mu_A\ S_C/S_A\right) \Big/ \left(S_A + S_C\right)$$

$$- \mu_B(S_A - S_C)/S_A/S_C$$

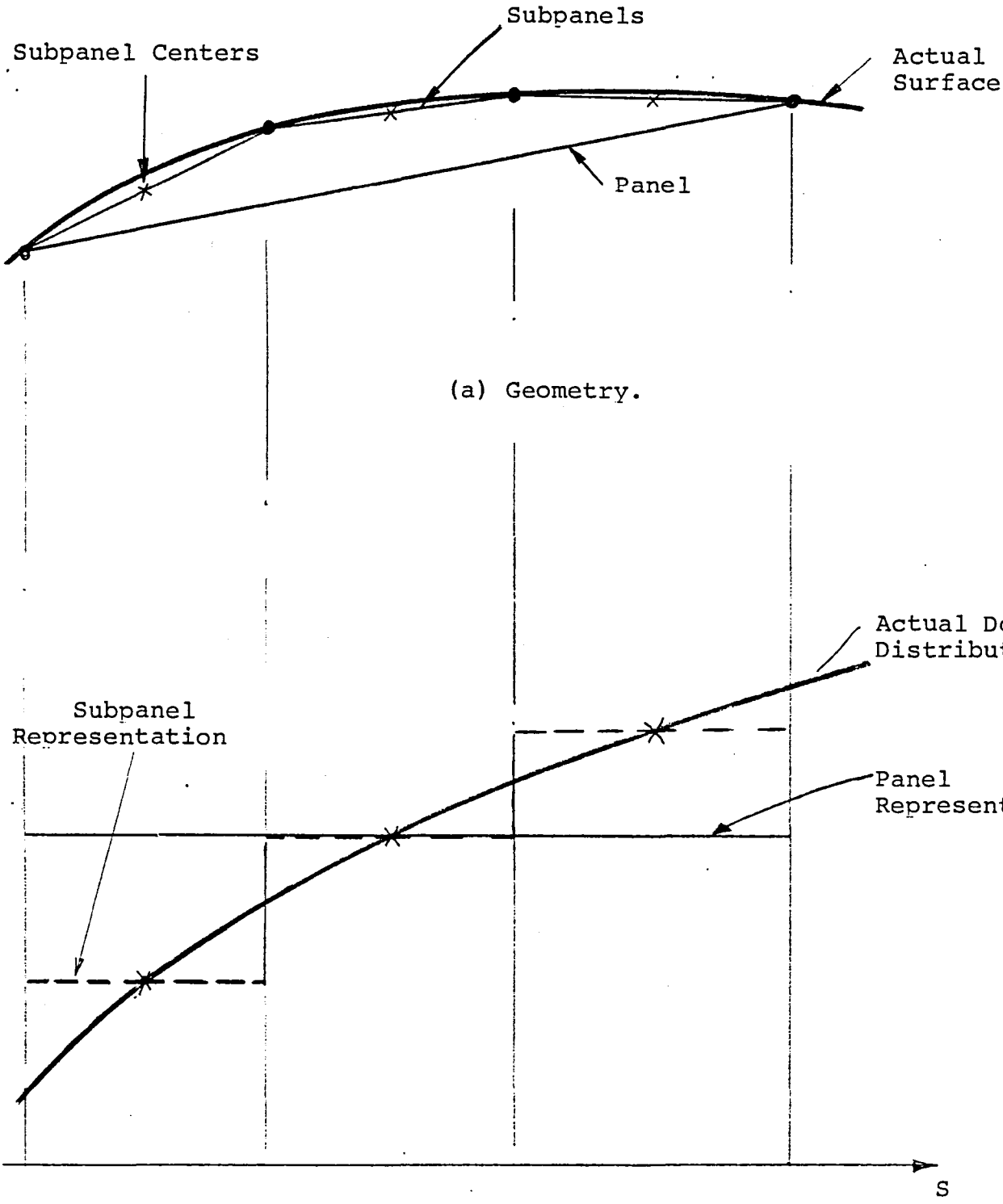

(a) Geometry.

(b) Singularity Distribution (e.g., Piecewise Constant).

Figure A1. Subpanel Model (NSUB = 3).

where S_A, S_c are, respectively, the surface distances betwen point A and B, and between points B and C.

Finally,

$$\gamma = - \frac{\partial \mu}{\partial s} .$$

APPENDIX B: BIQUADRATIC INTERPOLATION

Given a set of position vectors, $\underline{P}n$, n=1, 2, ..., N, defining a smooth space curve, we wish to interpolate for additional values in, say, the interval between $\underline{P}_n$ and $\underline{P}_{n+1}$, Figure B1. We first generate the integrand contour length, s_n, to each point from the beginning of the curve, i.e., from $\underline{P}_1$. For convenience, the straight segment lengths are used, i.e., $\Delta s_n = \left|P_{n+1} - \underline{P}_n\right|$ (but arc lengths could easily be substituted--or, indeed, any other parameter that varies smoothly and monotonically along the curve, i.e., without introducing multiple value problems. For example, the point subscript is used in some parts of the pilot program.)

Next, we generate two quadratic curves: $\underline{q}_1(\alpha,\alpha_{1_n})$ passing through points $\underline{P}_{n-1}$, $\underline{P}_n$, $\underline{P}_{n+1}$, and $\underline{q}_2(\alpha,\alpha_{2_n})$ passing through points $\underline{P}_n$, $\underline{P}_{n+1}$ and $\underline{P}_{n+2}$, Figure B1.

The normalized interpolation parameter, α, ranges from 0 to 1 in the n^{th} interval, and has value

$$\alpha_{1_n} \text{ at } \underline{P}_{n-1} \quad \text{and} \quad \alpha_{2_n} \text{ at } \underline{P}_{n+2}$$

where

$$\alpha_{1_n} = (s_{n-1} - s_n)/(s_{n+1} - s_n); \text{ and}$$

$$\alpha_{2_n} = (s_{n+2} - s_n)/(s_{n+1} - s_n).$$

In the n^{th} interval, we take a linear combination of $\underline{q}_1$ and $\underline{q}_2$ to define the biquadratic interpolation curve there:

$$\underline{P}(\alpha) = \alpha\underline{q}_2(\alpha,\alpha_{2_n}) + (1 - \alpha)\underline{q}_1(\alpha,\alpha_{1_n}).$$

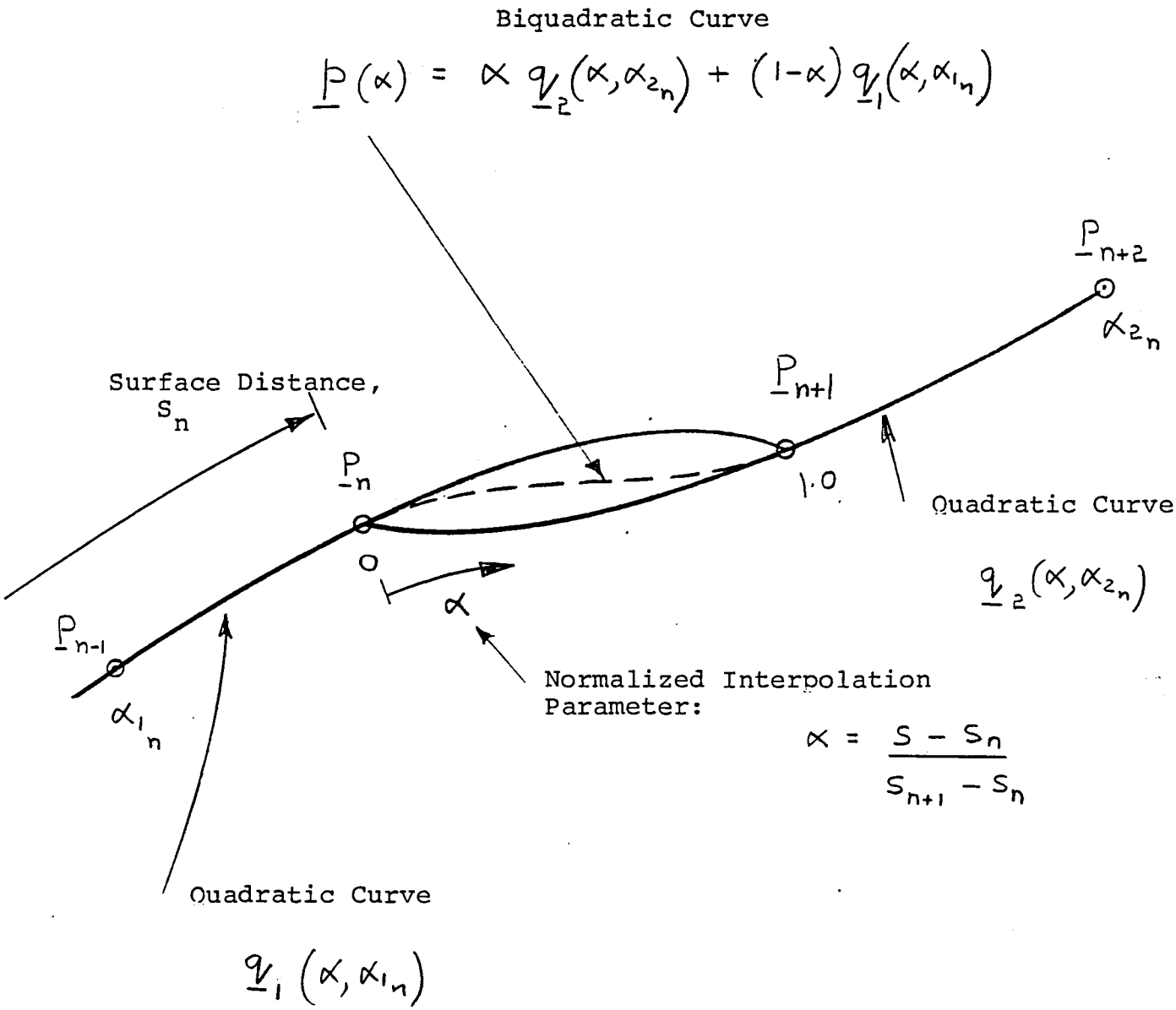

Figure B1. Biquadratic Interpolation.

The biquadratic is, therefore, a cubic, but is constrained to lie between two quadratic curves. It can't, therefore, behave wildly.

The value of α for a point distance, s, from the start of the curve (but located in the n^{th} interval) is

$$\alpha = (s - s_n)/(s_{n+1} - s_n)$$

The form of the interpolation curve can be expressed in terms of biquadratic multipliers, G1, G2, applied to the four local position vectors:

$$\underline{\bar{P}}(\alpha) = \underline{P}_{n-1}\, G1(\alpha, \alpha_{1_n}) + \underline{P}_n\, G2(\alpha, \alpha_{1_n}, \alpha_{2_n})$$

$$+ \underline{P}_{n+1}\, G2(1 - \alpha,\ 1 - \alpha_{2_n},\ 1 - \alpha_{1_n})$$

$$+ \underline{P}_{n+2}\, G1(1 - \alpha,\ 1 - \alpha_{2_n}) \ .$$

The forms of G1, G2 are:

$$G1(a,b) = a(1 - a)^2/(b(1 - b))$$

$$G2(a,b,c) = (1 - a)\left\{1 - a(1 - a)/b - a^2/c\right\}.$$

These are based on the linear combination of two quadratics, which gives continuous slope and a piecewise linear (but not necessarily continuous) variation of second derivative across each interval. Similar multipliers have been formed which give continuous second derivatives. In addition to the G1, G2 multipliers for position interpolation, other multipliers have been evaluated in the same convenient form to interpolate for first and second derivatives and also to integrate for area under the curve.

Besides interpolation for points on the curve, we can apply the same multipliers to other quantities varying along the curve, e.g., doublet values, μ, and pressure coefficient, C_p.

NASA Contractor Report 159334

Distribution List
NAS1-15495

	No. Copies
NASA Langley Research Center Hampton, VA 23665 Attn: Report and Manuscript Control Office, Mail Stop 180A W. Elliott Schoonover, Jr., Mail Stop 287	1 20
NASA Ames Research Center Moffett Field, CA 94035 Attn: Library, Mail Stop 202-3	1
NASA Dryden Flight Research Center P. O. Box 273 Edwards, CA 93523 Attn: Library	1
NASA Goddard Space Flight Center Greenbelt, MD 20771 Attn: Library	1
NASA Lyndon B. Johnson Space Center 2101 Webster Seabrook Road Houston, TX 77058 Attn: JM6/Library	1
NASA Marshall Space Flight Center Marshall Space Flight Center, AL 35812 Attn: Library, AS61L	1
Jet Propulsion Laboratory 4800 Oak Grove Drive Pasadena, CA 91103 Attn: Library, Mail Code 111-113	1
NASA Lewis Research Center 21000 Brookpark Road Cleveland, OH 44135 Attn: Library, Mail Stop 60-3	1
NASA John F. Kennedy Space Center Kennedy Space Center, FL 32899 Attn: Library, NWSI-D	1
National Aeronautics and Space Administration Washington, DC 20546 Attn: RTF-6	1
NASA Scientific and Technical Information Facility 6571 Elkridge Landing Road Linthicum Heights, MD 21090	30 plus original

End of Document